THE
PHYSICAL REVIEW
A Journal of Experimental and Theoretical Physics Established by E. L. Nichols in 1893

VOL. 52, NO. 7 OCTOBER 1, 1937 SECOND SERIES

The Induced Radioactivity of Scandium

HAROLD WALKE*
Radiation Laboratory, Physics Department, University of California, Berkeley, California
(Received August 10, 1937)

A study has been made of the radioactivities induced in scandium by bombardment with deuterons, alpha-particles and slow and fast neutrons. Sc^{46} has been produced by deuteron and slow neutron activation. This isotope emits low energy electrons and soft gamma-radiation. The energy distribution of the electrons has been investigated by means of a large hydrogen filled expansion chamber. The upper limit of the spectrum is at 0.89(5) Mev in reasonably good agreement with range measurements made using aluminum absorbers. The half-life of Sc^{46} is 85±2 days. Alpha-particle bombardment of scandium gives rise to V^{48} which emits positrons and gamma-rays and decays to half-value in 16.2±0.3 days. Irradiation of scandium with fast neutrons from the Be^9+H^2 reaction results in the formation of K^{42} only. Bombardment with the neutrons from the $Li+H^2$ reaction, however, yields K^{42} and both Sc^{43} and Sc^{44}. The scandium isotopes emit positrons and decay with half-lives of 4.0±0.1 hours and 52±2 hours, respectively. Under these conditions the reaction $Sc^{45}+n^1\rightarrow Sc^{43}+3n^1$ is twice as probable as $Sc^{45}+n^1\rightarrow Sc^{44}+2n^1$. No evidence has been obtained of the reaction $Sc^{45}+n^1\rightarrow Ca^{45}+H^1$.

INTRODUCTION

THE induced radioactivity of scandium was first studied by von Hevesy and Levi[1] who irradiated scandium oxide for a few days using a radon-beryllium source of 200–300 millicuries. These investigators observed the formation of K^{42} and Sc^{46} according to the reactions

$$Sc^{45}+n^1\rightarrow K^{42}+He^4; \quad K^{42}\rightarrow Ca^{42}+e^-;$$
$$Sc^{45}+n^1\rightarrow Sc^{46}+\gamma; \quad Sc^{46}\rightarrow Ti^{46}+e^-,$$

the half-lives of which were reported as 16 hours and two months, respectively. (Aston has shown that scandium has only one isotope, its mass number being 45.)

Recently Pool, Cork and Thornton[2] have irradiated scandium with the fast neutrons from a lithium target bombarded with deuterons and have observed the formation of Sc^{43} and Sc^{44} in addition to K^{42}.

The present paper is a report of an investigation of the radioactivities induced in scandium oxide by bombardment with deuterons, alpha-particles, slow neutrons, and fast neutrons from both beryllium and lithium targets bombarded with deuterons. On account of the high intensity of the effects observed more accurate values of the half-lives of Sc^{46} and K^{42} have been obtained. In addition, V^{48} has been identified.

APPARATUS

The activations with deuterons, alpha-particles and neutrons from beryllium were carried out using the Berkeley cyclotron under conditions already described.[3] The very high energy neutrons from the $Li+H^2$ reaction were produced by bombarding lithium metal which was compressed into a cavity in a brass plate and which was

* Commonwealth Fund Fellow.
[1] von Hevesy and Levi, Det. Kgl. Danske Videnskabernes Selskab Math. Fysiske Meddelelser. **14**, 5 (1936).
[2] Pool, Cork and Thornton, Phys. Rev. **52**, 41 (1937).
[3] Walke, Phys. Rev. **51**, 439 (1937).

efficiently water cooled. In consequence it was found possible to bombard the lithium with deuteron currents as high as 15 microamperes.

Measurements of the decay of the radioactive samples were carried out using a Lauritsen type quartz fiber electroscope.

Activation with Deuterons

Several samples of scandium oxide were bombarded with deuterons, and it was found that a long lived isotope was formed. In consequence chemical separations were carried out and Sc^{46} was isolated by several processes. For example, one sample of the oxide was activated for approximately 45 microampere-hours and was divided into three portions. To one portion which was dissolved in $6N$ HNO_3 was added inactive phosphoric acid followed by 5 cc of HNO_3 and 5 cc of $(NH_4)_2MoO_4$. The solution was heated to 70° and allowed to stand for 10–15 minutes. The precipitate of ammonium phosphomolybdate was found to be inactive showing that no radiophosphorus was present in the active sample.

The residual solution from this procedure was analyzed by the specific tests for scandium given by Noyes and Bray[4] as follows: Scandium hydroxide was precipitated from the nitrate solution by the addition of NH_4OH and was filtered off and washed. It was then dissolved in 5–10 cc of $6N$ HCl, the solution being subsequently evaporated almost to dryness. It was then transferred to a platinum dish being rinsed in with water. The solution was then evaporated completely to dryness and to the residue was added 2 cc of water and 0.5–1.0 cc of $27N$ HF, 1 cc of $6N$ HCl and 9 cc of water. The solution was heated to 100° for about 5 minutes and filtered through a waxed funnel.

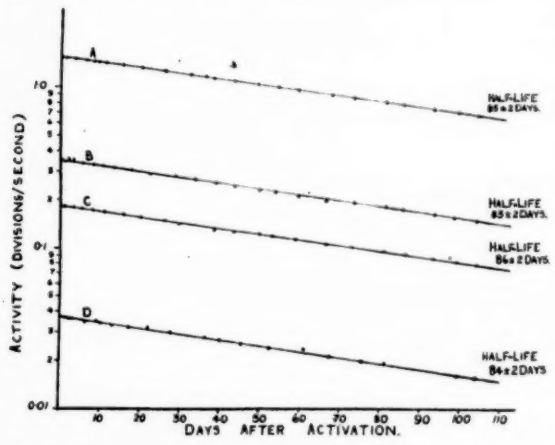

FIG. 1. Decay curves of various samples of Sc^{45}. *A* is the $\beta+\gamma$-ray decay curve of unseparated Sc_2O_3 after activation with deuterons. *B* is the decay curve of Sc_2O_3 recovered from Sc_2O_3 following activation with deuterons and separated chemically by the oxalate procedure. *C* is the decay curve of the γ-radiation from sample *A* filtered through 1 mm of lead and 3.2 mm of aluminum. *D* is the decay curve of spectroscopically pure Sc_2O_3 activated with slow neutrons.

[4] Noyes and Bray, *System of Qualitative Analysis for the Rare Elements.*

The precipitate was transferred to a platinum dish and to it was added 10 cc of $6N$ NH_4OH and 5 cc of $27N$ HF, the solution being heated nearly to boiling for 2–3 minutes. It was next filtered and to the filtrate was added 4 cc of $18N$ H_2SO_4. The mixture was allowed to stand for ten minutes and a white translucent precipitate formed. Finally 10 cc of water were added and sufficient $6N$ NH_4OH to make the solution alkaline. The $Sc(OH)_3$ precipitate was filtered off and found to be active. This test proves conclusively that the radioactive body formed is an isotope of scandium.

When it was thus established that the isotope Sc^{46} had been isolated the other portions of the sample were treated by different processes. From one $Sc(OH)_3$ was precipitated by the addition of $6N$ NH_4OH and from the other Sc_2O_3 was kindly recovered for the author by Dr. Philip Schutz of the department of chemistry. Dr. Schutz precipitated the scandium as oxalate in a solution of about $1N$ acidity. The oxalate was then filtered off and roasted for several hours at 700°C.

All the samples were found to be strongly active and observations of their decay have shown that the half-life of Sc^{46} is 85 ± 2 days. This value is somewhat higher than that given by Hevesy and Levi,[1] namely two months. The yield of Sc^{46} in the reaction

$$Sc^{45}+H^2 \rightarrow Sc^{46}+H^1$$

is approximately 9×10^7 deuterons per active atom.

Activation with Slow Neutrons

A further indication that the isotope concerned is Sc^{46} is given by the fact that the same active body has been formed by irradiating scandium oxide with slow neutrons. The sample

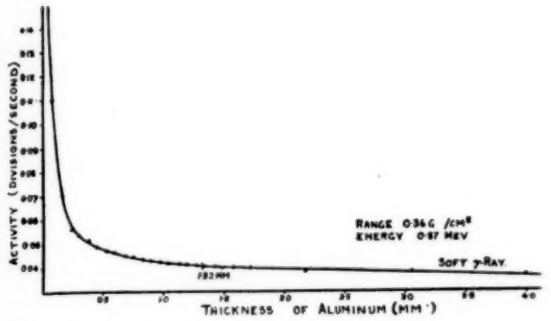

FIG. 2. Absorption curve in aluminum of radiations emitted by Sc_2O_3 recovered from the oxalate precipitate separated from Sc_2O_3 after activation with deuterons. Range of electrons 0.36 g/cm². Energy 0.87 Mev.

used in this experiment was spectroscopically pure. Several grams were activated in a cube of paraffin of side 10″ placed immediately behind the beryllium target which was bombarded with a current of 12 microamperes of deuterons. The radioactivity observed decayed with a single period of 84±2 days.

It is thus clear that Sc^{46} has been formed in the two reactions

$$Sc^{45}+H^2 \rightarrow Sc^{46}+H^1,$$
$$Sc^{45}+n^1 \rightarrow Sc^{46}+\gamma.$$

Decay curves of this isotope are shown in Fig. 1.

PROPERTIES OF Sc^{46}

Magnetic deflection of the particles emitted by Sc^{46} showed them to be negative electrons. It was observed that a gamma-ray was also present. The energy of the β-rays was then determined by measuring their range in aluminum. The absorption curve obtained is shown in Fig. 2. The range of the electrons is 0.36 g/cm² so that the maximum energy calculated according to Feather's formula is 0.87 Mev. The absorption curve when compared with that of Sc^{43} suggests that the energy of the gamma-ray is less than 0.5 Mev since it is much more absorbed by the aluminum than annihilation radiation.

The energy distribution of the electrons emitted by Sc_2O_3 recovered from the oxalate procedure has been studied by means of the large hydrogen filled expansion chamber mentioned in a previous paper.[5] The electrons were deflected in a field of 276 oersteds and their energy determined by the method already discussed[6] in considering the energy distribution of the positrons from Sc^{42} and Sc^{43}. Measurements were made on 312 tracks, the resulting momentum distribution being shown in Fig. 3. The upper limit of the spectrum is at $4350H\rho$, 0.89(5) Mev in good agreement with the value obtained from the range measurements. The dotted curve in Fig. 3 has been fitted to the distribution of tracks by inspection. It does not refer to any theoretical curve. The upper limit has also been determined by inspection. No attempt has been made to extrapolate beyond the observed track of highest energy nor has the end point been adjusted to fit any theory of β-decay.

The spectrum is characterized by the sharp maximum at $1500H\rho$.

ACTIVATION WITH ALPHA-PARTICLES

Following bombardment with 11 Mev alpha-particles scandium oxide was found to emit positrons and gamma-radiation. The activity decays to half-value in 16.2±0.3 days. The reaction involved is

$$Sc^{45}+He^4 \rightarrow V^{48}+n^1; \quad V^{48} \rightarrow Ti^{48}+e^+$$

as the emission of a proton yields the stable titanium isotope Ti^{48}.

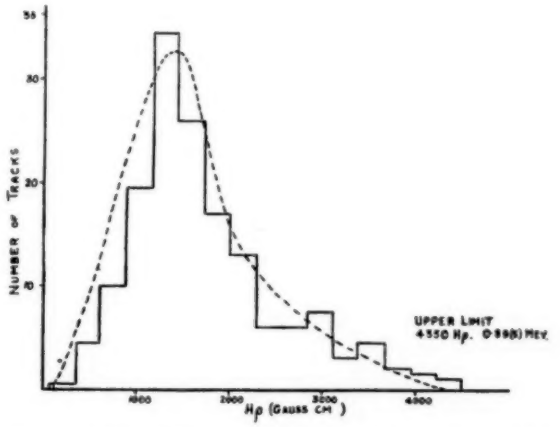

FIG. 3. Momentum distribution of electrons emitted by Sc_2O_3 recovered from oxalate procedure. Magnetic field 276 oersteds. Number of tracks measured 312. Upper limit 4350 $H\rho$. Energy 0.89(5) Mev. The dotted curve has been fitted to the distribution by inspection without reference to any theory. The upper limit has also been estimated by inspection of the distribution. No attempt has been made to extrapolate beyond the highest energy track observed nor to fit this to any theory.

[5] Walke, Phys. Rev. **52**, 400 (1937).

A chemical analysis showed that the active body is an isotope of vanadium.

The irradiated sample of scandium oxide was dissolved in 6*N* HCl and a little ammonium metavanadate was added. The equivalent quantity of lead nitrate was then added and 6*N* NH_4OH gently stirred into the mixture until the lead vanadate precipitate separated out. A little $Sc(OH)_3$ came down as well but the lead vanadate was redissolved in dilute HCl and inactive scandium was added to the solution. The vanadium was then reprecipitated as lead vanadate and after filtering and washing was thoroughly dried. This precipitate was found to be radioactive, decaying to half-value in 16.3 $\pm$0.3 days.

It is thus clear that bombardment of scandium with 11 Mev alpha-particles gives rise to V^{48}, this isotope having a half-life of 16.2$\pm$0.3 days. The same isotope has been separated chemically from titanium after activation with deuterons. In Fig. 4 are shown some decay curves of V^{48}. A comparison between the decay of two radioactive vanadium precipitates isolated from $Sc^{45}+He^4$ and $Ti^{47}+H^2$ is shown in this figure. By the deuteron activation of titanium very strong samples of V^{48} can be obtained so that it is proposed to consider the properties of this isotope in a subsequent paper.

The yield of V^{48} in the reaction studied is approximately 2×10^7 alpha-particles per active atom.

Activation with Fast Neutrons

A. Neutrons from beryllium bombarded with deuterons

When scandium oxide was bombarded with fast neutrons from beryllium+deuterons, a radioactive isotope was detected which decayed to half-value in 12.5$\pm$0.2 hours. Chemical analysis as already discussed in a previous paper[6] showed this to be an isotope of potassium namely K^{42}. The decay curve of the chemically separated potassium was published in the paper mentioned above.

After extracting the active potassium, scandium was precipitated from the solution and was found to be inactive and moreover calcium precipitated as oxalate was also inactive. This result agrees with the findings of Hevesy and Levi.[1] Thus the only reaction which takes place when scandium is bombarded with fast neutrons from the Be^9+H^2 reaction is that in which K^{42} is formed, namely

$$Sc^{45}+n^1\rightarrow K^{42}+He^4.$$

B. Neutrons from lithium bombarded with deuterons

Pool, Cork and Thornton[2] have recently obtained evidence for the formation of Sc^{43} and Sc^{44} from Sc^{45} when bombarded with the very energetic neutrons from the Li and H^2 reaction. During the course of the present investigation the same reactions were independently detected by the author. The results obtained are in good agreement with those reported by Pool, Cork and Thornton.

One sample which was contained in a cadmium box filled with boric oxide was irradiated for three hours close to a lithium target which was bombarded with 15 microamperes of deuterons. The scandium was separated from the lithium target by 1/4″ of brass, 1/32″ of cadmium and 1/4″ thickness of boric oxide. The sample was found to be very active and was chemically analyzed, as below.

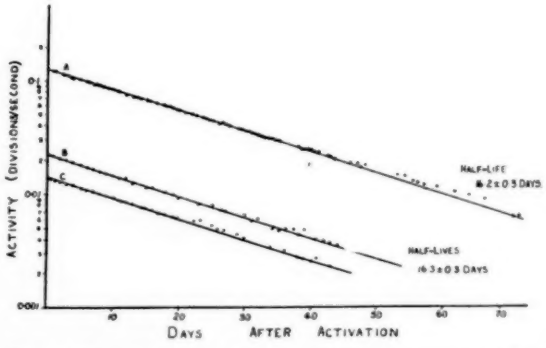

FIG. 4. Decay curves of V^{48}. *A* refers to a sample of Sc_2O_3 after activation with 0.2 microampere of 11 Mev alpha-particles for approximately three hours. *B* refers to a vanadium precipitate separated from titanium after activation with deuterons; *C*, vanadium precipitate separated chemically from Sc_2O_3 after activation with 11 Mev alpha-particles.

The Sc_2O_3 was dissolved in 6*N* HCl and a little inactive KCl, $CaCl_2$ and titanium nitrate were added. The solution was evaporated to 3 cc and 5 cc of 16*N* HNO_3 were added, the

[6] Hurst and Walke, Phys. Rev. **51**, 1033 (1937).

mixture being once more evaporated to 2–3 cc. Five cc of perchloric acid were then poured into the solution, the mixture being again evaporated to a few cc. The precipitated potassium perchlorate was filtered off and found to be weakly active. Ten cc of water were finally added to the filtrate, the solution being heated for about 15 minutes. In this way the titanium was precipitated as TiO_2. It was filtered off and found to be inactive.

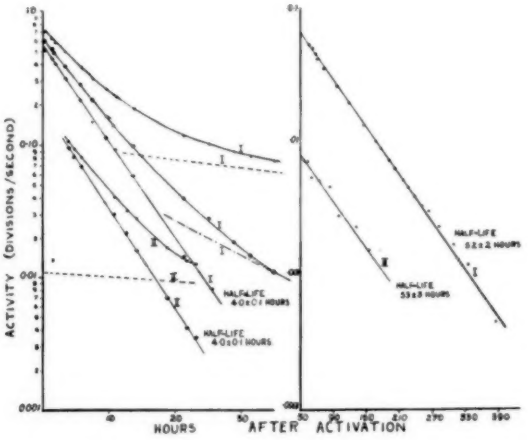

FIG. 5. Decay curves of Sc_2O_3 after irradiation with neutrons from the $Li+H^2$ reaction. The curves marked *I* refer to a spectroscopically pure sample of Sc_2O_3 which had been activated for 14 hours, the bombarding deuteron currents being 15 microamperes. This activity has been corrected for a trace of Sc^{46} formed by slow neutrons. The curves marked *II* refer to Sc_2O_3 separated chemically by the oxalate procedure from activated Sc_2O_3. The points shown by closed circles represent total activity. Those marked by open circles have been corrected for the activity due to K^{42} which is indicated by a dashed and dotted line (sample 1 only). The crosses have been corrected for the long period which is shown by dashed lines.

The scandium was then precipitated in acid solution as oxalate and filtered off. After washing it was converted to oxide by prolonged roasting at red heat. The scandium oxide was found to be very active. The particles emitted were investigated by means of a magnetic trochoid analyzer[7] and were found to be positrons. The decay of this sample showed the presence of two radioactive isotopes with half-lives of 4.0 ± 0.1 hours and 53 ± 3 hours, respectively.

In a subsequent experiment a spectroscopically pure sample of Sc_2O_3 was irradiated for about fourteen hours to intensify the long period. It was found with this sample that the longer period is 52 ± 2 hours in excellent agreement with previous results obtained by the author.[3, 6] Decay curves of these samples are shown in Fig. 5.

These results confirm the report of Pool, Cork and Thornton[2] that scandium whem bombarded with neutrons of energy 14–20 Mev can emit three neutrons as well as two neutrons. Thus we have the reactions:

$$Sc^{45}+n^1\rightarrow Sc^{43}+3n^1,$$
$$Sc^{45}+n^1\rightarrow Sc^{44}+2n^1.$$

By extrapolating to saturation it has been found that the reaction in which three neutrons are emitted is twice as probable under the conditions of these experiments as that in which two neutrons are ejected. It thus appears from these results that the Sc^{46} formed in a highly excited state by the reaction $Sc^{45}+n^1$ "evaporates" more readily three neutrons of relatively low energy than two neutrons of higher energy. This is in accord with recent views proposed by Professor Bohr.

In another experiment calcium was extracted from the active scandium oxide but it was found to be inactive. Thus the reaction

$$Sc^{45}+n^1\rightarrow Ca^{45}+H^1$$

appears to be a relatively improbable one.

ACKNOWLEDGMENTS

It is a pleasure once more for the author to record his gratitude to Professor E. O. Lawrence for continued encouragement. The author is also very grateful to Dr. W. Libby of the department of chemistry who kindly placed at his disposal several grams of the purest scandium oxide available and to Dr. Hugh C. Paxton who took the cloud chamber photographs of the electrons of Sc^{46}. The friendship and cooperation of the staff of the Radiation Laboratory is also gratefully acknowledged.

The research has been aided by grants to the laboratory from the Research Corporation, the Chemical Foundation and the Josiah Macy, Jr. Foundation.

[7] It is a pleasure to thank Mr. E. Lyman for the use of the trochoid analyzer.

A Search for Protons from Li Bombarded by Ra C′ α-Particles

W. G. SHEPHERD,* R. O. HAXBY AND E. L. HILL
Department of Physics, University of Minnesota, Minneapolis, Minnesota
(Received August 12, 1937)

A new search has been made for protons emitted from Li under bombardment by α-particles from Ra C′. The apparatus was designed to detect protons emitted between 50° and 120°. Protons were detected from the Li targets, but arguments are given supporting the idea that most, if not all of them arise from nitrogen contamination. Upper limits for the cross sections are computed for the two Li isotopes. A discussion is given of the relation of the emission of protons from Li^6 by α-particle bombardment, and of the reverse reaction, the emission of α-particles from Be^9 under proton bombardment which is known to be very prolific at low proton energies.

INTRODUCTION

A NUMBER of investigators[1] have looked unsuccessfully for protons from the reactions

$$_3Li^6+{}_2He^4\rightarrow[{}_5B^{10}]\rightarrow{}_4Be^9+{}_1H^1+Q_1, \quad (1)$$

$$_3Li^7+{}_2He^4\rightarrow[{}_5B^{11}]\rightarrow{}_4Be^{10}+{}_1H^1+Q_2. \quad (2)$$

The reverse reaction to (1); i.e.,

$$_4Be^9+{}_1H^1\rightarrow[{}_5B^{10}]\rightarrow{}_3Li^6+{}_2He^4-Q_1 \quad (3)$$

is well known at low proton energies. Its yield has been measured up to 140 kv proton energy by Allen,[2] and extended to 250 kv in this laboratory.[3] At these proton energies the yield from (3) is high, and is an exponentially increasing function of the energy, increasing by a factor of roughly 380 in the range from 100 kv to 250 kv.

A direct comparison of the yields from (1) and (3) is of considerable interest since this is almost the only reaction with charged particles which it seems feasible to reverse at the present time. Unfortunately (2) is not reversible since the Be^{10} nucleus is not known naturally.

Schintlmeister and Stetter[4] have made a careful search for protons emitted in the backward direction, using Po α-particles as a source and a double ionization chamber as detector. Their result was negative.

We have undertaken new experiments on (1) and (2) using Ra C′ α-particles and somewhat improved geometrical conditions. Consideration of the previous experiments shows that some improvement can be made in the choice of the angular range over which the protons are collected. Measurements in the forward and the right-angle directions are disadvantageous; in the first case because of the long ranges of the "natural" protons, and in the second because of the possibility of contamination with recoil aggregates if foils of low stopping-power are used.

The value of Q_1 is known from the measurements of Oliphant, Kempton and Rutherford on the range of the α-particles from (3). Because of difficulties in measuring the short ranges accurately there is some uncertainty in the exact value. We take Q_1 to be somewhere between -1.86 and -2.3 Mev. The value of Q_2 is determined from the masses[5] as ~-2.4 Mev.

EXPERIMENTAL DETAILS

Calculations on the expected proton ranges for Ra C′ α-particles indicate that the most favorable angular range for detection extends down to about 40°. The apparatus was accurately constructed to restrict the angle of collection of the protons to the range 50°–120° with respect to the direction of the incident α-particles. The minimum stopping power of 9.29 cm was sufficient to prevent the entrance of recoil protons into the ionization chamber. A schematic diagram of the apparatus is shown in Fig. 1.

The detecting chamber was a parallel-plate ionization chamber used in conjunction with a

* Now at Bell Telephone Laboratories, New York, N. Y.
[1] E. Rutherford and J. Chadwick, Proc. Phys. Soc. London **36**, 417 (1924); J. Chadwick, J. Constable and E. Pollard, Proc. Roy. Soc. **A130**, 463 (1930).
[2] J. S. Allen, Phys. Rev. **51**, 182 (1936).
[3] To be submitted for publication in the Physical Review.
[4] J. Schintlmeister and G. Stetter, Wiener Sitzungsberichte **143**, 597 (1934).
[5] M. L. Oliphant, Nature **137**, 396 (1936).

linear amplifier. The counts could be observed both on a counter and visually with a cathode-ray oscillograph. To minimize the γ-ray background, the ionization chamber was constructed of aluminum and was shielded with lead. A magnetic field was used to prevent the entry of β-rays into the chamber.

The most feasible method of making the measurements appeared to be to compare directly the yield from Li with that from N, which is known from Haxel's work.[6] Consequently the arrangement was such that targets could be readily interchanged while readings were being made with a given source. The sources were deposited from radon on small stainless steel buttons, and were covered with a thin film of collodion to prevent the spreading of recoil aggregates into the apparatus. Our usual sources were of 15 to 50 mC in initial strength.

For a nitrogen target we used dicyandiamide ($C_2N_4H_4$) fused onto the brass target holder. For the Li target we used at times fused LiOH, but most of the runs were made with metallic Li. We encountered much difficulty in maintaining a really clean surface of metallic Li. The formation of the nitride (Li_3N) on a freshly cut surface seems to be extremely rapid under normal laboratory conditions.[7] As a fresh surface did not tarnish under Bacol (a heavy mineral oil) we tried leaving a very thin film of oil on it, but some blackening did occur during a run. We also tried putting a thin gold film on the surface, but even this did not prevent the blackening.

Experimental Results

Although the counting rate was low we did observe an increase in proton counts with the Li targets over the background count. For reasons to be detailed later we incline to the belief that these counts did not arise from the disintegration of Li, but were due rather to nitrogen contained in the film on the target. In view of this we shall not present a detailed analysis of our data here. From our observations we have, however, computed what we think are safe *upper limits* to the cross sections for reactions (1) and (2).

If we assume that all of the counts which we observed from the Li targets above background were due to the disintegration of Li, then we can compute an "average thick target" cross section

$$\sigma = Y/nR = \int_0^R \sigma_{\text{thin}}(\lambda)d\lambda/R,$$

where Y is the total yield, n the number density of nuclei, and R the range of the α-particles in the target. Even if some of the counts were due to a nitrogen impurity, the values which we get in this way will be upper limits to the true cross sections. For comparison with the cross section for nitrogen we have

$$\sigma_{\text{Li}} = \sigma_{\text{N}}(n_{\text{N}}R_{\text{N}}/n_{\text{Li}}R_{\text{Li}})(Y_{\text{Li}}/Y_{\text{N}}).$$

The protons from nitrogen arise from the reaction

$$_7N^{14} + {}_2He^4 \rightarrow [{}_9F^{18}] \rightarrow {}_8O^{17} + {}_1H^1 - 1.3 \text{ Mev}. \quad (4)$$

The dynamical conditions for (4) are similar to those for (1) and (2), although a more efficient collection of the protons from it is to be expected, due to the higher energies of the protons and the smaller dependence of their energies on the angle of emission. We have attempted to make a proper correction for this in computing the relative yields from the Li and the dicyandiamide targets.

From our measurements on the relative yields, and from Haxel's data on σ_N, which we take as 5×10^{-26} cm^2 for Ra C′ α-particles, we estimate finally that

$$\sigma_1 < 10^{-26} \text{ cm}^2 \ (\text{Li}^6), \quad \sigma_2 < 10^{-27} \text{ cm}^2 \ (\text{Li}^7).$$

σ_1 and σ_2 are the cross sections for (1) and (2) for "pure" targets of the corresponding atoms.

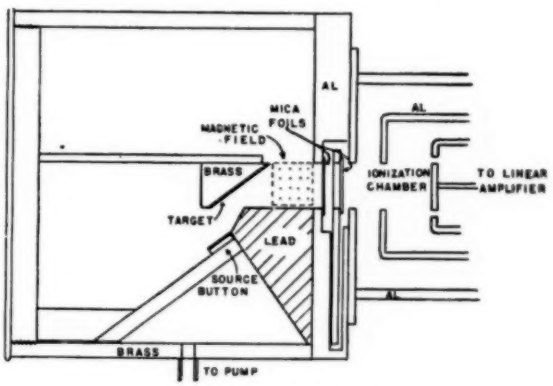

FIG. 1. Diagram of apparatus.

[6] O. Haxel, Zeits. f. Physik **93**, 400 (1935).
[7] Cf. Gmelin's *Handbuch der anorganischen Chemie*, eighth edition, Teil 20: Lithium.

From our experience it seems to us most likely that the true cross sections for (1) and (2) are much less than the upper limits given above, and we incline to the belief that most, if not all, of the counts observed with the Li targets were due to nitrogen contamination. There are several reasons for this belief:

(1) The actually observed yield from the dicyandiamide target was about 50 times that from the Li target. Hence a film of Li_3N having a thickness of 0.03 times the range of the α-particles in the dicyandiamide should be sufficient to produce the observed numbers of counts.[8]

(2) At least some of the protons from the Li targets appeared to have too long ranges to arise from the disintegration of Li nuclei. We attempted to determine numbers-range curves for the protons from both targets, but could not do so successfully for Li because of the small numbers of counts. From the dicyandiamide target the protons appeared to form a homogeneous group as expected, extending out to 25 cm, the inhomogeneity due to poor geometrical definition being marked, and extending over some 10 cm range. From the dynamical conditions of (1), (2) and (4), the protons from the last reaction should be the more penetrating. Those expected from (1) and (2) should have had ranges at most of about 18.5 cm, but so far as we were able to tell they seemed to continue with some intensity to over 22 cm.

Discussion

Coming now to a discussion of these results, their most interesting implications arise in the comparison of the data on (1) and its reverse (3). Since we have no data on the reverse of (2) we shall not discuss it further at the present time.

In the appendix we have given a brief discussion of the relation between the cross sections for reverse reactions on the basis of the principle of detailed balancing. The result is that within our accuracy, the cross sections for (1) and (3) are equal, when "corresponding" energy values are used for the two. If ϵ_α is the energy of the α-particle relative to the Li^6 nucleus, the "corresponding" energy of the proton; i.e., the kinetic energy of the proton with respect to the Be^9 nucleus is

$$\epsilon_H = 0.67\epsilon_\alpha + 1.1Q_1.$$

For α-particles from Ra C′ ($\epsilon_\alpha = 7.68$ Mev) we have $\epsilon_H = 2.9$ Mev, and for α-particles from Po ($\epsilon_\alpha = 5.3$ Mev), $\epsilon_H = 1.3$ Mev.

At 100 kv proton energy Allen[2] found for (3) a cross section of 5×10^{-29} cm². In the range from 100 to 250 kv the yield increases by about 380-fold. Making due correction for increasing penetration of the protons into the Be target, we compute a cross section of 7×10^{-27} cm² at 250 kv. Estimated conservatively, the rate of increase is 100 percent per kv at 250 kv.

Since the upper limit which we find for σ_1 corresponds to that for 3 Mev protons, we conclude from our value of $\sigma_1 < 10^{-26}$ cm² that the extremely rapid rise in σ_1 manifested at the low proton energies is not maintained, and that somewhere between 0.25 and 3 Mev the cross section for (3) rises to a maximum and then diminishes rapidly.

The results of Schintlmeister and Stetter[4] who used Po α-particles and looked for protons ejected in the backward direction (90°–160°) give added weight to this conclusion. Calculations which we have made from their data on the total yield from nitrogen give nearly the same cross section for (4) as we used above. In the case of Li they state that the yield was less than 2 protons per 10^7 α-particles. Adopting this as an upper limit we compute values for the upper limits to σ_1 and σ_2 almost identical with ours. Although this is an undoubtedly fortuitous numerical agreement it is strong evidence that the cross section for (3) has already become small for 1.3 Mev protons.[9]

In considering possible explanations for the failure to observe protons from (1) we early considered the possibility that in reaction (3) the resulting Li^6 nucleus might be left in an excited state, subsequently emitting a γ-ray, in which case considerations of reversibility become

[8] However, it should be remarked that even with our most blackened targets we did not obtain any such large increase in the counting rate as we would have expected if a thick film of Li_3N had formed.

[9] In *Tables Annuelles de Constantes et Données Numériques* Vol. 11, Curie-Joliot, Grinberg and Walen state a yield for (3) of 4×10^{-8} α-particles per proton at 0.5 Mev, while the value found in this laboratory is 5×10^{-7} at 0.25 Mev. If this is correct it means that the cross section for (3) has already passed its maximum at 0.5 Mev proton energy. However, we have not been able to trace the origin of this value.

invalid. Accordingly a search was conducted at 250 kv for a γ-ray[10] accompanying (3), but none was found with the expected intensity. That the detecting apparatus should have been amply sensitive was shown by its success in the measurement of the γ-ray accompanying the formation of Li^7 from Li^6 by deuteron bombardment, and the γ-ray from the resonance in boron under proton bombardment.[11]

As a general type of explanation for the decrease in the cross section of (3) at the higher energies, it may be supposed that some one or more of the alternative reactions become more probable, at the expense of (3). This notion has already been employed for some other cases by Newson.[12] The most likely of these appears on general grounds to be

$$_4Be^9+{}_1H^1\rightarrow[{}_5B^{10}]\rightarrow{}_5B^9+{}_0n^1$$
$$_5B^9\rightarrow{}_4Be^9+e^+.$$

However, Schnetzler[13] and Eckardt[14] have looked for radioactivity accompanying the corresponding reaction

$$_3Li^6+{}_2He^4\rightarrow[{}_5B^{10}]\rightarrow{}_5B^9+{}_0n^1$$

without success. On the other hand the difficulties of measurement in the latter case make the results somewhat uncertain.[14a] Another possibility would be for a large increase to occur in the emission of deuterons from the reaction

$$_4Be^9+{}_1H^1\rightarrow[{}_5B^{10}]\rightarrow{}_4Be^8+{}_1D^2$$

which has almost equal probability with (3) at low proton energies.[2]

On the other hand it may be that the reaction should really be considered as an incipient resonance in spite of the fact that it appears to follow a normal Gamow curve. This would explain why the yield is high even at low proton energies and increases so rapidly, and would also give a plausible explanation for a rapid rise to a maximum followed by a sharp decrease in the cross section.

Although we do not feel that our experiments settle the question of the emission of protons from (1) and (2), we do feel, as the result of our efforts, that little further can be done in this direction until better sources of α-particles, free from γ-ray background, are available from the cyclotron, or otherwise. It would also be of special interest to push the measurement of the yield from (3) to higher proton energies. The chief difficulty in this appears to be that of separating the α-particles from the recoil protons.

We wish to express our thanks to Dr. K. Stenstrom and Dr. I. Vigness of the University Hospital, and to the department of chemistry for generous gifts of radon, as well as to Dr. Herb and his co-workers for the gift of the Li metal. We are also grateful to Professor J. H. Williams for his interest and encouragement. To Mr. Rudolph Thorness we express our thanks for his painstaking construction of apparatus.

[10] W. G. Shepherd, R. O. Haxby and J. H. Williams, Phys. Rev. **52**, 247 (1937). This agrees with the negative result of Oliphant, Kempton and Rutherford, Proc. Roy. Soc. **A150**, 241 (1935).

[11] There is a bare possibility that the value used for Q_1 may be sufficiently inaccurate to make the search for protons uncertain. This does not seem likely since the α-particles from (3) have been studied independently by Oliphant, Kempton and Rutherford and by Allen with substantially equivalent results. The worst value of Q_1 (for our purposes) which has been suggested is -2.3 Mev. With this value we believe that we should have been able to detect the protons if the yield had been sufficient.

[12] H. W. Newson, Phys. Rev. **51**, 620 (1937).

[13] K. Schnetzler, Zeits. f. Physik **95**, 302 (1935).

[14] A. Eckardt, Ann. d. Physik (5) **29**, 497 (1937).

[14a] It is probable that radioactivity could not be detected from this reaction with Po α-particles, since with the present mass of the neutron it should begin only when the corresponding energy of the proton is about 2 Mev with respect to the Be nucleus. For this reason also it could not be invoked to explain a diminishing cross section for (3) below 2 Mev proton energy.

Appendix

The relation between the cross sections for reversed reactions

We shall not attempt a fundamental treatment here, but shall content ourselves with a simple extension of the usual application of the principle of detailed balancing to collisions of the second kind. The most significant change comes from the circumstance that when coordinates are taken at the center of mass of the system, the reduced mass is altered by a finite amount during the course of the reaction.

Confining our attention specifically to (1) and (3) we define the state of each of the four "particles" by the coordinates and momenta of its center of mass, and by a set of quantum numbers which describe the internal states and the spin vector. In the following we consider only a given type of accurately defined collision in which the

initial and final states of the reactants are uniquely given. Following the usual arguments for collisions of the second kind between complex systems[15] we find as the condition for detailed balancing

$$(\mu_+)^{\frac{1}{2}}(v_\alpha)^2\sigma_+(v_\alpha)=(\mu_-)^{\frac{1}{2}}(v_H)^2\sigma_-(v_H)$$

where the subscripts + and − refer to the reaction (1) going from left to right and from right to left, respectively. v_α and v_H are the relative velocities of the α-particle and Li nucleus, and of the proton and Be nucleus, respectively, while

$$\mu_+=m_\alpha m_{Li}/(m_\alpha+m_{Li});\qquad \mu_-=m_H m_{Be}/(m_H+m_{Be}).$$

Hence we get

$$\sigma_+(\epsilon_\alpha)/\sigma_-(\epsilon_H)=(m_\alpha m_{Be}/m_H m_{Li})^{\frac{1}{2}}(\epsilon_H/\epsilon_\alpha),$$

where ϵ_α and ϵ_H are the corresponding energies of the α-particle and proton with respect to their partner nuclei. For Ra C′ α-particles

$$\epsilon_\alpha\sim 7.7 \text{ Mev},\qquad \epsilon_H\sim 3 \text{ Mev},$$

so that

$$\sigma_+/\sigma_-\approx 0.95.$$

For Po α-particles $\epsilon_\alpha\sim 5.3$ Mev, $\epsilon_H\sim 1.3$ Mev

$$\sigma_+/\sigma_-\approx 0.6.$$

Within the accuracy of our measurements we can accordingly treat the cross sections for (1) and (3) as equal *for corresponding energies on the two sides.*

In the experiments as performed the conditions are not those of complete reversibility as required in this formulation. In performing (1) the Li nucleus is initially effectively at rest and the α-particle incident from a particular direction with a given energy while the final products are both in motion, only the direction of motion of the collected protons being determined by the construction of the apparatus. In performing (3) the Be nuclei are at rest and the ejected α-particles measured in some other specified direction. To complete the conditions for reversibility we must first make the *relative* velocities of the reactants the same in (1) and (3). This has been considered as stated in the text. Second, the different characteristics of the two sets of apparatus with respect to the angles at which particles are collected must be considered. It is conceivable that the angular distribution of the final products from (1) or (3) might be marked, and might depend on the energy of the incident α-particle or proton. We have assumed that this is not the case. Since in our experiments combined with those of Shintlmeister and Stetter the range from 40° to 160° has been covered for (1), while the measurements on (3) have been made at 90°, this seems to be a fairly safe assumption. It hardly seems likely that the disintegration products would concentrate appreciably in the forward direction.

[15] Cf. e.g., Fowler, *Statistical Mechanics*, second edition, p. 683.

OCTOBER 1, 1937 PHYSICAL REVIEW VOLUME 52

The Scattering of Protons by Neutrons*

P. GERALD KRUGER, W. E. SHOUPP AND F. W. STALLMANN
Department of Physics, University of Illinois, Urbana, Illinois

(Received July 13, 1937)

The scattering of neutrons by protons has been investigated by observing recoil proton tracks with a liquid-filled cloud chamber. The neutrons used were produced by bombarding frozen heavy water with 1 Mev deuterons from a small cyclotron. The tracks of 870 recoil protons have been measured. Of these tracks 635 satisfied our length selection criteria and are used as the basis of the calculations. Random track, area, and azimuthal correction factors are calculated and applied. The final curve indicates that the scattering for the energy of neutrons used in this experiment is approximately spherically symmetrical about the center of gravity. This is in agreement with the current theory.

THE success of the neutron-proton model in explaining many of the phenomena in nuclear physics, attaches a great significance to the law of force between these fundamental particles. Since it is not possible to measure the force between the neutron and the proton directly, one must infer the law of force from the way it manifests itself in various physical experiments. One of the most cogent experiments apposite to the determination of the law of force between the neutron and the proton is the study of the angular distribution of the recoil protons produced when a substance, rich in hydrogen, is bombarded with neutrons.

Several investigators[1–5] have examined the

* A preliminary report of these data was given at the Washington meeting of the American Physical Society, April 1937; Kruger, Shoupp and Stallmann, Phys. Rev. **51**, 1021A (1937).

[1] Monod-Herzen, J. de phys. et rad., Feb. (1934).
[2] Meitner and Philipp, Zeits. f. Physik **87**, 484 (1934).
[3] Kurie, Phys. Rev. **44**, 461 (1933).
[4] Harkins, Kamen, Newson and Gans, Phys. Rev. **50**, 980 (1936).
[5] Lampson, Mueller and Barton, Phys. Rev. **51**, 1021A (1937).

scattering of protons by neutrons but their results are contradictory. None of them except Lampson[5] used neutrons of homogeneous energy and most of them have studied so few tracks that their results are subject to large statistical fluctuations. These difficulties together with uncertain geometrical factors make the interpretation of their results difficult.

The neutrons used in the experiment discussed in this paper were produced by bombarding a target of frozen heavy water with 1 Mev deuterons from a small cyclotron.[6] The target chamber was sealed on the end of the beam exit tube. This allowed the cloud chamber, in which the recoil protons were stereoscopically photographed, to be placed 41 cm from the ice target and at right angles to the direction of the incident deuteron beam. Thick paraffin blocks were placed near the cyclotron vacuum chamber to prevent high energy neutrons originating from places other than the ice target from entering the cloud chamber. The effectiveness of this screening is seen from the fact that only one recoil proton track per five pictures was observed when the deuteron beam did not strike the ice target. With the deuteron beam incident on the target as high as ten tracks per picture were observed.

The liquid-filled (four part ethyl alcohol and one part water) cloud chamber is sylphon actuated, and is 13 cm in diameter with a usable depth of 3.2 cm. A light beam from four 100-volt movie projector bulbs illuminated the usable portion. For this experiment the chamber was filled with methane to a pressure of 102 cm of Hg, the pressure variation during an expansion being ± 14 cm of Hg. The methane gave many more tracks per picture than hydrogen which was tried also.

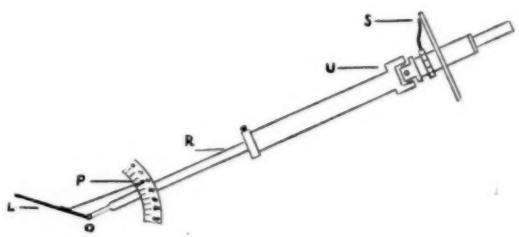

FIG. 1. Measuring engine to measure ϕ and θ.

[6] Kruger and Green, Phys. Rev. **51**, 699 (1937).

Stereoscopic photographs of the tracks were taken by means of a Sept camera chassis equipped with a f 1.9 lens and two vertical mirrors each arranged so that it gives an image of slightly more than half of the chamber nearest it. The central light beam is allowed to go through the lens also and when the images are reprojected they redefine the object at its original position.

The scattering angle, ϕ, is the angle between the forward direction of the incident neutron and the direction of the recoil proton, and the azimuthal angle, θ, is the angle between a horizontal line lying in a plane perpendicular to the direction of the incident neutron and through the origin of the track, and the projection of the recoil proton track onto this plane. The angles ϕ and θ for 870 recoil proton tracks have been measured. Of these tracks 635 met the selection requirements discussed below and after multiplication by the total correction factor represent an effective 1163 tracks.

The track images were reprojected through the same stereoscopic camera used to photograph them, and were viewed on a translucent onion skin paper screen so that it was easy to get the stereoscopic images in coincidence. The measurements of ϕ and θ can be described best with the use of Fig. 1. It shows the side view of the measuring engine used. The center of the universal joint U was placed at the position of the neutron source. The sliding square rod R makes it possible to match the point O with the origin of the track without rotation. Then the thin rod L is placed in coincidence with the reprojected track and ϕ read on scale P, θ on scale S. The length of the track was measured with a small scale to $\pm 1/16$ inch ($\leqq 1.5$ mm). It was found that the measurement of ϕ could be reproduced to $\pm 1°$ and θ to $\pm 4°$ on average sharp tracks.

ANALYSIS OF DATA

In the analysis of these data it is necessary to consider only the recoil proton tracks caused by neutrons which have sufficient momentum to have come directly from the target. Due to the variation of pressure in the cloud chamber during an expansion ($\Delta P = \pm 14$ cm of Hg), the energy variation in the neutron beam caused by

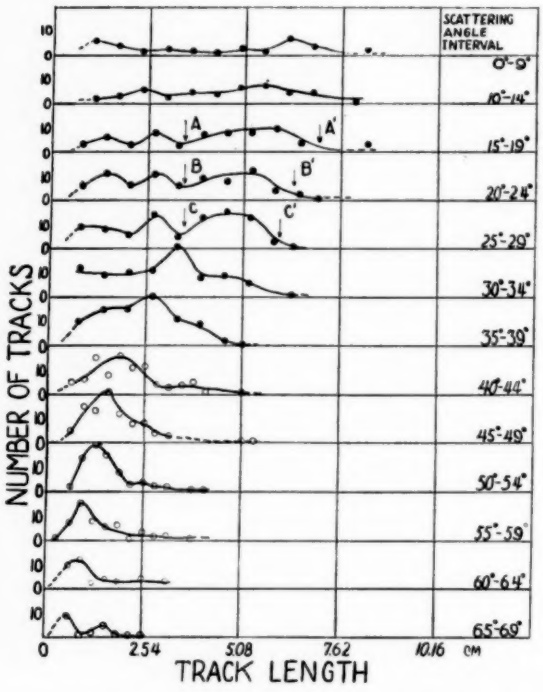

FIG. 2. Number of tracks *vs.* length of track for various scattering angle intervals. All tracks used.

a thick ice target ($\Delta E = 0.25$ Mev), and the finite scattering angle interval (5°) used (except 0°–9°), the tracks of recoil protons may have various lengths in a given scattering angle interval. For this reason it is necessary to set up a criterion for selecting the tracks of allowable length in any scattering angle interval. This is done with the aid of the graphs in Fig. 2, in which the number of tracks *vs.* track length is plotted for all scattering angle intervals. In the intervals (15°–19°), (20°–24°), and (25°–29°) the main groups of tracks fall between points AA', BB', and CC'. The lengths corresponding to A and A' are taken from the graph and with the use of the approximate relation $R = A V_0^3 \cos^3 \phi$, where R is the range of the proton and V_0 is the velocity of a proton scattered at $\phi = 0°$, the maximum and minimum allowable track length for all $\Delta\phi$'s are calculated. This procedure is repeated for the points BB' and CC' and the three sets of upper and lower limits to the track lengths thus obtained are averaged to obtain the maximum and minimum track lengths which are used to make the length selection. The results of these calculations (with ±1.6 mm to take care of estimated error in measurement of track length) are given in Table I.

By using the maximum track length for a proton at $\phi = 0°$ as given in Table I, the stopping power of the gas and vapors in the cloud chamber, and the range-energy curve for protons,[7] it is possible to calculate the maximum energy of our neutrons. This yields 2.49±0.1 Mev. Due to the thick ice target used 0.25 Mev must be subtracted from this value to get the energy of the neutrons which have received no energy from the bombarding deuterons. This gives 2.24±0.1 Mev which is to be compared with Bonner and Brubaker's[8] value of $2.55 - 0.12 = 2.43 \pm 0.1$ Mev. The agreement is good and substantiates our method of making the track length selection.

A clock diagram showing the azimuthal angle distribution of the tracks selected according to the above criteria is shown in Fig. 3. Here each track is plotted at its observed angle of scattering and azimuth. By counting the number of tracks occurring in $\Delta\phi = 0°$–9° and $\Delta\theta = 0°$–19°, 20°–39°, etc. (also $\Delta\theta = 15°$–24°, etc.) in Fig. 3, the curves in Fig. 4 are constructed. These curves are smoothed by averaging the number of tracks in a given $\Delta\phi$ and $\Delta\theta$ in all four quadrants of the azimuthal plane. (For example, in $\Delta\phi = 30°$–34°, average the tracks in $\Delta\theta = 50°$–59°, 120°–129°, 230°–239° and 300°–309°.) This is allowable since the symmetry of the geometrical arrangement of the chamber and the light beam

TABLE I. *Maximum and minimum track length allowed in each scattering angle interval.*

SCATTERING ANGLE INTERVAL	MAXIMUM TRACK LENGTH	MINIMUM TRACK LENGTH
0°–9°	8.40cm	4.10cm
10°–14°	8.10	3.95
15°–19°	7.60	3.65
20°–24°	7.00	3.20
25°–29°	6.35	2.85
30°–34°	5.55	2.40
35°–39°	4.60	1.90
40°–44°	3.80	1.40
45°–49°	3.00	1.10
50°–54°	2.40	0.80
55°–59°	1.75	0.50
60°–64°	1.25	0.25
65°–69°	0.80	0.05

[7] Private communication from Livingston and Bethe.
[8] Bonner and Brubaker, Phys. Rev. **49**, 19 (1936).

will entail the same loss of tracks in all four quadrants.

If the limited height of light beam did not prevent the observation of tracks in certain $\Delta\phi$'s and $\Delta\theta$'s the curves in Fig. 4 should be horizontal straight lines. The fact that they are not straight lines means that the selected data must be corrected so as to account for the impossibility of observing all of the scattered protons. The proper correction factor can be obtained from the curves in Fig. 4 by getting the ratio, A/A', of the area under the straight line to the area under the curve in each scattering angle interval. The results are shown in Table II.

The geometrical azimuthal angle correction factors were computed by numerical integration in the following way. The divergence of the neutron beam was taken into account only along the direction of the depth of the chamber. The origins of all tracks were referred to the segment of the vertical central axis of the chamber which is illuminated by the light beam, and which is observed to be about 3.2 cm long. The geometrical correction factor is defined as the ratio of the total solid angle to the usable solid angle in a given $\Delta\phi$. Thus the correction factor

$$C_{\text{ave}}=\int_0^h \frac{C_h dh}{32},$$

where

$$C_h=\frac{2\pi(\cos\phi_1-\cos\phi_2)}{2\int_{\phi_1}^{\phi_2}\int_{\theta=0}^{\theta_1}\sin\phi d\phi d\theta+2\int_{\phi_1}^{\phi_2}\int_{\theta=0}^{\theta_2}\sin\phi d\phi d\theta}=\frac{\pi(\cos\phi_1-\cos\phi_2)}{\int_{\phi_1}^{\phi_2}(\theta_1+\theta_2)\sin\phi d\phi}$$

and where

$$\theta_1=\sin^{-1}(h/R\sin\phi),$$
$$\theta_2=\sin^{-1}[(32-h)/R\sin\phi)],$$

h is the distance of the origin of a track from the top of the light beam, and R is the minimum track length in the $\Delta\phi$ interval under consideration. The minimum ranges were used because all tracks whose lengths are greater than the minimum have been included in the selected data, while those under the minimum length, though they may have gone partly out of the light beam, have been discarded. In evaluating

$$\int_{\phi_1}^{\phi_2}\sin^{-1}\left(\frac{h}{R\sin\phi}\right)\sin\phi d\phi$$

by numerical integration according to Simpson's rule one degree $\Delta\phi$ subintervals are used and C_h is calculated for each $\Delta\phi=2°$ and for each $h=0$, 2, 4, $\cdots$ 32 mm. Then C_{ave} is the integral mean of C_h over the depth of the light beam. The results of these calculations are given in Table II also.

Figure 5 shows a plot of the data in Table II, and a composite curve made up partly from

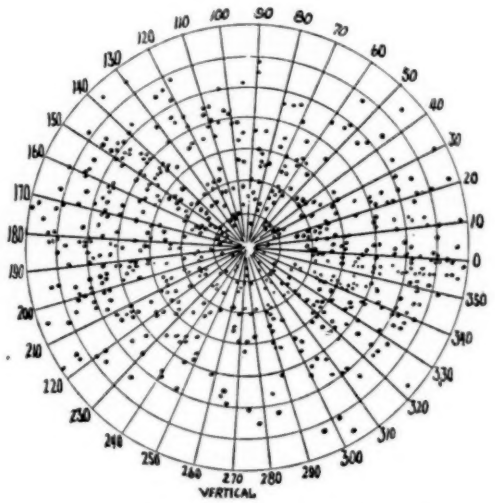

FIG. 3. Clock diagram: The scattering angle ϕ is the radial variable and the azimuthal angle is the angle variable.

TABLE II. *Graphically and geometrically calculated azimuthal angle correction factors.*

Scattering Angle Interval	Correction Factor From Curve Fig. 4 $R=A/A'$	Geometrically Calculated Correction Factor
0°–9°	1.00	1.15
10°–19°	1.00	1.34
20°–29°	1.41	1.43
30°–39°	1.94	1.42
40°–49°	1.76	1.32
50°–59°	2.53	1.14
60°–69°	3.22	1.08

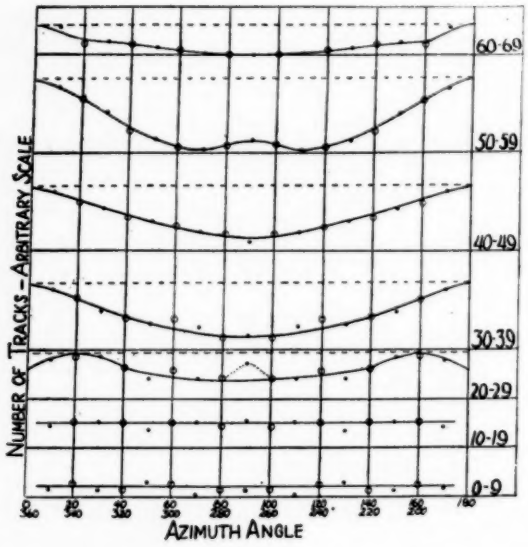

FIG. 4. Number of tracks *vs.* azimuthal angle for each scattering angle.

calculated points and partly from graphical points. The azimuthal correction factors used to correct our data are taken from the solid curve. This procedure is justified because the geometrically calculated points are more accurate than the experimentally determined correction factors at small $\phi(0°–20°)$, whereas the converse is true at large ϕ. At small ϕ so few tracks are observed that statistical fluctuations are large and the shape of the curves in Fig. 4 ($\phi=0°–20°$) are not accurately known. At large ϕ (50°–70°) it is hard to measure the short tracks occurring in the azimuthal regions 60°–120° and 240° to 300°. It is likely that we have failed to measure a large number of tracks in these regions and that that accounts for the large correction factor, and large deviation from the geometrical correction factor at large ϕ. Final azimuthal correction factors are tabulated in Table III.

Though we consider the solid curve in Fig. 5 to represent the best azimuthal correction factors, in treating the final data (Table IV and Fig. 7) all three types of azimuthal correction factors have been tried to see how they affect the result. When the geometrical factors are used the curve representing the completely corrected data has the same general shape as curve B in Fig. 7 but falls farther below the cosine curve (A) at large ϕ. When using the experimentally determined

TABLE III. *Correction factors*

Scattering Angle Interval	Random Factor	Area Factor	Azimuthal Factor	Total Factor
0°–9°		1.45	1.15	1.67
10°–14°		1.48	1.30	1.92
15°–19°		1.41	1.35	1.90
20°–24°		1.28	1.43	1.83
25°–29°		1.28	1.50	1.92
30°–34°	1.00	1.21	1.70	2.06
35°–39°	0.97	1.11	1.90	2.04
40°–44°	0.87		2.00	1.73
45°–49°	0.81		2.15	1.73
50°–54°	0.77		2.40	1.85
55°–59°	0.70		2.70	1.88
60°–64°	0.71		3.05	2.17
65°–69°	0.85		3.35	2.84

factors, the peak in the curve B at $\phi=15°$ is accentuated and moved to $\phi=25°$.

From the curves in Fig. 2 it is obvious that a correction for random tracks is necessary. From the data represented by Fig. 2, and the allowable track lengths in Table I, one can tabulate the number of random tracks in each scattering angle interval and for each range variation. These must be corrected for azimuthal angle and reduced to the average number of tracks per unit solid angle per scattering angle interval. From this one can calculate the average number of random tracks to be expected in each range interval and the appropriate correction factor which is given in Table III.

It is necessary to make an area correction also. This is due to the fact that a part of the area of the cloud chamber (represented by crosshatched section of Fig. 6) will not record the total length of all tracks occurring at small ϕ. Since no tracks are counted if they originate closer to the wall of the cloud chamber than one-half inch, except in region C of Fig. 6, the correction factor is given by the ratio $(A+B+C)/(B+C)$, where A is the

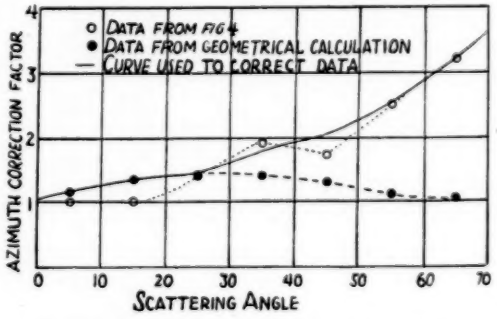

FIG. 5. Azimuthal angle correction curves.

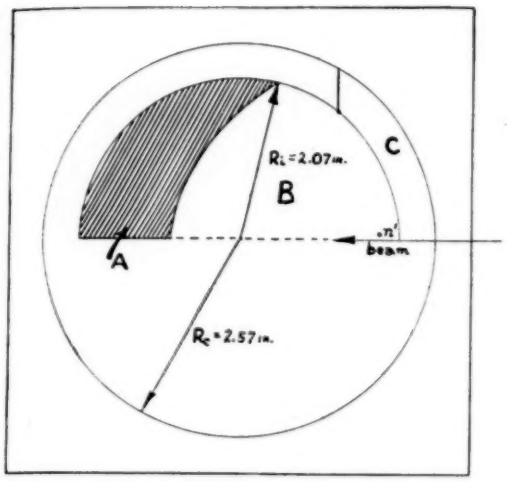

FIG. 6. Area correction.

cross hatched section of Fig. 6, $A+B$ is the half-area of the region of the cloud chamber where $R_i=$ 2.07 inches, and C is the region in the one-half inch ring where tracks were counted. The cross hatched section is determined as follows. For a given scattering angle interval (i.e., $\Delta\phi=0°$–$9°$) and the effective average minimum track length for this interval (slightly smaller than those given in Table I), points are laid out on several lines making an angle of 9° with the diameter of the chamber, and at a distance from the chamber wall equal to the effective average minimum track length. The area enclosed by a curve connecting these points and the inner circle ($R_i=R_c-\frac{1}{2}$ inch) is the crosshatched area and represents the area of the cloud chamber in which tracks having a length greater than the average minimum track length for the interval $\Delta\phi$, will hit the chamber wall and will not be counted in the length selected data because they are too short. This results in the above definition of the area correction factor. The results of repeating this process for each $\Delta\phi$ are tabulated in Table III.

Table IV gives the number of selected tracks in each scattering angle interval, the corresponding number of tracks when corrected by the correction factors in Table III, the number of tracks in each scattering angle interval when grouped in 10° intervals, the solid angle correction factors, the number of tracks per unit solid angle times a constant C, and the percent of the total number of tracks which occur in a $\Delta\phi=10°$. At the right of the table, the subintervals $\Delta\phi=5°$ have been regrouped into $\Delta\phi=10°$ intervals which overlap the first groups by $\pm5°$. This is done to smooth the statistical fluctuations and obtain a better curve (B) in Fig. 7.

TABLE IV. *Data on selected tracks. ϕ denotes the scattering angle interval, N the number of selected tracks, C_T the total correction factor, N_c the number of tracks after correction, $N_c/10°$ the total number of corrected tracks in 10° intervals, $\Delta\cos\phi$ the solid angle correction factor ($\cos\phi_1-\cos\phi_2$), Q the number of tracks per unit solid angle times a constant C, and P the percent number of tracks per ten degree ($\Delta\phi$) per unit solid angle. $N_c/10°$*, $\Delta\cos\phi$*, Q* and P* represent the corresponding data for the regrouped 10° intervals.*

ϕ	N	C_T	N_c	$N_c/10°$	$\Delta\cos\varphi$	Q	P	$N_c/10°$*	$\Delta\cos\varphi$*	Q*	P*
0°–9°	29	1.67	49	49	0.015	3260	20.2±3.9				
10°–14°	32	1.92	61								
				158	.045	3510	21.6±2.4				
15°–19°	51	1.90	97								
								190	0.060	3170	19.6±1.9
20°–24°	51	1.83	93								
				224	.074	3030	18.7±1.6				
25°–29°	68	1.92	131								
								240	.087	2760	17.1±1.6
30°–34°	53	2.06	109								
				254	.100	2540	15.7±1.5				
35°–39°	71	2.04	145								
								259	.112	2310	14.3±1.2
40°–44°	66	1.73	114								
				239	.123	1930	11.9±1.2				
45°–49°	72	1.73	125								
								227	.133	1710	10.6±1.0
50°–54°	55	1.85	102								
				189	.143	1320	8.2±0.8				
55°–59°	46	1.88	87								
								143	.151	950	5.9±0.8
60°–64°	26	2.17	56								
				93	.158	590	3.7±0.6				
65°–69°	13	2.84	37								

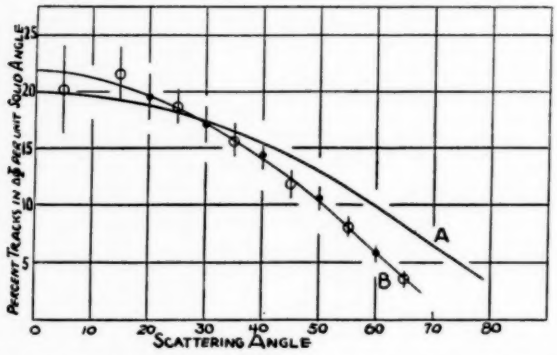

FIG. 7. Final data: Percent number of tracks per $\Delta\phi$ per unit solid angle.

The open circles on curve B of Fig. 7 represent the data in column 8 of Table IV. The full circles represent the points obtained by regrouping the $\Delta\phi = 5°$ intervals. The limits of probable statistical fluctuations as calculated from the number of selected tracks in column 2 of Table IV, are given by the vertical lines through the points on curve B.

Bethe and Bacher,[9] and Morse, Fisk and Schiff[10] have concluded that, under their assumptions and for the energy of neutrons used in this experiment, the scattering should be S scattering. Consequently curve B of Fig. 7 should be a cosine curve (A) if our data were in complete agreement with the current theory. That curve B is nearly a cosine curve means that the scattering must be essentially S scattering. The suggestion of a small peak at $\phi = 15°$ is probably due to statistical fluctuations. On the other hand, the greater than cosine slope of curve B at large ϕ seems to be real since curve B falls farther below the cosine curve A than our probable statistical fluctuations allow. In spite of this the apparent deviation may not be real and more data are necessary to decide that point. If further experimentation does support the reality of the deviation, it does not necessarily lead to a difficulty, for it appears that under less simple assumptions than those used in the current theory, deviations from S scattering can be explained.[11]

At present it seems sufficient to say that curve B Fig. 7 surely cannot be concave, as would be necessary if these data agreed with those of Kurie,[3] Harkins *et al.*[4] Fig. 8 shows how much different our data are from their data.

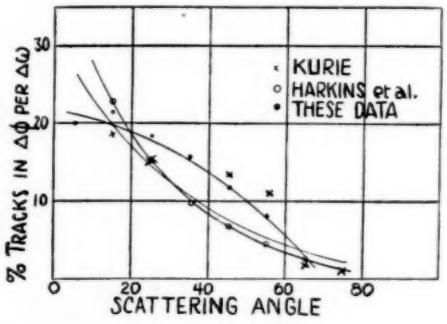

FIG. 8. Comparison of these data with those from other investigators.

The authors wish to express their thanks to R. E. Watson for his help in measuring tracks and making part of the calculations. One of us (P. G. K.) also wishes to acknowledge a grant-in-aid from the National Research Council and generous support from the Graduate School Research Board of the University of Illinois.

[9] Bethe and Bacher, Rev. Mod. Phys. **8**, 82 (1936).
[10] Morse, Fisk and Schiff, Phys. Rev. **51**, 706 (1937).
[11] Bartlett, Phys. Rev. **51**, 889L (1937). At the time Professor Bartlett made these comments the authors had not made azimuthal angle corrections. Thus our communication to him was based on incomplete and preliminary data so that his remarks no longer apply specifically to the data in this paper.

Neutron-Proton Scattering and the Disintegration of Deuterium by Deuterons

T. W. BONNER
Rice Institute, Houston, Texas
(Received July 31, 1937)

The angular distribution of the scattering of neutrons by protons has been observed by the method of recoil protons in a cloud chamber. The source of neutrons was the reaction $_1H^2+{}_1H^2 \rightarrow {}_2He^3+{}_0n^1+Q_1$ which gave 2.6 Mev neutrons at right angles to the bombarding deuterons. The value of Q_1 was found to be 3.36 ± 0.20 Mev. The recoil proton distribution showed a maximum at 45° as measured in laboratory coordinates. The distribution agreed with the theoretical one which predicts a spherical symmetry with respect to the center of mass of the moving system.

THE angular distribution of the neutrons scattered by protons is of fundamental significance since such a distribution will tell us whether the present ideas of neutron-proton interaction are correct. Numerous experiments[1] have been carried out to determine this angular distribution. Experimentally there are two different methods of attack. The first method is the observation of the scattered neutrons and the second method is the observation of the recoil-protons projected by the neutrons. At present the second method of observing the angular distribution of the recoil protons (usually observed in a cloud chamber) seems capable of greater precision than the first method. Of course the same information would be obtained by either method, since the distribution of the scattered neutrons is uniquely determined by the distribution of recoil protons.[2]

Many experiments on the angular distribution of recoil-protons (from neutrons) have been carried out with highly contradictory results.[1] The interpretation of most of the earlier results has been complicated by two factors. First, neutrons of widely differing energies have usually been employed and, second, much scattering material has been present near the neutron source and cloud chamber. For the latter reason many of the neutrons did not come directly from the source.

In view of the difficulties inherent in the earlier results, the present experiment was undertaken for the purpose of obtaining data under better experimental conditions. The source of neutrons was the nuclear reaction

$$_1H^2+{}_1H^2 \rightarrow {}_2He^3+{}_0n^1+Q_1. \qquad (1)$$

This reaction is known to give neutrons which have an energy of about 2.5 Mev.

Experimental Arrangement

The experimental arrangement for the production of neutrons is shown in Fig. 1. The source of potential was a 200 kv kenetron rectifier doubler circuit of the Cockcroft and Walton type. The ion source was a filament controlled low voltage arc. It was similar in design to one described by Crane.[3] The ion source was operated in synchronism with the cloud chamber so that ions only came down the tube at the time of expansion of the chamber. With such an arrangement a total ion current of 200 microamperes reached the deuterium target. The ion spot on the target was less than a cm in diameter.

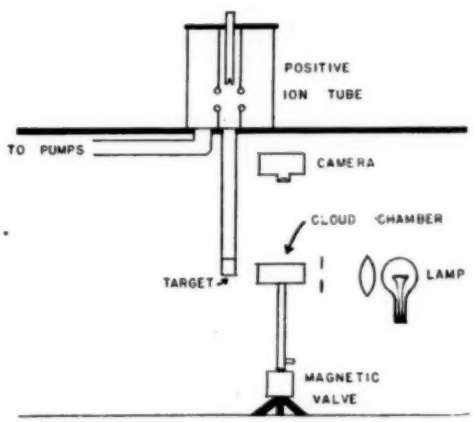

FIG. 1. Diagram of apparatus.

[1] Kurie, Phys. Rev. **44**, 463 (1933); Monod-Hertzen, J. de phys. **5**, 95 (1934); Meitner and Philipp, Zeits. f. Physik **87**, 484 (1934); N. Dobrotin, Comptes rendus de L'Acad. des Sci. U. S. S. R. **4**, 179 (1934); Harkins, Kamen, Newson and Gans, Phys. Rev. **50**, 980 (1936); Kruger, Schoupp and Stallman, Bull. Am. Phys. Soc. April (1937); Lampson, Mueller and Barton, Bull. Am. Phys. Soc. April (1937).

[2] Assuming the conservation of energy and momentum in the collision.

[3] H. R. Crane, Phys. Rev. **52**, 11 (1937).

Since it was only important to get as large a yield of neutrons as possible, no magnetic analysis was made on the ion beam. The deuterium target was made from a mixture of P_2O_5 and heavy water. This target was placed in a thin brass cup at the end of the ion tube. When such a target was bombarded continuously by large ion currents, it lasted only a short time. However, phosphoric acid targets lasted for a much longer period when the current was flashed only during the sensitive time of the chamber.

The cloud chamber, which was used to observe the recoil protons, was of the rubber diaphragm type. All the parts of the chamber were made as light as possible to reduce neutron scattering by such material. The electromagnetic valve, which was opened to produce the expansion, was 80 cm below the cloud chamber. The chamber was 17 cm in diameter and 4.5 cm deep. The distance from the ion spot to the center of the chamber was 18.5 cm. The cloud chamber was filled with a mixture of CH_4 and C_2H_6 at an expanded pressure of 1.1 atmospheres. The stopping power of the gas mixture was determined by using the alpha-particles from polonium as a standard.

Results

One thousand stereoscopic pairs of pictures were taken when the tube was operated at a potential of 100 kv; on these pictures 303 recoil proton tracks were measured. This measurement included the track length and the angle of projection of the recoil proton assuming that the neutron came directly from the ion spot on the deuterium target. The probable errors in the measurements were approximately 1 mm in track length and 5° in the angle of projection.

Calculation of the Energy of the Neutrons

The energy of the neutrons can be determined in two different ways. One method is to calculate the energy of the neutron from the relation $E_H = E_N \cos^2 \phi$, where E_H is the proton energy, E_N the neutron energy, and ϕ the angle of projection of the proton. Another and more reliable method is to use only those tracks which are in nearly the forward direction and to make no correction for the $\cos^2 \phi$ factor. When ϕ is small the value of $\cos^2 \phi$ is nearly unity so the recoil protons have essentially the energy of the primary neutrons. Fig. 2 gives the distribution with energy of the recoil protons in the forward direction (0−21°). This curve indicates a neutron group with an energy of 2.60±0.15 Mev which is approximately the result obtained in the experiments of Bonner and Brubaker.[4] There is also some indication of a weaker group at about 1 Mev. However, further work will have to be done in order to be certain whether these low energy neutrons come from reaction (1) in which the He^3 nucleus is left in an excited level of about 2 Mev.

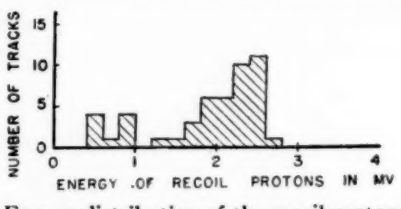

Fig. 2. Energy distribution of the recoil protons in the forward direction (0°–21°).

The energy of disintegration Q_1 can be calculated from the neutron energy of 2.60±0.15 Mev observed at an angle of 90°±10° to the direction of the 100 kv deuterons. This value of $Q_1 = 3.36 \pm 0.20$ is a little greater than that given by Bonner and Brubaker. However, it is believed that the new value is more reliable since the stopping power of the gas was determined with polonium alpha-particles.[5]

Figure 3 gives the calculated energy distribution of the neutrons when all the tracks were used and corrected for the $\cos^2 \phi$ term. There is a maximum in the curve at 2.5 Mev. There are also neutrons with calculated energies extending far beyond the known end point. This of course is to be expected because of the errors in determination of ϕ[6] and because of a few recoil protons from "scattered neutrons." Although such a method is obviously not reliable for getting neutron energies, it does indicate that there are some low energy neutrons present. This conclusion is inferred from the fact that there are

[4] Bonner and Brubaker, Phys. Rev. **49**, 19 (1936).

[5] A correction of three percent was applied for the difference in stopping power of the gas for particles of 10 cm and 3.8 cm range.

[6] If an error is made in the determination of ϕ for a recoil proton, the calculated neutron energy will have a larger error the greater the value of ϕ. For example, if the angle of projection of a proton recoiling from a 2.6 Mev neutron were measured as 60°, but actually was 50°, the calculated energy of the neutron would be 4.3 Mev.

more calculated neutron energies less than 2.5 Mev than with greater energies.

The disintegration energy of reaction (1) together with reaction

$$_1H^2+{}_1H^2\rightarrow{}_1H^3+{}_1H^1+Q_2 \qquad (2)$$

gives an experimental method for getting the difference between the binding energies of He^3 and H^3. This difference is equal to Q_2-Q_1. If neutron-neutron forces are equal to proton-proton forces, then the difference in the binding energies of He^3 and H^3 should alone be due to the Coulomb repulsion between the two protons in He^3. Bethe[7] has shown that the experimental values of Q_1 and Q_2 are consistent with this viewpoint.

The value of Q_2 has been accurately determined by Oliphant, Kempton, and Rutherford,[8] and is 3.97 ± 0.02 Mev. If the new value of Q_1 is used, the difference between Q_2 and Q_1 is 0.61 Mev instead of 0.76 Mev. This is very nearly the expected value of the Coulomb factor as given by recent theoretical calculations.[9]

Angular Distribution of the Recoil Protons

The angular distribution of the recoil-protons is shown in Fig. 4. The data are plotted in two ways. The open circles represent the distribution with angle of all the measured tracks. Such a distribution should be the correct one if all the neutrons which traversed the chamber came directly from the source and if all recoil protons were observable independent of the angle of projection. With the present experimental arrangement, protons projected by 2.6 Mev

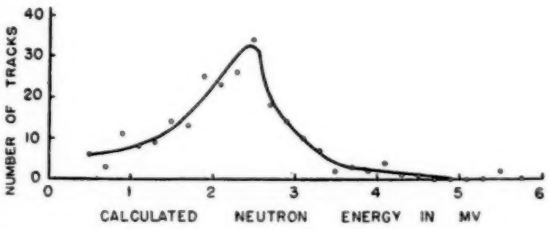

Fig. 3. Distribution of calculated neutron energies.

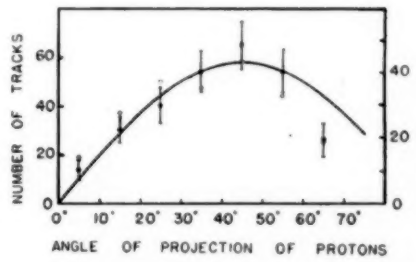

Fig. 4. Angular distribution of the recoil proton tracks. Ordinates on the left side of the graph refer to the open circles; these include all measured tracks. Ordinates on the right refer to the closed circles; these include only those tracks which satisfy the momentum conditions.

neutrons at an angle of 70° would have a track length of 0.5 cm and so would usually be distinguishable. Tracks shorter than this would generally have been missed. Lower energy neutrons, whose presence is indicated, would not have been observable at large angles and so would distort the curve toward the small angles. All the observed tracks were not used because of the low energy neutrons and also because a few neutrons did not come directly from the source (of the order of 5 percent). All tracks were rejected which were not consistent with a 2.6 Mev neutron energy assuming a possible error of as much as 10° in ϕ and one mm in track length.[10] Ninety-six of the observed tracks were rejected for this reason.

The corrected distribution of the recoil protons is given in Fig. 4. The smooth curve of Fig. 4 gives the theoretical distribution of the recoil protons in laboratory coordinates. This corresponds to a spherical symmetry with respect to the center of mass of the moving system. Such a distribution should be expected since the de Broglie wave-length of 2.6 Mev neutrons is large with respect to the currently accepted range of interaction of the neutron-proton forces. The experimental points agree with the theoretical curve within the probable errors. The fact that the experimental point at 65° is too low may be attributed to missing some of the shorter range protons.

In conclusion it may be said that the experiment indicates that there is no large deviation from theory in the scattering of 2.6 Mev neutrons by protons.

[7] Bethe and Bacher, Rev. Mod. Phys. **8**, 82 (1936).
[8] Oliphant, Kempton and Rutherford, Proc. Roy. Soc. **A149**, 406 (1935).
[9] Bethe and Bacher, Rev. Mod. Phys. **8**, 82 (1936); Share, Phys. Rev. **50**, 488 (1936), Rarita and Present, Phys. Rev. **51**, 788 (1937).
[10] Tracks which ended in the walls of the cloud chamber were said to be consistent with this criterion unless they gave neutron energies that were too great.

Conductivity of Monovalent Metals*

J. BARDEEN†
Harvard University, Cambridge, Massachusetts
(Received July 27, 1937)

The conductivity of monovalent metals is computed from the Bloch theory under the assumption that the wave functions of the electrons are nearly the same as those of free electrons throughout the major part of the volume. The perturbation potential resulting from the Debye elastic waves, which produce transitions between the electronic states, is the sum of two terms: (1) the change in the total potential of the ions, which are assumed to move rigidly with the elastic waves, and (2) the change in the potential of the self-consistent field of the valence electrons. The second part tends to compensate the first. Scattering of electrons through angles greater than $2\sin^{-1}2^{-\frac{1}{2}}$ ($\sim$79°) results from the "*Umklappprozesse*" of Peierls. It is shown that the probability of these transitions joins smoothly with the probability of transitions of the ordinary type, so that the probability is a continuous function of the angle of deflection, and transitions through all angles are possible. Comparison with experiment is made through Bethe's interaction constant C, which is a measure of the average scattering power of the elastic waves. Table I gives the theoretical and experimental values of C/ζ, where ζ is the Fermi energy. Reasonable agreement is obtained for Na and K, but the theoretical values of C for the remaining monovalent metals are somewhat too small.

I. INTRODUCTION

THE modern quantum theory of the electrical conductivities of metals has been very successful in giving a qualitative, and in some cases a quantitative, explanation of such experimental results as the following: the Wiedemann-Franz law, the dependence of conductivity on temperature (in particular, the infinite conductivity at zero temperature), the effect of impurities, and the conductivities of solid solutions. It seems, however, to be very difficult to make an accurate calculation of the absolute value of the conductivity of a metal. The resistance of a pure metal results from the interaction of the electron waves with the lattice vibrations, and little is known about either the electronic wave functions or the frequency spectrum of the vibrations of most metallic crystals.

An attempt is made in the present paper to calculate the conductivity of a monovalent metal under the usual assumption that the wave functions of the electrons are nearly the same as those of free electrons throughout the major part of the volume. The Debye theory is used to obtain the frequency spectrum of the elastic waves. Our treatment differs from previous theories in two respects: (1) the perturbation resulting from the elastic waves, which is responsible for the transitions between the electronic states, is determined in a consistent manner by calculating the change in the self-consistent field of the valence electrons when the crystal is distorted, and (2) the probability of transitions resulting from the "*Umklappprozesse*" is determined. These latter transitions are responsible for the scattering of electrons through angles greater than $2\sin^{-1}2^{-\frac{1}{2}}(\sim 79°)$.

The main outlines of the theory of conductivity are rather definite. According to Bloch,[1] the wave functions of the electrons moving in the periodic potential field of the undistorted crystal are of the form:

$$\psi(\mathbf{k}) = \exp[i\mathbf{k}\cdot\mathbf{x}]U(\mathbf{k},\mathbf{x}), \qquad (1)$$

where $U(\mathbf{k},\mathbf{x})$ has the translational period of the lattice. The configuration of the electrons may be described by giving the distribution of electrons in $\mathbf{k}$ space. If an electric field acts on the metal, the distribution of electrons will no longer by symmetric about the origin of $\mathbf{k}$ space, but will be displaced in the direction of the field. The new distribution results from an equilibrium between the transitions due to the field, and those due to the lattice vibrations. Bloch[1] obtained an integral equation for the new distribution by setting up the conditions for equilibrium. Due to mathematical difficulties, it has so far been possible to solve this equation only with the following simplifications:

* Presented at the American Physical Society, Madison meeting, June 22, 1937.
† Society of Fellows, Harvard University.

[1] F. Bloch, Zeits. f. Physik **52**, 555 (1928).

(1) The energy of an electron in the state $\mathbf{k}$ is a function of $|\mathbf{k}|$, and is independent of the direction of $\mathbf{k}$.

(2) The probability of a transition from a state $\mathbf{k}$ to a state $\mathbf{k}'$ due to the lattice vibrations depends only on the angle between $\mathbf{k}$ and $\mathbf{k}'$ (or, equivalently, on $|\mathbf{k}-\mathbf{k}'|$).

These conditions are approximately satisfied only by the monovalent metals.[2]

The thermal motion of the ions is generally analyzed into a system of independent sound waves, after the manner of Debye. The displacement of an ion at the lattice point $\mathbf{R}_n$ is then of the form:

$$\delta\mathbf{R}_n=\Sigma(\mathbf{q}j)\{\mathbf{A}_{qj}\exp(i\mathbf{q}\cdot\mathbf{R}_n-i\omega_{qj}t) +\mathbf{A}_{qj}^*\exp(-i\mathbf{q}\cdot\mathbf{R}_n+i\omega_{qj}t)\}, \quad (2)$$

in which $\mathbf{q}$ is the propagation vector, and ω_{qj} is the angular frequency of the wave. The index $j=(1, 2, 3)$ refers to the three possible directions of motion of the ions. Transitions between the electronic states are due to the displacement of the ions from their equilibrium positions.

A calculation of the probability of the transition $\mathbf{k}\rightarrow\mathbf{k}'$ due to the thermal motion of the ions depends on the evaluation of the matrix element:

$$M(\mathbf{k}\mathbf{k}')=\int\psi(\mathbf{k}')^*V_p\psi(\mathbf{k})d\tau, \quad (3)$$

where V_p is the perturbation potential resulting from the lattice vibrations. Several different forms for V_p have been chosen by the authors who have discussed the subject. Bethe and Bloch[3] have used the hypothesis of a "deformable potential." If the potential at the point $\mathbf{r}$ in the undistorted crystal is $V(\mathbf{r})$, the potential at the same point in a crystal subject to the distortion $\delta\mathbf{r}$ is assumed to be $V(\mathbf{r}-\delta\mathbf{r})$, and V_p is then the difference between these, $V(\mathbf{r}-\delta\mathbf{r})-V(\mathbf{r})$. Nordheim[4] introduced the idea of a "rigid ion." If $v(\mathbf{r})$ is the potential of a single ion, the total potential of the ions is $\Sigma_n v(\mathbf{r}-\mathbf{R}_n)$. The ionic potential of the distorted lattice will then be $\Sigma_n v(\mathbf{r}-\mathbf{R}_n-\delta\mathbf{R}_n)$. Nordheim supposed that the perturbation potential, V_p, is the difference between these, and thus neglected the distortion in the electronic potential. Both of these hypotheses result in an interaction between electrons and lattice vibrations which is too large, and therefore in a value for the resistance which is much greater than the experimental value. Mott and Jones[5] assume that in each atomic cell, the potential is due entirely to the ion in the center of the cell. Then, in the nth cell, V_p is $v(\mathbf{r}-\mathbf{R}_n-\delta\mathbf{R}_n)-v(\mathbf{r}-\mathbf{R}_n)$. Due to the neglect of the potential of an ion outside of its own cell, they obtain a value for the resistance which is somewhat too small.

The most recent discussion of the subject is that of Peterson and Nordheim.[6] These authors object to the method discussed above of describing the effect of the lattice vibrations as a perturbation acting on the wave functions of the electrons in the undistorted crystal, because the perturbation potential and wave functions are both large in the neighborhood of the ions. An attempt is made to construct approximate wave functions of the progressive wave type for electrons in the distorted crystal, and transitions between these functions are considered. The method is applicable when the periodic part of the wave function of an electron in the undistorted crystal, $U(\mathbf{k},\mathbf{r})$, is reasonably independent of the propagation vector $\mathbf{k}$. For "starting" wave functions they take functions of the form $\exp[i\mathbf{k}\cdot\mathbf{r}]\ U_d(\mathbf{r})$ where $U_d(\mathbf{r})$ is the *exact* wave function of an electron in its lowest state in the *distorted* crystal. It is assumed that $(U_d(\mathbf{r}))^2$ is proportional to the electronic charge density. In order to obtain the charge density, it is assumed that the atomic cells are distorted by the lattice vibrations, and that the total electronic charge in each cell is equal to the charge of one ion. A knowledge of the perturbation potential is not required, as the matrix element required for the transition probability depends essentially on a Fourier component of the charge density, and is independent of the potential. Approximate agreement with the experimental

[2] A discussion appropriate to divalent and transition metals, where two Brillouin zones are of importance, has been given by Mott, Proc. Roy. Soc. **A153**, 699 (1936).

[3] A. Sommerfeld and H. A. Bethe, *Handbuch der Physik*, Vol. 24, II (Berlin, 1933); Bloch, reference 1.

[4] L. W. Nordheim, Ann. d. Physik **9**, 607 (1931).

[5] N. F. Mott and H. Jones, *Theory of the Properties of Metals and Alloys* (Oxford, 1936). These authors use the Einstein model, instead of the Debye model, for the thermal motion, and so do not need to consider the "*Umklappprozesse*."

[6] E. L. Peterson and L. W. Nordheim, Phys. Rev. **51**, 355 (1937).

values of the resistances of Na and K is obtained, but these authors neglect transitions due to the "*Umklappprozesse*" of Peierls,[7] which would greatly increase the resistance if included.

Furthermore, the assumption concerning the form of U_d is not correct, as the density of electrons in the distorted crystal is not proportional to U_d^2. According to the theory of Peterson and Nordheim, the conductivity at low temperatures should be proportional to T^9 instead of T^5. The latter follows from the theory of Bloch, and is justified by experimental data (cf. Section 5).

While the general procedure of these authors is undoubtedly correct, we believe that the ordinary perturbation procedure is also correct as long as the displacement of the ions is small compared with the interatomic distance. If U_d is computed correctly, both methods should lead to the same result. Regions near the ions, where the perturbation is large, make a negligible contribution to the matrix element.[8]

The perturbation potential acting on a given electron consists of two parts: (1) the change in the potential of the ions[9] (which is given by the "rigid ion" hypothesis of Nordheim above) and (2) the change in the potential of the self-consistent field of the valence electrons. The second part tends to cancel the first. Let us consider the transitions due to a single elastic wave of wave number $\mathbf{q}$. It is well known that the allowed transitions $\mathbf{k}\rightarrow\mathbf{k}'$ are such that

$$\mathbf{k}-\mathbf{k}'=\pm\mathbf{q}+\mathbf{K}_n, \tag{4}$$

where $\mathbf{K}_n$ is a vector of the reciprocal lattice space, such that $\mathbf{K}_n\cdot\mathbf{R}_m$ is a multiple of 2π. Furthermore, we have the requirement of the conservation of energy:

$$E_{k'}=E_k\pm\hbar\omega_q. \tag{5}$$

The few electrons for which these conditions are satisfied do not contribute appreciably to the self-consistent field. The wave functions of the remaining electrons charge adiabatically with the elastic waves. The field acting on an electron is the potential of the ions together with the adiabatically varying potential of the self-consistent field. The perturbation potential, V_p, is the difference between the fields in the distorted and the undistorted crystals.

A calculation of the self-consistent field is carried out in detail for a simple model in Section 3. It is assumed that the wave functions of the electrons in the undistorted crystal are sufficiently close to the plane wave functions, $\psi(\mathbf{k})=\exp[i\mathbf{k}\cdot\mathbf{r}]$ so that the latter may be used to determine the charge distribution. This requires that the periodic part of the actual wave function, $U(\mathbf{k},\mathbf{r})$, be fairly flat throughout the major part of the volume. The calculations of Wigner and Seitz and of Slater[10] show that this assumption is valid for Na, and it probably holds reasonably well for other monovalent metals as well.

It has been found possible to determine the probability of transitions resulting from the "*Umklappprozesse*" (values of $\mathbf{K}_n\neq 0$ in Eq. (4)). The probability is of the same order of magnitude as the probability of an ordinary transition and does not depend markedly on the direction of the propagation vector $\mathbf{k}$ of the initial state, so that the theory of Bloch may be applied. Transitions are possible for all angles between $\mathbf{k}$ and $\mathbf{k}'$; the transitions through angles greater than 2 sin $2^{-\frac{1}{2}}$ ($\sim 79°$) are due to the "*Umklappprozesse*."

II. General Theory of Conductivity

Reviews of the theory of conductivity as developed by Sommerfeld and Bloch may be found in many places in the literature,[11] so only the results we shall need later will be quoted here. For temperatures well above the characteristic temperature of Debye, the formula for the conductivity may be written in the Drude-Lorentz-Somerfeld form:

$$\sigma=(Ne^2/\hbar k_m)v_m\tau. \tag{6}$$

The notation is as follows: N is the number of

[7] R. Peierls, Ann. d. Physik **12**, 154 (1932).

[8] Cf. reference 5, p. 254.

[9] It is assumed that the ions may be replaced by a central force field which follows the motion of the ions. This assumption is probably justified for the alkali metals, since the ionic radii are small compared with the interatomic distance; it is more questionable for the noble metals.

[10] E. Wigner and F. Seitz, Phys. Rev. **43**, 804 (1933); **46**, 509 (1934); J. C. Slater, Phys. Rev. **45**, 794 (1934); Rev. Mod. Phys. **6**, 209 (1934).

[11] The recent books of Mott and Jones (reference 5), Frohlich, *Electronentheorie der Metalle* (Berlin, 1936), and Wilson, *The Theory of Metals* (Cambridge, 1936), may be found useful. The notation of the present paper follows more closely that of the older article of Sommerfeld and Bethe (reference 3).

valence electrons per unit volume, v_m is the group velocity of an electron in a state, k_m, at the top of the Fermi distribution, and τ is the mean lifetime of an electron in the state k_m. The value of τ, as determined from the integral equation of Bloch is given by

$$(1/\tau)=(k_m^2/\pi\hbar)(dk/dE)_m\int_0^\pi |M(\mathbf{kk}')|^2 \times(1-\cos\theta)\sin\theta d\theta, \quad (7)$$

where θ is the angle between $\mathbf{k}$ and $\mathbf{k}'$. In the derivation of (7), it has been assumed that E is a function of $|\mathbf{k}|$, and that $M(\mathbf{kk}')$ is a function of $|\mathbf{k}-\mathbf{k}'|$. The matrix element is defined by (1).

In computing the matrix element, one may suppose that the elastic waves with different wave numbers scatter independently. Since the motion of the ions is slow compared with that of the electrons, it is possible to consider the scattering of a stationary wave. The displacement of the ion at the point $\mathbf{R}_n$ due to an elastic wave of wave number $\mathbf{q}$ is

$$\delta\mathbf{R}_n=N^{-\frac{1}{2}}\mathbf{n}_q(a_q\exp[i\mathbf{q}\cdot\mathbf{R}_n] +a_q^*\exp[-i\mathbf{q}\cdot\mathbf{R}_n]), \quad (8)$$

where $\mathbf{n}_q$ is a unit vector in the direction of motion of the ions, and N is the number of atoms per unit volume. At high temperatures, $T\gg\Theta$ the amplitude of the vibration is given by:

$$|a_q|^2=\kappa T/2M\omega_q^2, \quad (9)$$

where κ is the Boltzmann constant, M is the mass of the atom, and ω_q is the angular frequency of the vibration. According to the elementary treatment of Debye, the frequency is given by

$$\omega_q=qc, \quad (10)$$

where c is the velocity of the wave, which is assumed to be independent of $\mathbf{q}$ and of the direction of motion of the ions. The maximum value of $\mathbf{q}$ may be expressed in terms of Θ, the Debye characteristic temperature:

$$\hbar q_m=\hbar(6\pi^2N)^{\frac{1}{3}}=\kappa\Theta/c. \quad (11)$$

While the Debye treatment is not very accurate, one is almost forced to use it in the present stage of the theory, because little is known about the actual frequency spectrum of metallic crystals. Furthermore, Bloch's integral equation has not yet been solved for the general case.

At low temperatures ($T<\Theta$), the sound waves must be quantized, and the energy of the sound quantum may no longer be neglected in comparison with κT. A brief discussion of the conductivity at low temperatures is given in Section 5.

III. Calculation of the Matrix Element

We consider the scattering due to a single elastic wave of wave number $\mathbf{q}$, defined by (8) above. The perturbation potential, V_p, resulting from this wave is the sum of two terms: V_i, the change in potential of the ions, and V_ρ, the change in the potential of the self-consistent field of the valence electrons. Since the amplitude of the vibration is small, it is possible to determine V_ρ by a perturbation procedure in which terms of higher order than the first in the amplitude are neglected. For V_i we have simply:

$$V_i=-N^{-\frac{1}{2}}a_q\Sigma_m\exp[i\mathbf{q}\cdot\mathbf{R}_m]\mathbf{n}_q\cdot\operatorname{grad}v(\mathbf{r}-\mathbf{R}_m)+\text{comp. conj.} \quad (12)$$

The potential $v(\mathbf{r})$ is the potential of a single ion, and the sum runs over all N ions in the unit volume.

It is more difficult to compute the potential V_ρ which results from the modification of the electronic charge distribution. In order to simplify the calculation, we assume that the wave functions of the electrons in the undistorted crystal run close to the free electron wave functions, $\psi^0(\mathbf{k})=\exp[i\mathbf{k}\cdot\mathbf{r}]$ throughout most of the volume. The self-consistent field is computed by a perturbation procedure in which the wave functions of the electrons in the distorted crystal are expanded in terms of the wave functions of the electrons in the undistorted crystal.

If we expand $V_i\psi(\mathbf{k})$ in terms of the wave functions, $\psi(\mathbf{k}')$, of the electrons in the undistorted crystal, the only values of $\mathbf{k}'$ which enter are those which satisfy condition (4) above. Thus,

$$V_i\psi(\mathbf{k})=\Sigma_n\{V_{in+}\psi(\mathbf{k}+\mathbf{q}+\mathbf{K}_n)+V_{in-}\psi(\mathbf{k}-\mathbf{q}-\mathbf{K}_n)\}, \tag{13}$$

where the sum is over all points of the reciprocal lattice space, and

$$V_{in+}=\int\psi(\mathbf{k}+\mathbf{q}+\mathbf{K}_n)^*V_i\psi(\mathbf{k})d\tau=-N^{-\frac{1}{2}}a_q\int\exp\left[-i(\mathbf{q}+\mathbf{K}_n)\cdot\mathbf{r}\right]$$
$$\times\{\Sigma_m\exp\left[i\mathbf{q}\cdot\mathbf{R}_m\right]\mathbf{n}_q\cdot\operatorname{grad}v(\mathbf{r}-\mathbf{R}_m)\}U(\mathbf{k}+\mathbf{q}+\mathbf{K}_n)^*U(\mathbf{k})d\tau. \tag{14}$$

Interchanging the order of summation and integration, we have, after summation over m,

$$V_{in+}=-N^{-\frac{1}{2}}a_q\int\exp\left[-i(\mathbf{q}+\mathbf{K}_n)\cdot\mathbf{r}\right]\mathbf{n}_q\cdot\operatorname{grad}v(\mathbf{r})\,U(\mathbf{k}+\mathbf{q}+\mathbf{K}_n)^*U(\mathbf{k})d\tau. \tag{15}$$

The integration is throughout space. We have made use of the fact that $U(\mathbf{k})$ is periodic. There is a similar expression for V_{in-}. In the approximation of nearly free electrons, V_{in} is independent of the propagation vector $\mathbf{k}$ of the initial state.

The wave functions, $\Psi(\mathbf{k})$, of the electrons in the distorted crystal may be expanded in a similar series,

$$\Psi(\mathbf{k})=\psi(\mathbf{k})+\Sigma_m\{b(\mathbf{k}n+)\psi(\mathbf{k}+\mathbf{q}+\mathbf{K}_n)+b(\mathbf{k}n-)\psi(\mathbf{k}-\mathbf{q}-\mathbf{K}_n)\}. \tag{16}$$

In computing the charge density and potential resulting from these wave functions, we assume that $\psi(\mathbf{k})$ for the undistorted crystal is approximately,

$$\psi(\mathbf{k})=\exp\left[i\mathbf{k}\cdot\mathbf{n}\right]U_0(\mathbf{r}) \tag{17}$$

and that $U_0(\mathbf{r})$ is flat throughout most of the volume.

The density of electrons is, to the first order,

$$\rho=\Sigma(\mathbf{k})\Psi(\mathbf{k})^*\Psi(\mathbf{k})=\rho_0+\Sigma(\mathbf{k},n)U_0^2\{(b(\mathbf{k}n+)+b(\mathbf{k}n-)^*)\exp\left[i(\mathbf{q}+\mathbf{K}_n)\cdot\mathbf{r}\right]$$
$$+(b(\mathbf{k}n+)^*+b(\mathbf{k}n-))\exp\left[-i(\mathbf{q}+\mathbf{K}_n)\cdot\mathbf{r}\right]\}, \tag{18}$$

where ρ_0 is the density of electrons in the undistorted crystal. The summation over $\mathbf{k}$ is over all occupied states.

From the equation,

$$\Delta V_\rho=-4\pi e^2(\rho-\rho_0), \tag{19}$$

we may determine the change is the electrostatic potential of the electrons resulting from the distortion of the crystal. We make the further approximation that $U_0^2\simeq 1$, so that (19) may be easily integrated. This approximation should be satisfactory for the terms in which we are interested; i.e., those for which $\mathbf{q}+\mathbf{K}_n$ is small. To this approximation, the potential is:

$$V_\rho=\Sigma_n\{V_{\rho n}\exp\left[i(\mathbf{q}+\mathbf{K}_n)\cdot\mathbf{r}\right]+V_{\rho n}^*\exp\left[-i(\mathbf{q}+\mathbf{K}_n)\cdot\mathbf{r}\right]\}, \tag{20}$$

where

$$V_{\rho n}=4\pi e^2|\mathbf{q}+\mathbf{K}_n|^{-2}\Sigma(\mathbf{k})(b(\mathbf{k}n+)+b(\mathbf{k}n-)^*). \tag{21}$$

The $b(\mathbf{k}n)$ are to be determined from the Schrödinger equation,

$$-(\hbar^2/2m)\Delta\Psi(\mathbf{k})+(V_0+V_i+V_\rho)\Psi(\mathbf{k})=E(\mathbf{k})\Psi(\mathbf{k}), \tag{22}$$

where V_0 is the total potential, ionic plus electrostatic, in the undistorted crystal. The energy of an electron is unchanged in the first order by the distortion of the crystal. In the free electron approximation,

$$E_k=E_0+\hbar^2k^2/2m. \tag{23}$$

Substituting (13), (16) and (20) in Eq. (22), and keeping only first-order terms, we obtain the following set of equations for the $b(\mathbf{k}n)$:

$$\begin{aligned}(E(\mathbf{k}+\mathbf{q}+\mathbf{K}_n)-E(\mathbf{k}))b(\mathbf{k}n+)+V_{in+}+V_{\rho n}=0,\\ (E(\mathbf{k}-\mathbf{q}-\mathbf{K}_n)-E(\mathbf{k}))b(\mathbf{k}n-)+V_{in-}+V_{\rho n}{}^{*}=0.\end{aligned} \tag{24}$$

These equations serve to determine the $b(\mathbf{k}n)$ except for $\mathbf{k}$ such that

$$E(\mathbf{k})\sim E(\mathbf{k}+\mathbf{q}+\mathbf{K}_n);\quad E(\mathbf{k})\sim E(\mathbf{k}-\mathbf{q}-\mathbf{K}_n); \tag{25}$$

when the simple perturbation procedure breaks down. It is, of course, just these $\mathbf{k}$ for which transitions are possible. Solving (24), we find

$$\begin{aligned}b(\mathbf{k}n+)=(V_{in+}+V_{\rho n})(E(\mathbf{k})-E(\mathbf{k}+\mathbf{q}+\mathbf{K}_n))^{-1},\\ b(\mathbf{k}n-)=(V_{in-}+V_{\rho n}{}^{*})(E(\mathbf{k})-E(\mathbf{k}-\mathbf{q}-\mathbf{K}_n))^{-1}.\end{aligned} \tag{26}$$

The $V_{\rho n}$ still involve the $b(\mathbf{k}n)$. An equation for $V_{\rho n}$ may be obtained by substituting the values of $b(\mathbf{k}n)$ given by (26) into (21). Some care must be taken in carrying out the summation over $\mathbf{k}$, because the $b(\mathbf{k}n)$ become large for certain values of $\mathbf{k}$. It will be convenient to define an average energy, $W(\mathbf{q}+\mathbf{K}_n)$ which is a function of $|\mathbf{q}+\mathbf{K}_n|$ to be determined below, by

$$[W(\mathbf{q}+\mathbf{K}_n)]^{-1}=N^{-1}\Sigma(\mathbf{k})(E(\mathbf{k}+\mathbf{q}+\mathbf{K}_n)-E(\mathbf{k}))^{-1}, \tag{27}$$

so that we have the following equation for $V_{\rho n}$:

$$V_{\rho n}=-(V_{in+}+V_{\rho n})(8\pi e^2N)\,|\mathbf{q}+\mathbf{K}_n|^{-2}[W(\mathbf{q}+\mathbf{K}_n)]^{-1}. \tag{28}$$

Solving, we obtain

$$V_{\rho n}=-V_{in+}(1+(8\pi e^2N)^{-1}|\mathbf{q}+\mathbf{K}_n|^{2}[W(\mathbf{q}+\mathbf{K}_n)])^{-1}. \tag{29}$$

In our approximation, the matrix element, $M(\mathbf{k}\mathbf{k}')$, corresponding to the transition $\mathbf{k}\rightarrow\mathbf{k}'=\mathbf{k}+\mathbf{q}+\mathbf{K}_n$ is:

$$M(\mathbf{k}\mathbf{k}')=V_{in+}+V_{\rho n}=V_{in+}(1+8\pi e^2N|\mathbf{q}+\mathbf{K}_n|^{-2}[W(\mathbf{q}+\mathbf{K}_n)]^{-1})^{-1}. \tag{30}$$

The factor multiplying V_{in+} is a measure of the compensation of the distortion of the ionic potential by the shift in the charge density of the valence electrons. For elastic waves of long wave-length ($\mathbf{q}$ small, $\mathbf{K}_n=0$) the compensation is almost complete; the compensation is less effective for waves of shorter wave-length.

There remains to determine $W(\mathbf{q}+\mathbf{K}_n)$ from from (27) and V_{in} from (15). The summation over $\mathbf{k}$ in (27) may be replaced by an integration over the occupied states in $\mathbf{k}$ space. We introduce cylindrical coordinates $(\zeta,\ \rho,\ \alpha)$, in $\mathbf{k}$ space, with the axis in the direction of $\mathbf{K}\equiv\mathbf{q}+\mathbf{K}_n$. From a consideration of the behavior of the $b(\mathbf{k}n)$ for those values of $\mathbf{k}$ for which (24) is satisfied, it is easily shown that the integral we require is:

$$\begin{aligned}[W(\mathbf{K})]^{-1}=\lim_{\epsilon\rightarrow 0}\frac{3m}{\hbar^2k_m{}^3}\Bigg\{\int_{-k_m}^{-(K/2)-\epsilon}\frac{d\zeta}{[(K+\zeta)^2-\zeta^2]}\int_0^{(k_m{}^2-\zeta^2)^{\frac{1}{2}}}\rho d\rho\\ +\int_{-(K/2)+\epsilon}^{k_m}\frac{d\zeta}{[(K+\zeta)^2-\zeta^2]}\int_0^{(k_m{}^2-\zeta^2)^{\frac{1}{2}}}\rho d\rho\Bigg\}.\end{aligned} \tag{31}$$

We have used (23) for E_k. The integration may easily be carried out by elementary methods, and we find:

$$W(\mathbf{K})=\frac{4}{3}\frac{\hbar^2k_m^2}{2m}\left\{\frac{1}{2}+\frac{4k_m^2-K^2}{8k_mK}\log\frac{2k_m+K}{2k_m-K}\right\}^{-1}. \tag{32}$$

In calculating V_{in} from (15), it will be convenient to divide the integration over space into two parts: the integration over the central cell, and the integration over the remainder of space. The former may be transformed into a surface integral; the latter may be simplified by the approximations $U(\mathbf{k})\backsimeq 1$; $v(\mathbf{r})\backsimeq -e^2/r$. In carrying out the integration, we replace the central cell by a sphere of equal volume (radius r_s). We then have

$$V_{in+}=-N^{\frac{1}{2}}a_q(I_1+I_2), \tag{33}$$

with

$$\begin{aligned} I_1&=\int_{\text{cell}}\exp\left[-i(\mathbf{q}+\mathbf{K}_n)\cdot\mathbf{r}\right]\mathbf{n}_q\cdot\operatorname{grad}v(r)\,U(\mathbf{k}+\mathbf{q}+\mathbf{K}_n)^*U(\mathbf{k})d\tau,\\ I_2&=-\int_{r_s}^{\infty}\int_0^{2\pi}\int_0^{\pi}\exp\left[-i(\mathbf{q}+\mathbf{K}_n)\cdot\mathbf{r}\right]\mathbf{n}_q\cdot\operatorname{grad}(e^2/r)d\tau. \end{aligned} \tag{34}$$

By elementary methods, we find:

$$\begin{aligned} I_2&=4\pi e^2\cos(\mathbf{n}_q,\mathbf{q}+\mathbf{K}_n)\int_{r_s}^{\infty}\int_0^1 u\sin(|\mathbf{q}+\mathbf{K}_n|ru)dudr\\ &=-(4\pi ie^2/|\mathbf{q}+\mathbf{K}_n|)\cos(\mathbf{n}_q,\mathbf{q}+\mathbf{K}_n)(\sin x/x), \end{aligned} \tag{35}$$

where

$$x=|\mathbf{q}+\mathbf{K}_n|r_s. \tag{36}$$

In any cell, the undistorted potential V_0 is approximately equal to the potential of the ion in the center of the cell plus the potential of the electron cloud within the cell, since the potential of the ions in neighboring cells is very nearly cancelled by the potential of the electrons in those cells. The potential of the electron cloud, with the assumption of uniform density, is equal to $(3e^2/2r_s)-(e^2r^2/2r_s^3)$. We thus have

$$V_0(r)=v(r)+(3e^2/2r_s)-(e^2r^2/2r_s^3). \tag{37}$$

The integral I_1 is then,

$$\begin{aligned} I_1=\int_{\text{cell}}\psi(\mathbf{k}')^*\mathbf{n}_q\cdot\operatorname{grad}v(r)\psi(\mathbf{k})d\tau&=\int_{\text{cell}}\psi(\mathbf{k}')^*\mathbf{n}_q\cdot\operatorname{grad}V_0\psi(\mathbf{k})d\tau\\ &+\int_{\text{cell}}\psi(\mathbf{k}')^*\mathbf{n}_q\cdot\operatorname{grad}(e^2r^2/2r_s^3)\psi(\mathbf{k})d\tau. \end{aligned} \tag{38}$$

The first integral on the right-hand side of (38) may be transformed into a surface integral which is rather small in magnitude; the second may easily be evaluated directly.

According to Mott and Jones,[12]

$$\int_{\text{cell}}\psi(\mathbf{k}')^*\mathbf{n}_q\cdot\operatorname{grad}V_0\psi(\mathbf{k})d\tau=(\hbar^2/2m)\mathbf{n}_q\cdot\int\left[\psi(\mathbf{k}')^*(\partial/\partial n)\operatorname{grad}\psi(\mathbf{k})-\operatorname{grad}\psi(\mathbf{k})(\partial/\partial n)\psi(\mathbf{k}')^*\right]dS, \tag{39}$$

the second integral being over the surface of the cell. With the approximation of nearly free electrons,

$$\psi(\mathbf{k})\backsimeq\exp\left[i\mathbf{k}\cdot\mathbf{r}\right]U_0(r);\quad U_0(r_s)\backsimeq 1;\quad U'(r_s)=0; \tag{40}$$

[12] Reference 5, p. 253.

it is easily shown that the surface integral is equal to:

$$-4\pi i r_s^2 \cos(\mathbf{n}_q, \mathbf{q}+\mathbf{K}_n)(V_0(r_s)-E_0)(\sin x - x\cos x)/x^2, \tag{41}$$

where E_0 is the energy of an electron in its lowest state. The potential in each cell is given by (37), and the wave function of an electron in its lowest state satisfies the Schrödinger equation,

$$-(\hbar^2/2m)\Delta U + V_0 U = E_0 U. \tag{42}$$

It should be noted that E_0 includes the Coulomb energy, which, for free electrons is $1.2e^2/r_s$. The values of E_0 should be quite small for most monovalent metals. Since $v(r) \backsimeq -e^2/r$, $V_0(r_s) \backsimeq 0$.

In the second integral on the right-hand side of (38), we may set with sufficient accuracy, $\psi(\mathbf{k}) = \exp[i\mathbf{k}\cdot\mathbf{r}]$ so that

$$\int_{\text{cell}} \psi(\mathbf{k}')^* \mathbf{n}_q \cdot \text{grad}\,(e^2r^2/2r_s^3)\psi(\mathbf{k})d\tau = \int_{\text{cell}} \exp[-i(\mathbf{q}+\mathbf{K}_n)\cdot\mathbf{r}]\mathbf{n}_q \cdot \text{grad}\,(e^2r^2/2r_s^3)d\tau. \tag{43}$$

Integration by elementary methods gives the following value for the integral:

$$-(4\pi i e^2/|\mathbf{q}+\mathbf{K}_n|)\cos(\mathbf{n}_q, \mathbf{q}+\mathbf{K}_n)[3(\sin x - x\cos x) - x^2 \sin x]/x^3. \tag{44}$$

From (35), (41), and (44), we have, finally,

$$I_1+I_2 = -\frac{i|\mathbf{q}+\mathbf{K}_n|}{N}\left(\frac{4\pi e^2 N}{|\mathbf{q}+\mathbf{K}_n|^2} + V_0(r_s) - E_0\right)\cos(\mathbf{n}_q, \mathbf{q}+\mathbf{K}_n)\left(\frac{3(\sin x - x\cos x)}{x^3}\right) \tag{45}$$

and $M(\mathbf{k}\mathbf{k}')$ may easily be obtained from (30) and (33). An explicit expression will be given in the next section.

IV. Calculation of the Conductivity

The reciprocal mean lifetime, $1/\tau$, is to be obtained by expressing the matrix element $M(\mathbf{k}\mathbf{k}')$ as a function of the angle of scattering, θ, and then integrating over all angles from 0 to π, as indicated by Eq. (7). For the transitions of interest, we must satisfy the conservation of energy, which, in our approximation, gives

$$k'^2 = |\mathbf{k}+\mathbf{q}+\mathbf{K}_n|^2 = k^2,$$

or
$$|\mathbf{q}+\mathbf{K}_n|^2 = -2\mathbf{k}\cdot(\mathbf{q}+\mathbf{K}_n). \tag{46}$$

Given any $\mathbf{k}$ and $\mathbf{k}'$ such that $k^2 = k'^2$, one can always choose $\mathbf{q}$ and $\mathbf{K}_n$ in such a way that (46) is fulfilled. If the angle θ between $\mathbf{k}$ and $\mathbf{k}'$ is less than $2\sin^{-1}2^{-\frac{1}{2}}(\sim 79°)$, $\mathbf{K}_n = 0$. For angles greater than 79°, one must take the $\mathbf{K}_n$ which connect the nearest neighbors to the origin of the reciprocal lattice space (these transitions correspond to the "*Umklappprozesse*" of Peierls). In order that the Bloch theory may be applied, the matrix element $M(\mathbf{k}\mathbf{k}')$ must be independent of the direction of $\mathbf{k}$, and depend only on the angle between $\mathbf{k}$ and $\mathbf{k}'$, which may be expressed in terms of $|\mathbf{q}+\mathbf{K}_n|$. This requirement is satisfied if $\mathbf{K}_n = 0$. All the factors in $M(\mathbf{k}\mathbf{k}')$ are functions of $|\mathbf{q}+\mathbf{K}_n|$ except a_q, which is a function of q. According to (10) and (11), a_q is inversely proportional to q. For most transitions resulting from the "*Umklappprozesse*," q is quite large, and is close to its maximum value, q_m. We will therefore set $q = q_m$ in a_q for those transitions for which $\mathbf{K}_n \neq 0$, and thus underestimate the resistance to some extent. The theory of Bloch may then be applied in its usual form.

In order to simplify the equations, the following notation will be introduced:

$$\begin{aligned}
&u = \sin(\theta/2);\\
&|\mathbf{q}+\mathbf{K}_n|^2 = 2k_m^2(1-\cos\theta) = 4k_m^2u^2;\\
&f(u) = \tfrac{1}{2} + ((1-u^2)/4)\log((1+u)/(1-u));\\
&\xi(u) = \begin{cases} 1, & u < 2^{-\frac{1}{2}} \\ 2^{\frac{1}{2}}u, & u > 2^{-\frac{1}{2}}; \end{cases}\\
&g(u) = 3(\sin x - x\cos x)/x^3;\\
&x = |\mathbf{q}+\mathbf{K}_n| r_s = 2k_m r_s u = 3.84u;\\
&\zeta = \hbar^2 k_m^2/2m;\\
&\beta = e^2 k_m/\pi\zeta.
\end{aligned} \tag{47}$$

Using (30), (32), (33), (45) and (47), and summing over the three directions of motion of the ions, we find, after some reduction, that

$$\Sigma(\mathbf{n}_q)|M(u)|^2=(4/9N)|\mathbf{q}a_q|^2(G(u))^2, \quad (48)$$

where

$$G(u)=g(u)\xi(u)[1+(Vr_s)-E_0)(3u^2/\beta\zeta)] \times[f(u)+(2/\beta)u^2]^{-1}\zeta. \quad (49)$$

As u approaches zero (deflection through small angles) the factor multiplying ζ in (49) approaches unity. As u increases, $G(u)$ decreases, and becomes rather small when $u=1$ (deflection through an angle of 180°). It is to be noted that there is no discontinuity in $G(u)$ at $u=2^{-\frac{1}{2}}(\theta\sim 79°)$. The probability of transitions due to the "*Umklappprozesse*" joins smoothly with the probability of transitions of the ordinary type.

The reciprocal mean lifetime is obtained by substituting (48) into (7). The integration over θ is changed to an integration over u, and we have

$$(1/\tau)=2^{-5/3}(k_m^2/\pi\hbar)(dk/dE)_m \times(4/9N)|qa_q|^2C^2, \quad (50)$$

in which it has been convenient to introduce a mean square value of $G(u)$ defined by

$$C^2=4u_m^{-4}\int_0^1(G(u))^2u^3du =2^{14/3}\int_0^1(G(u))^2u^3du, \quad (51)$$

where $u_m=2^{-\frac{1}{2}}$ is the maximum value of u for an ordinary transition. As thus defined, C is the interaction constant of Sommerfeld and Bethe.[13]

[13] Reference 3, p. 513.

We may simplify (50) to some extent by use of (9), (10), and (11). The substitution for $|qa_q|^2$ gives, after some reduction,

$$(1/\tau)=\hbar^2\pi^3Nk_m^{-2}(dk/dE)_m(T/M\kappa\Theta^2)C^2. \quad (52)$$

The conductivity is obtained by substitution of (52) into (6):

$$\sigma=Me^2(\hbar\pi)^{-3}k_m(dE/dk)_m^2(\kappa\Theta^2/T)C^{-2}, \quad (53)$$

which is Eq. (36.11) of Sommerfeld and Bethe.

As the characteristic temperatures are not known accurately for most of the monovalent metals, it is perhaps best to compare the directly calculated quantity with the experimental values of σ/Θ^2, which may be expressed in terms of the interaction constant C^2. If we use the free electron value for E, we have

$$k_m(dE/dk)_m=2\zeta. \quad (54)$$

Eq. (53) may then be written in the form

$$(\zeta/C)^2=\pi\sigma mhT/4\beta M\kappa\Theta^2. \quad (55)$$

Table I gives a comparison of the experimental and theoretical values of C/ζ for the monovalent metals. The relevant data for the calculation of C/ζ from the experimental values of σ and Θ are also given. As the characteristic temperatures of the alkalis are rather uncertain, two values have been given for Na and K. The lower values are those of Fuchs[14] as derived from the specific heat at low temperatures; the higher values are those of Gruneisen[15] as obtained from the variation of conductivity with temperature. The former values are perhaps to be preferred, because the theory of conductivity at intermediate temperatures is rather uncertain. Row (8) of Table I

[14] K. Fuchs, Proc. Roy. Soc. **A153**, 622 (1936).
[15] Gruneisen, Ann. d. Physik **16**, 530 (1933).

TABLE I. *Comparison of the experimental and theoretical values of C/ζ for the monovalent metals.*

1	METAL	Na	K	Rb	Cs	Cu	Ag	Au
2	Atomic Wgt.	23	39	85.5	133	63.6	108	197
3	$\sigma(\Omega^{-1}\,\mathrm{cm}^{-1};\ 0°C)$	22.6	15.3	8.2	5.4	64	67	68
4	Θ	150–202	100–126	~85	~55	315	215	175
5	$r_s\times10^8$	2.12	2.56	2.81	3.13	1.41	1.58	1.58
6	β	1.33	1.60	1.77	1.9	0.89	1.00	1.00
7	C/ζ (exp)	0.77–1.04	0.87–1.10	1.6	1.65	1.32	1.21	1.30
8	C/ζ (theor.*)	0.72	0.77	0.80	0.82	0.61	0.64	0.64
9	$V_0(r_s)-E_0$ (ev)	0.2				1.3	1.1	(3.7)
10	C/ζ (theor.)	0.77				0.80	0.83	0.90

* Assuming that $V_0(r_s)-E_0=0$.

gives the theoretical values of C/ζ, computed under the assumption that $V_0-E_0=0$. This assumption should be very nearly correct for the alkalis (except Li). Row (9) gives the theoretical values of E_0 for Na, Cu and Ag as determined from the work of Wigner and Seitz[10] and of Fuchs.[16] The value given for Au was estimated from the ionization potential and the heat of sublimation. It should be noted that the theoretical values of C/ζ for all the metals listed are close to 0.8, and are thus very close to the theoretical values of Peterson and Nordheim[6] (0.84 for all monovalent metals). Since we have underestimated the effect of "*Umklappprozesse*," the true theoretical values should be larger (by perhaps ten or fifteen percent).

The agreement obtained for Na and Rb is satisfactory, but the calculated values for the noble metals and for Rb and Cs are somewhat too small. It is perhaps not surprizing that the values for the noble metals are too low, because our assumptions are very likely not justified for these metals, but one would expect closer agreement for Rb and Cs in view of the fact that many properties of these metals can be explained on the assumption of free electron wave functions.

The accuracy that can be expected from the one-electron picture on which the Bloch theory is based is uncertain. The effect of electron exchange on the conductivity will be discussed by the author in a forthcoming paper.

V. Conductivity at Low Temperatures

At low temperatures ($T\ll\Theta$), the only elastic waves which will be excited are those with small wave number $\mathbf{q}$, and the electrons can be scattered only through small angles. The theory has been discussed by Bloch[1] with the following simplifying assumptions:

(1) Debye theory for eastic waves,
(2) Thermal equilibrium of elastic waves,
(3) $E(\mathbf{k})$ a function of $|\mathbf{k}|$ alone,
(4) $G(u)=$constant,
(5) Neglect of "*Umklappprozesse.*"

If T_1 and T_2 are two temperatures such that

$$T_1\ll\Theta\ll T_2 \tag{56}$$

and σ_1 and σ_2 are the corresponding conductivities, it was shown that

$$\sigma_2/\sigma_1=497.6(T_1/\Theta)^4(T_1/T_2). \tag{57}$$

According to the present theory, the numerical factor will be slightly different. As θ (or u) approaches zero, $G(u)$ approaches ζ. It is easily seen that (57) must be multiplied by ζ^2/C^2, so that we have

$$\sigma_2/\sigma_1=497.6(\zeta^2/C^2)(T_1/\Theta)^4(T_1/T_2). \tag{58}$$

For Na, the numerical factor is increased by a factor of about 1.6. Gruneisen has shown that the T^5 law is obeyed by most metals at low temperatures, but it is difficult to estimate the numerical factor from experimental data because of the uncertainty in Θ, which enters in a high power.

The criticism of Peierls[7] of the theory of conductivity at low temperatures must not be forgotten. It is difficult to see how the elastic waves in a monovalent metal can be in thermal equilibrium when a current is flowing.

[16] K. Fuchs, Proc. Roy. Soc. **A151**, 585 (1935).

Excitation Functions of the Auroral Bands of N_2^+ and the Comet-Tail Bands of CO^+, Excited by Electron Impact

F. P. BUNDY*
Mendenhall Laboratory of Physics, Ohio State University, Columbus, Ohio
(Received August 10, 1937)

The excitation functions of the auroral bands of N_2^+ and the comet-tail bands of CO^+, excited by electron impact, have been determined by the method of photographic intensitometry. A discharge tube is described in which electrons were accelerated from three filaments into the inside of a hollow cylindrical grid where the discharge took place. The discharge tube was operated at a pressure of 0.001 mm Hg with an electron current of 25 ma. The mean free path of the electrons was large in comparison to the interelectrode distances. It was found by probe electrode measurements that the "transparency" of the grid to electrons from the filaments diminished with the voltage for voltages less than 150 volts. Because of this effect it was necessary to correct the intensity measurements to correspond to a constant *excitation* current.

The intensities of the 4018 and 4271A bands of CO^+ and the 3914 and 4278A bands of N_2^+ were measured. The excitation functions that were obtained rise rapidly from zero at the excitation potential to sharp maxima at 2.5 times the excitation potential, then diminish rapidly in an exponential fashion. The functions for N_2^+ and CO^+ are very similar and are regarded to be representative of the general type of excitation function associated with the excitation of the electronic states of these ionized molecules by single electron impacts.

INTRODUCTION

EXPERIMENTAL investigations of the electron-impact excitation function of the auroral bands of N_2^+ have not up to the present time given consistent results. Lindh[1] obtained a function with three maxima,—a low one at 80 volts, a high one at 165 volts, and a very weak one at 270 volts. Such a function is not at all to be expected from theoretical considerations and it is likely that Lindh's measurements suffered from errors due to multiple electron impact and to secondary emission of electrons from the anode. Recently Bernard[2] has shown that the shape of the experimentally determined excitation function for these bands is very sensitive to the conditions of discharge. He found that when multiple electron impact starts in the discharge, the maximum of the excitation function shifts rapidly to higher voltages. Knowing this, he interpreted his results to indicate that the maximum of the true excitation function really lies at about 48 volts, but since his best curves showed the effects of multiple electron impact in the discharge, they could not be relied upon for giving accurate quantitative information.

To obtain a reliable excitation function, for excitation by electron impact, the conditions of the discharge must permit only single impacts of the primary electrons, and the primary electrons must all have the same energy. The first of the conditions can be realized by producing the discharge at a pressure sufficiently low to make the mean free path of the electrons large in comparison to the interelectrode distances. The second of the conditions may be attained by drawing the electrons from a nearly equipotential surface, such as a very low voltage filament. These conditions were attained quite successfully in the discharge tube used in this investigation.

It has been shown experimentally by Lees[3] and others, and theoretically by Massey and Mohr,[4] that the electron-impact excitation functions of the helium atom differ widely for the singlet and triplet terms, as to the relative positions of their maxima with respect to the excitation potential. The maxima of the functions for the triplet terms are reached very shortly after the excitation potential, while those of the functions for the singlet terms are reached at two to four times the excitation potential. The author has been unable to find any theoretical work on the excitation functions for the electron impact excitation of the doublet states of atoms or molecules, but in a general way these functions would be expected to rise to

* Now at Ohio University, Athens, Ohio.
[1] A. E. Lindh, Zeits. f. Physik **67**, 67 (1931).
[2] R. Bernard, Comptes rendus **204**, 488 (1937).
[3] J. H. Lees, Proc. Roy. Soc. **A137**, 173 (1932).
[4] Massey and Mohr, Nature **127**, 234 (1931) and Proc. Roy. Soc. **A140**, 613 (1933).

their maxima at two to three times the excitation potential.

To investigate whether there is a similarity between the excitation functions for the doublet states of isoelectronic molecules, the excitation-function for the comet-tail bands of CO^+ was determined for comparison with that of the auroral bands of N_2^+, since CO^+ and N_2^+ are isoelectronic molecules. The auroral bands arise from the $B^2\Sigma \rightarrow X^2\Sigma$ electronic transition in N_2^+ while the comet-tail bands arise from the $A^2\Pi \rightarrow X^2\Sigma$ transition in CO^+. The excitation functions for these two sets of bands should be similar and should be representative of the electron-impact excitation efficiency for doublet states of ionized molecules.

Experimental

The essential parts of the discharge tube are shown in Fig. 1(a). The glass shell of the tube was about 7.5 cm in diameter and 30 cm in length. Electrons from the filaments *F* were accelerated by the cylindrical grid *G*, into the region of discharge *R*. The filaments consisted of flat spirals of 15 mil tungsten wire and the grid was constructed of 8 mil tungsten wire wrapped around an iron-wire framework. This grid was 4.5 cm in diameter and 6.5 cm long. Scattered light from the incandescent tungsten filaments was prevented from entering the spectrograph by the collimating disks *C* and the blackened absorption horn *H*. This arrangement made it possible to obtain spectra which were quite free from continuous background, as may be seen from the spectrograms in Fig. 2.

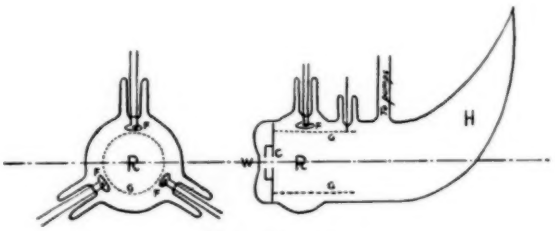

Fig. 1(a). Discharge Tube.

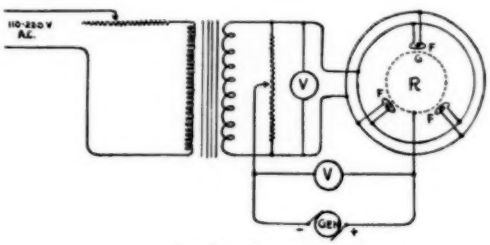

Fig. 1(b). Circuit Diagram.

Fig. 1. Discharge tube and circuit.

The circuit used in connection with the discharge tube is shown in Fig. 1(b). The three filaments were connected in parallel to a large a.c. step-down transformer. When the filaments were heated to electron emission temperatures the r. m. s. potential drop across them was about 10 volts. The negative terminal of the grid voltage supply was connected to the center tap of an external resistance across the filament terminals so that the total energy width of the electron beam was about 10 volts, and the actual electron energies ranged about 5 volts each way from the grid potential. Because most of the electrons were emitted from the hot centers of the filaments, the effective energy width of the electron beam was less than 10 volts. In any case, because of the center tapped filaments, the energy width of the electron beam would not affect the position of the maximum of the excitation function unless the true maximum were very unsymmetrical.

The nitrogen was taken from a steel cylinder containing the pure gas, passed through a liquid-air trap containing activated charcoal, and stored in a 12-liter reservoir flask. The reservoir was connected to the discharge tube by an adjustable gas leak. During the operation of the discharge tube a continuous stream of fresh gas was pumped from the reservoir flask through the discharge tube by the vacuum pumps. The CO was produced by passing formic acid vapor over anhydrous P_2O_5. This "dehydrated" the acid to CO. Last traces of condensible vapor were removed by passing the gas through a liquid air trap. The gas was stored in the large reservoir flask.

The discharge tube was "cleaned-up" by baking it at a temperature of 400°C at high vacuum for several hours. Then, before any spectrograms were taken for measurement, the tube was operated for about 5 hours with an electron current of 700 to 900 ma in order to further clean up the metal electrodes.

An image of the hole in the collimating disk of the discharge tube was projected upon the slit of the spectrograph by use of an *f*:3.5

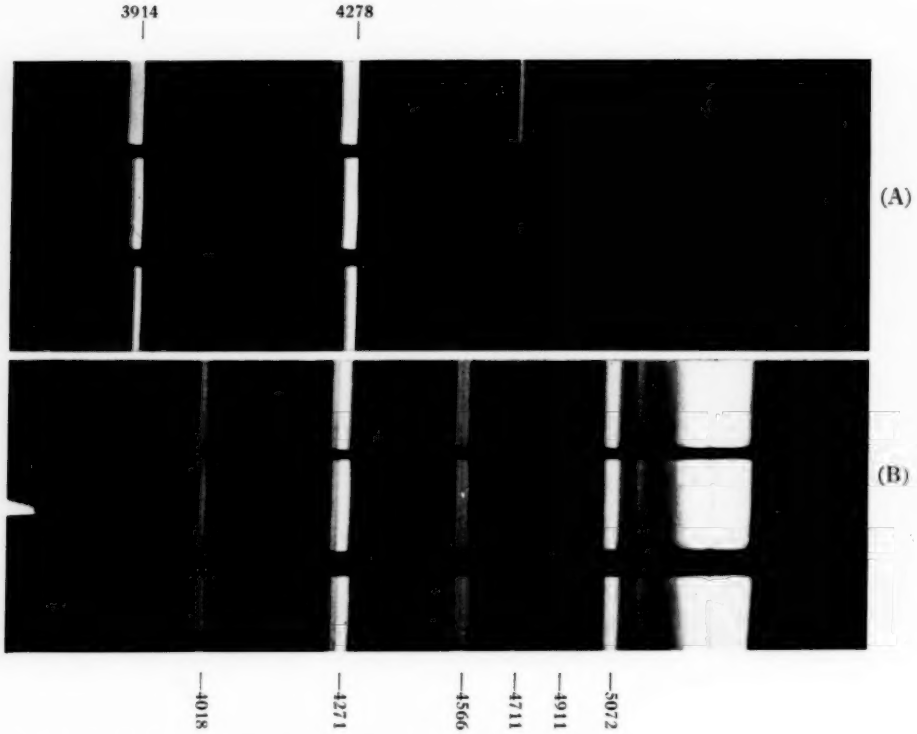

FIG. 2. Typical spectrograms. (A) auroral bands of N_2^+; (B) comet-tail bands of CO^+.

achromatic lens. With a pressure of 0.001 mm and an electron current of 25 ma the glow in the discharge tube was sufficiently bright to give satisfactory exposures in 30 seconds. It was possible to take forty spectrograms on one plate. Twenty of these were devoted to excitation function measurements and the rest were used for densitometer calibration markings. For the determination of the excitation functions a series of exposures was made at various grid voltages ranging from 30 to 450 volts while the grid current was held constant at 25 ma and the pressure at 0.001 mm Hg. Four of these series were taken for the CO^+ measurements and three for the N_2^+ measurements. The intensities of the 4018 and 4271A bands of CO^+ and the 3914 and 4278A bands of N_2^+ were measured.

The densitometer calibration markings were made in the following way: the discharge tube was operated at constant current and voltage while a series of exposures of constant time was made with a series of calibrated neutral wire screen filters[5] interposed between the discharge tube and the condensing lens. This gave a series of exposures which yielded intensity-density calibrations for the particular wavelength regions of the appropriate bands. The spectrograph gave low dispersion, and with a wide slit the band images on the plate were sufficiently diffused that the densitometer readings were representative of the entire band and not some particular part of it.

There was some question as to whether at all voltages the part of the electron current which penetrated the grid into the region of discharge (i.e., the *excitation* current) was a constant proportion of the current to the grid itself. To investigate this matter of the "transparency" of the grid to electrons, a probe electrode was inserted into the region of discharge and a series of measurements was made of the ratio of the probe current to the grid current. The analysis[6] of these probe grid data showed that the ratio of the excitation current to the grid current diminished with the grid voltage for voltages less than 150 volts. This ratio is shown graphi-

[5] G. R. Harrison, J. O. S. A. **18**, 492 (1929) and J. O. S. A. **19**, 267 (1929).

[6] F. P. Bundy, Ph. D. dissertation, Ohio State University (1937).

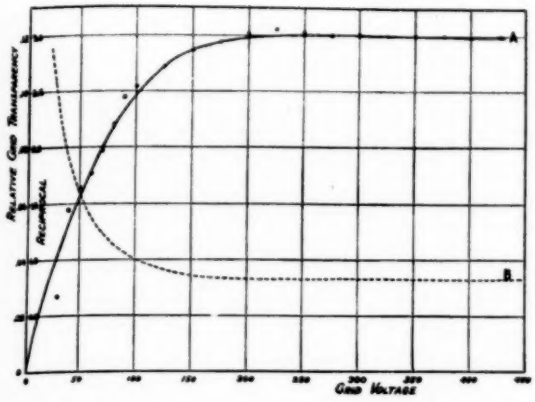

FIG. 3. Relative transparency of grid to electrons as a function of the grid voltage. (*A*) transparency; (*B*) reciprocal of transparency.

cally in curve *A* of Fig. 3. Because of this effect, the excitation functions already determined,—which corresponded to a constant *grid* current,—had to be corrected to correspond to a constant excitation current. This was done by multiplying the ordinates of the constant-grid-current excitation function by the reciprocal of the electron transparency of the grid for the corresponding grid voltages. The reciprocal values are shown by the dotted curve *B* of Fig. 3.

RESULTS AND DISCUSSION

The excitation function for the auroral bands of N_2^+, uncorrected for the electron transparency of the grid, is shown by curve *A* of Fig. 4. Curve *B* shows the same function corrected for the grid transparency. The sharp maximum at 49 ± 2 volts agrees well with Bernard's[2] value of 48 volts. Bernard's best results are shown by curve *C* of Fig. 4. He explains the second rise in his curve to be due to multiple impacts of the electrons, since this was possible in his discharge tube at the pressures he used. Curve *D* of Fig. 4 shows the results of Lindh.[1] His results were subject to three errors: multiple impacts of the electrons due to the comparatively high gas pressures used (0.1 mm); transparency of grid to primary electrons from the filament; and secondary emission of electrons from the anode. Because of these errors his results are not comparable with those of Bernard and the author. The fact that the excitation function obtained in the present investigation has the general form of a theoretical excitation function shows that this discharge was particularly free from multiple impacts and secondary emission.

The results for the comet-tail bands of CO^+ are shown in Fig. 5. Curve *A* shows the uncorrected function and curve *B* the corrected one. This excitation function has the same general shape as that of the N_2^+ function, but the maximum comes at 42 ± 2 volts. One should expect this maximum to come at a lower voltage than that of the N_2^+ because the excitation potential of the CO^+ bands (16.7 volts) is less than that of the N_2^+ bands (19.6 volts). The rise which starts in the CO^+ curve at about 200 volts is not believed to exist in the true excitation function. It is suggested that this rise of intensity results from a slight increase of pressure in the discharge tube due to outgassing of the electrodes by bombardment of the higher energy electrons. Carbon monoxide is known to be strongly absorbed by "clean" metals and for this reason the discharge tube was operated at 800 to 900 ma for at least an hour before each series of spectrograms in order to eliminate the absorbed gas. But in the case of carbon monoxide the gas started reabsorbing as soon as the electron current was diminished. The irregular outgassing and reabsorption caused the raw

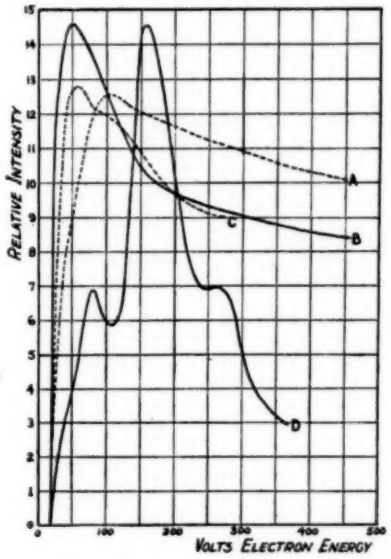

FIG. 4. Excitation functions of the auroral bands of N_2^+. (*A*) uncorrected function; (*B*) corrected function; (*C*) Bernard's curve; (*D*) Lindh's curve.

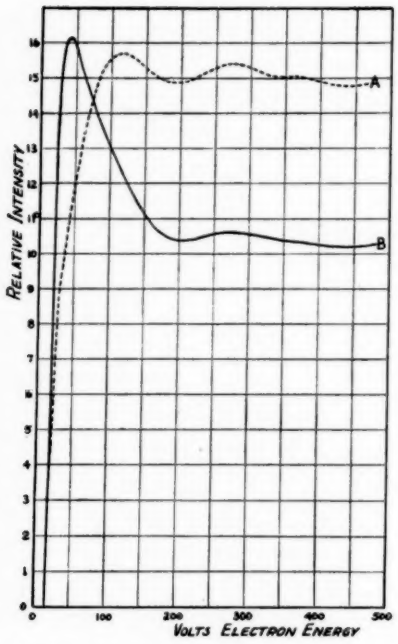

FIG. 5. Excitation function curves of comet-tail bands of CO^+. (*A*) uncorrected curve; (*B*) corrected curve.

experimental data for CO^+ to be much more irregular than that of nitrogen.

In Fig. 6 are shown the excitation functions for CO^+ and N_2^+. The abscissae are the electron energies divided by the excitation potentials. The purpose of this figure is to compare the characteristics of the two curves, and not their absolute magnitudes. For this reason the scales of the ordinates for the two curves are independent. It is interesting to note that the maxima of both the functions are reached at 2.5 times the excitation potential, and that they die away in much the same manner. The hump in the CO^+ curve has been discussed in the preceding paragraph. Were it not for this experimental irregularity the CO^+ curve would probably continue parallel to the N_2^+ curve as

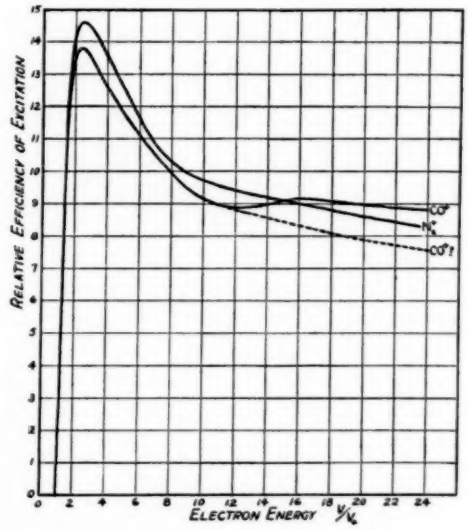

FIG. 6. Excitation functions of auroral bands of N_2^+ and the comet-tail bands of CO^+.

indicated on the graph. These curves show clearly that the isoelectronic molecules, N_2^+ and CO^+, respond in a very similar manner to excitation by electron impact.

The fact that these bands do not appear in the spectrum until the energy of the exciting electrons reaches the excitation potential shows that the process of excitation from the singlet ground state of the neutral molecule to the doublet state of the ionized molecule takes place at a single step. The probability of this type of excitation as a function of the energy of the exciting electrons should be calculable from theoretical considerations. The results of this experimental determination are believed to be sufficiently accurate to justify comparison with theoretical calculations whenever the calculations are made.

The author wishes to express his most sincere appreciation for the valuable discussions of Dr. M. L. Pool and Dr. H. P. Knauss during the progress of this investigation.

Theory of the Townsend Method of Measuring Electron Diffusion and Mobility

W. P. ALLIS AND HARRIET W. ALLEN
Massachusetts Institute of Technology, Cambridge, Massachusetts

(Received June 18, 1937)

The Lorentz method is applied to the combined drift and diffusion of the electron stream in the Townsend experiment. The zeroth-order approximation is found to lead to the equation found by Townsend. It is shown how the next approximation is obtained. The same method is then applied to the drift of electrons in crossed electric and magnetic fields. It is found that the magnetic field changes the energy distribution as well as the direction of drift. The latter is found in close agreement with Townsend, but not with Huxley.

TOWNSEND[1] measures the random motion of electrons in gases under the influence of an electric field E by means of an apparatus sketched in Fig. 1. Electrons liberated from the plate P pass through a circular hole at A and on down to a circular electrode C_2 with a ring electrode C_1C_3 around it. Potentials are applied to the various parts of the apparatus so as to insure a uniform field E from P to C. The ratio of the current to C_1C_3 to that to C_2 determines the ratio of the diffusion constant D to the drift velocity u_E, and hence the temperature T by the relation

$$T=eED/ku_E. \tag{1}$$

The drift velocity u_E is measured in a similar apparatus in which the circular hole is replaced by a slit and the electrodes C_1, C_2, C_3 are sections of a disk. The electron stream is deviated

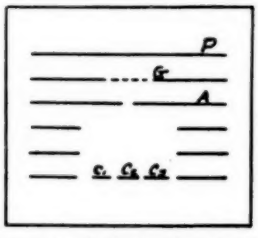

FIG. 1. Arrangement of electrodes used by Townsend for measuring random motion of electrons in gases.

by a magnetic field H directed parallel to the slit, and the angle of deviation is given by

$$\tan\theta=Hu/E. \tag{2}$$

The derivation of these relations is, however, not free from objections. The existence of a "temperature" implies a Maxwell distribution of velocities, yet it is known that the distribution cannot be Maxwellian. Druyvesteyn[2] has derived a distribution similar to the Maxwellian but with the energy squared, instead of to the first power, in the exponent.

The authors have therefore applied to the theory of these experiments the method originated by Lorentz[3] and extended by Morse, Allis and Lamar[4] to give both the drift velocities and the energy distribution. The method is superior to "mean free path" methods in that one does not average over velocities until the very last step, and hence can easily handle any velocity distribution or mean free paths which are a function of the velocity. Townsend[5] has recently tried to avoid the difficulty by considering groups of electrons of the same energy, but this is difficult as the groups do not stay together. The Lorentz method considers the electrons entering and leaving an element of volume fixed in phase space. It therefore resembles the Euler method in hydrodynamics whereas Townsend follows Lagrange.

The as yet unknown distribution f is expanded in surface harmonics in velocity space and only the linear terms are kept. This is well justified, as random motions are always much larger than the drift velocity. The thermal motions of the gas atoms are neglected compared to the motions of the electrons. Davydov[6] has shown how to correct for the thermal motions if it is necessary to do so. Collisions with atoms are considered to be elastic. This imposes an upper limit on the parameter E/p which will be investigated in the following paper by one of

[1] Townsend and Tizard, Proc. Roy. Soc. **88**, 336 (1913); Townsend and Bailey, Phil. Mag. **42**, 873 (1921).

[2] M. J. Druyvesteyn, Physica **10**, 61 (1934).
[3] H. A. Lorentz. *Theory of Electrons*, p. 269.
[4] Morse, Allis and Lamar, Phys. Rev. **48**, 412 (1935).
[5] J. S. E. Townsend, Phil. Mag. **22**, 145 (1936).
[6] D. Davydov, Physik. Zeits. Sowjetunion **8**, 59 (1935).

us. The probability of elastic scattering, $\sigma(v, \Theta)$ is, however, an arbitrary function of angle and velocity. The cross section for momentum transfer is then defined by

$$Q(v)=\int_0^\pi 2\pi(1-\cos\Theta)\sigma(v,\Theta)\sin\Theta d\Theta \quad (3)$$

and the mean free path by

$$\lambda(v, p)=1/NQ. \quad (4)$$

Interactions between electrons are neglected, and hence the theory applies only to electron densities which are very small in comparison to that of the gas.

The two cases of a circular hole and a slit at A are treated quite separately as cylindrical coordinates are appropriate to the first and cartesian coordinates to the second.

Mobility and Diffusion Coefficients

As a first approximation we shall neglect the diffusion sideways and assume the energy distribution to be that for the homogeneous case[7]

$$f_0=A\exp\left[-2\mu\int_0^\epsilon \epsilon d\epsilon/\epsilon_0^2\right], \quad (5)$$

where $\mu=3m/M$, $\epsilon_0=\lambda eE$, $\epsilon=\frac{1}{2}mv^2$ and the electron density

$$n=4\pi\int_0^\infty f_0 v^2 dv. \quad (6)$$

Eq. (7) of Morse, Allis and Lamar can then be applied directly, giving

$$f_1=(2\mu\epsilon/\epsilon_0)f_0-(\lambda/n)(dn/dz)f_0, \quad (7)$$

where we are using z instead of x. The drift velocity is then given by

$$u=-\frac{1}{n}\int\frac{\dot z^2}{v}f_1 d\gamma=\frac{8\pi}{3nm^2}\times\left[\int\frac{2\mu\epsilon^2}{\epsilon_0}f_0 d\epsilon-\frac{1}{n}\frac{dn}{dz}\int\lambda\epsilon f_0 d\epsilon\right]=u_E-(1/n)(dn/dz)D, \quad (8)$$

where u_E is the drift due to the field and D the diffusion constant. If the mean free path is constant, the two integrals are easily evaluated and give

$$u_E=\frac{\mu^{\frac{1}{2}}}{3\Gamma(3/4)}\left(\frac{2\pi\epsilon_0}{m}\right)^{\frac{1}{2}}.$$
$$D=\frac{\lambda}{3\Gamma(3/4)\mu^{\frac{1}{2}}}\left(\frac{2\epsilon_0}{m}\right)^{\frac{1}{2}}. \quad (9)$$

The cases of greatest interest, however, are those where λ is not constant and the above quantities must be determined by integrating.

Energy Distribution

Let r, θ, z be cylindrical coordinates, $\dot r$, $r\dot\theta$, $\dot z$ the corresponding velocities. Following Lorentz, we have

$$\frac{df}{dt}=\frac{\partial f}{\partial t}+\dot r\frac{\partial f}{\partial r}+\dot\theta\frac{\partial f}{\partial\theta}+\dot z\frac{\partial f}{\partial z}+\ddot r\frac{\partial f}{\partial\dot r}+\ddot\theta\frac{\partial f}{\partial\dot\theta}+\ddot z\frac{\partial f}{\partial\dot z}=b-a. \quad (10)$$

The first, third, and sixth term in the above expression vanish because we are considering a stationary state with cylindrical symmetry. In the fifth and seventh terms

$$\ddot r=r\dot\theta^2 \quad \text{and} \quad \ddot z=eE/m, \quad (11)$$

but the nature of these two accelerations is entirely different. The second is due to the applied electric field and takes place independently of the orthogonal velocity components $\dot r$ and $r\dot\theta$ and these therefore have to be kept constant in the partial derivative. On the other hand the radial acceleration is due to the curvature of the coordinate lines and takes place as the electron moves uniformly along a straight line. The derivative is therefore to be taken with v constant.

[7] Morse, Allis and Lamar, Eq. (14) which is incorrectly written.

$$\frac{df}{dt}=\dot{r}\frac{\partial f}{\partial r}+\dot{z}\frac{\partial f}{\partial z}+r\dot{\theta}^2\left(\frac{\partial f}{\partial \dot{r}}\right)_v+\frac{eE}{m}\left(\frac{\partial f}{\partial \dot{z}}\right)_{\dot{r},\,\dot{\theta}}=b-a. \tag{12}$$

We now substitute

$$f=f_0+(\dot{z}/v)f_1+(\dot{r}/v)f_2 \tag{13}$$

and replace the resulting quadratic terms by their average values

$$\langle\dot{z}^2\rangle_{Av}=\langle\dot{r}^2\rangle_{Av}=r^2\langle\dot{\theta}^2\rangle_{Av}=v^2/3,\quad \langle\dot{z}\dot{r}\rangle_{Av}=0 \tag{14}$$

$b-a$ can readily be obtained from Morse, Allis and Lamar by an obvious extension of their Eq. (6a). Equating separately the terms in v alone, in $\dot{z}$, and in $\dot{r}$ gives

$$\frac{\partial f_1}{\partial z}+\frac{1}{r}\frac{\partial}{\partial r}(rf_2)+\frac{eE}{mv^3}\frac{\partial}{\partial r}(v^2f_1)=\frac{\mu}{v^3}\frac{\partial}{\partial v}\left(\frac{v^4f_0}{\lambda}\right),\quad \frac{\partial f_0}{\partial z}+\frac{eE}{mv}\frac{\partial f_0}{\partial v}=-\frac{f_1}{\lambda},\quad \frac{\partial f_0}{\partial r}=-\frac{f_2}{\lambda}. \tag{15}$$

It is convenient now to use energy units

$$\zeta=zeE,\quad \rho=reE,$$

and further to substitute as independent variable $\eta=\epsilon-\zeta$ in place of ζ.

The above equations then become

$$\frac{1}{\rho}\frac{\partial}{\partial\rho}(\rho f_2)+\frac{1}{\epsilon}\frac{\partial}{\partial\epsilon}(\epsilon f_1)=\frac{2\mu}{\epsilon}\frac{\partial}{\partial\epsilon}\left(\frac{\epsilon^2f_0}{\epsilon_0}\right)+2\mu\frac{\epsilon}{\epsilon_0}\frac{\partial f_0}{\partial\eta},\quad \partial f_0/\partial\epsilon=-f_1/\epsilon_0,\quad \partial f_0/\partial\rho=-f_2/\epsilon_0. \tag{16}$$

It is noticed that the variable η which has replaced z no longer appears on the left-hand sides with the diffusion terms, but enters only in the term arising from the energy loss in collisions. If there were no energy losses, η, the total energy, would be a constant of the motion and hence fixed by the initial conditions and have no place in the differential equation.

It is now easy to eliminate f_1 and f_2 and separate the variables

$$\frac{1}{\rho}\frac{\partial}{\partial\rho}\left(\rho\frac{\partial f_0}{\partial\rho}\right)+\frac{1}{\epsilon_0\epsilon}\frac{\partial}{\partial\epsilon}\left(\epsilon_0\epsilon\frac{\partial f_0}{\partial\epsilon}\right)+\frac{2\mu}{\epsilon_0\epsilon}\frac{\partial}{\partial\epsilon}\left(\frac{\epsilon^2f_0}{\epsilon_0}\right)+\frac{2\mu\epsilon}{\epsilon_0^2}\frac{\partial f_0}{\partial\eta}=0. \tag{17}$$

Set

$$f_0=R(\rho)Z(\eta)E(\epsilon), \tag{18}$$

$$(1/\rho)(\partial/\partial\rho)(\rho\partial R/\partial\rho)=-a^2R,\quad R=J_0(a\rho),\quad \partial Z/\partial\eta=bZ,\quad Z=e^{b\eta}=e^{b(\epsilon-\zeta)}, \tag{19}$$

where a and b are the separation constants to be determined by the boundary conditions and the equation for $E(\epsilon)$ is

$$\frac{1}{\epsilon_0\epsilon}\frac{\partial}{\partial\epsilon}\left(\epsilon_0\epsilon\frac{\partial E}{\partial\epsilon}+\frac{2\mu\epsilon^2}{\epsilon_0}E\right)+\left(\frac{2b\mu\epsilon}{\epsilon_0^2}-a^2\right)E=0.$$

Substituting

$$E=\exp\left[-b\epsilon-2\mu\int_0^{\epsilon}\epsilon d\epsilon/\epsilon_0^2\right]G(\epsilon), \tag{20}$$

$$G''+\left(\frac{1}{\epsilon}+\frac{\epsilon_0'}{\epsilon_0}-2b-\frac{2\mu\epsilon}{\epsilon_0^2}\right)G'+\left(b^2-a^2-\frac{b}{\epsilon}-\frac{b\epsilon_0'}{\epsilon_0}+\frac{4b\mu\epsilon}{\epsilon_0^2}\right)G=0, \tag{21}$$

and finally the solution is expressed as a series

$$f_0=\exp\left[-2\mu\int\epsilon d\epsilon/\epsilon_0^2\right]\sum_i A_iJ_0(a_i\rho)\sum_k B_{ik}\exp\left[-b_{ik}\zeta\right]G_{ik}(\epsilon), \tag{22}$$

where the constants are determined by the boundary conditions at the plane $z=0$.

$$\sum B_{ik}G_{ik}(\epsilon)=1, \quad \sum_i A_i J_0(a_i\rho)=\begin{cases} A & \text{for } \rho<\rho_0 \text{ the radius of the hole,} \\ 0 & \text{for } \rho>\rho_0. \end{cases} \tag{23}$$

The equation for G is, however, not one that has been studied and therefore it would be difficult to determine the coefficients B_{ik} even if the characteristic values b_{ik} were known. It is better therefore to determine a single mean value $\bar{b}_i$ corresponding to each Bessel function $J_0(a_i\rho)$ and then solve Eq. (21) by power series or asymptotic series. The resulting function f_0 will satisfy the equation exactly but will not give quite the correct energy distribution at the hole.

To determine the best value for b one can first assume the energy distribution to be the same everywhere and given by Eq. (5). Townsend's[8] equation, converted to our notations, is then correct

$$\bar{b}_i^2+u\bar{b}_i/eED=a_i^2 \tag{24}$$

and u and D are given by Eq. (8). Solving for $\bar{b}_i$ and substituting in (21) one finds how much the energy distribution differs from that assumed, and substituting in (22) without summing over k one finds how the energy distribution varies from point to point, in first approximation.

Magnetic Deflection

We shall not attempt here the complete theory of the experiment with the magnetic field, but simply that of crossed electric and magnetic fields, leaving out diffusion. Using Cartesian coordinates and taking E and H along the x and z axes respectively, the problem reduces to the $x-y$ plane only. We have

$$\ddot{x}(\partial f/\partial\dot{x})+\ddot{y}(\partial f/\partial\dot{y})=b-a \tag{25}$$

with

$$\ddot{x}=(eE/m)+(eH/m)\dot{y}, \qquad \ddot{y}=-(eH/m)\dot{x}. \tag{26}$$

Setting

$$f=f_0+(\dot{x}/v)f_1+(\dot{y}/v)f_2 \tag{27}$$

and proceeding as before one obtains

$$\frac{eE}{mv^3}\frac{\partial}{\partial v}(v^2f_1)=\frac{\mu}{v^3}\frac{\partial}{\partial v}\left(\frac{v^4f_0}{\lambda}\right), \tag{28}$$

$$\frac{eE}{mv}\frac{\partial f_0}{\partial v}-\frac{eH}{mv}f_2=-\frac{f_1}{\lambda}, \tag{29}$$

$$(eH/mv)f_1=-f_2/\lambda. \tag{30}$$

The last two equations correspond to Huxley's[9] Eq. (24). Huxley has, however, already averaged over all velocities. Defining θ by

$$\tan\theta=f_2/f_1$$

and following Huxley one gets

$$\frac{f_1}{\partial f_0/\partial v}=-(E/2H)\sin 2\theta.$$

Averaging over velocities now does not lead to Huxley's Eq. (25).

Equations (28), (29), (30) are easily integrated and give

$$\log f_0=-\int\frac{2\mu\epsilon}{\epsilon_0^2}d\epsilon-\frac{\mu\epsilon}{m}\frac{H^2}{E^2}, \tag{31}$$

$$f_1=\frac{2\mu\epsilon}{\epsilon_0}f_0, \tag{32}$$

$$f_2=\frac{H\epsilon_0}{Emv}f_1=-\mu\frac{Hv}{E}f_0. \tag{33}$$

Eq. (31) shows that the magnetic field reduces the number of high velocity electrons. Eq. (32) shows that the drift down the electric field of electrons of a given energy is not altered by the magnetic field. This is, however, because of the change in the energy distribution. If f_0 were not allowed to change, (32) would not be true. Eq. (33) shows that the sideways drift increases with v. Comparing (32) and (33) shows that $\tan\theta$ varies inversely as v, so that the high velocity electrons are relatively little affected.

The average drift velocities are given by

$$u_x=\frac{1}{n}\int\frac{\dot{x}^2}{v}f_1d\gamma=\frac{2\pi}{3n}\frac{8\mu}{m^2}\int\frac{\epsilon^2}{\epsilon_0}f_0d\epsilon,$$
$$u_y=\frac{1}{n}\int\frac{\dot{y}^2}{v}f_2d\gamma=\frac{4\pi}{3n}\frac{H}{E}\mu\int v^4f_0dv. \tag{34}$$

[8] J. J. Thomson and G. P. Thomson, *Conduction of Electricity through Gases*, p. 82.

[9] L. G. H. Huxley, Phil. Mag. **23**, 226 (1937).

These integrals are easily evaluated as power series in $\sqrt{\mu}(Hv_0/E)^2$, where $\frac{1}{2}mv_0^2=\lambda eE$, and give, in terms of the drift velocity without the magnetic field u_E

$$u_x=u_E[1-0.195(\mu)^{\frac{1}{2}}(Hv_0/E)^2+\cdots], \quad (35)$$

$$\frac{u_y}{u_x}=\frac{3}{2(2)^{\frac{1}{2}}}\frac{Hu_E}{E}=1.06\frac{Hu_E}{E}. \quad (36)$$

It is this last formula which Townsend used to measure u_E and it is seen that the numerical factor differs insignificantly from his value 1.

OCTOBER 1, 1937 PHYSICAL REVIEW VOLUME 52

Electron Temperatures and Mobilities in the Rare Gases

HARRIET W. ALLEN
Massachusetts Institute of Technology, Cambridge, Massachusetts

(Received June 28, 1937)

The results of the theory developed by Allis and Allen are applied to the computation of electron "temperatures" and drift velocities in the rare gases; helium, neon and argon. Curves are given showing the effect of the variable cross sections on the distribution function in the three cases. A distribution function is derived to account for energy lost by inelastic impact at higher values of E/p. This distribution function depends on an adjustable parameter, ϵ_1 which has a value between the first resonance potential and the ionization potential, since it is assumed that the number of electrons with energies above ϵ_1 is negligible. Curves are given comparing the computed values of electron "temperatures" and drift velocities with experimental values. In most cases the check is good.

1. ELASTIC COLLISIONS ONLY

THE rare gases helium, neon, and argon offer an excellent opportunity to check the results of the theory developed in the previous paper by Allis and Allen, of the diffusion and drift velocity of electrons in these gases. The angular distribution of electrons scattered from these gases has been measured down to very low velocities by Ramsauer and Kollath[1] and by Normand[2] and these measurements allow the computation of cross sections for momentum transfer Q. It is found that helium has a falling curve, neon one which is practically flat, while argon has one which rises sharply (Fig. 1). The energy distribution in these three gases will consequently vary greatly on this account as well as because of the greatly differing masses. The argon curve cuts off more sharply on the high energy side. Furthermore the drift velocity u_E and the diffusion coefficient D correspond to the averages of $(\mu/\lambda E)v^3$ and λv, respectively; $\mu=3m/M$, three times the ratio of the masses of the electron and the gas molecule, λ is the mean free path, $1/NQ$. The quantity which is given by Townsend[3] as a result of his measurements is

$$T=eED/ku_E \quad (1)$$

and would be the temperature if the electrons had a Maxwell distribution. In the above expression e is the electron charge, E the field strength and k the Boltzmann constant. Formulae (9) of Allis and Allen show that for a constant cross section T should be proportional to $E\lambda/\mu^{\frac{1}{2}}$ but when the cross section varies it is

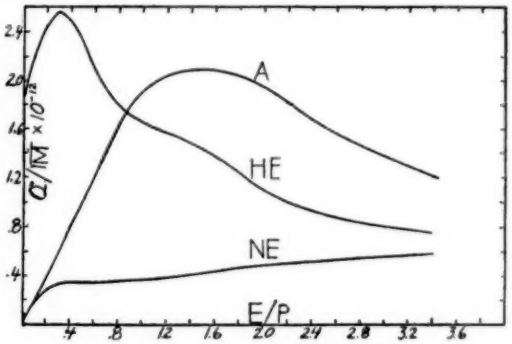

FIG. 1. Cross section in sq. A divided by the square root of the mass. This is the quantity which determines the mean energy $\bar{\epsilon}$ of the electrons.

[1] C. Ramsauer and R. Kollath, Ann. d. Physik (5) **12**, 529 (1932).
[2] C. E. Normand, Phys. Rev. **35**, 1217 (1930).
[3] J. S. Townsend, *Electricity in Gases* (Clarendon Press, Oxford, 1915).

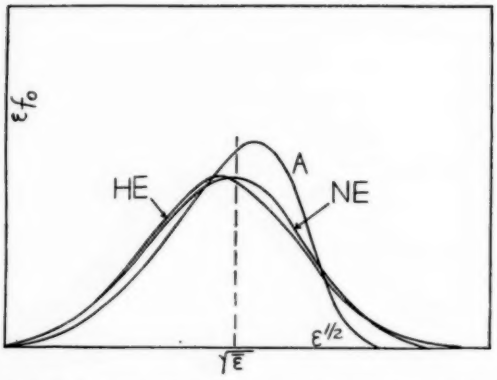

FIG. 2. Effect of variable cross section on the distribution function. The abscissae are chosen so as to give the same mean energy.

proportional to the more complicated function given by the ratio of the above averages (Fig. 2).

In the case of argon there are also probe measurements of "temperature" by Seeliger and Hirchert[4] and by Groos.[5] These are difficult to interpret since the probe measurement curves are not given. They should, if the theory is correct, be parabolic, and if the best representative straight were passed through the points at low currents where the scale is stretched the resulting "temperature" would tend to be lower than $2\bar{\epsilon}/3k$ where $\bar{\epsilon}$ is the average energy. The curve for the average energy as a function of E/p, expressed in volts per cm per mm of mercury gas pressure, is given on the figure for comparison.

The drift velocities agree fairly well with the experimental points for low E/p but are in all cases somewhat too low.

2. Inelastic Collisions

For higher values of E/p the experimental results depart markedly from the theory; "temperatures" approach a constant value and drift velocities increase more rapidly. It is evident from this that electrons with energies above the first resonance potential are undergoing inelastic collisions. This will modify the distribution function not only in the high energy range but also where collisions are purely elastic, as Smit[6] has shown. Indeed as electrons of high energy are being continually removed from the distribution and returned with very little energy, there must be an excess of energy all through the lower energy brackets. Eq. (10) of Morse, Allis and Lamar[7] representing energy unbalance can be written

$$8\pi eE\epsilon/3m^2[f_1-2\mu\epsilon f_0/\epsilon_0]=-j, \qquad (2)$$

where j measures the degree of unbalance. $-j$ represents the net number of electrons crossing a certain energy level per second, f_0 and f_1 determine the random distribution in velocity and the electron drift respectively and $\epsilon_0=\lambda eE$. Let us write F_0 for the equilibrium distribution,

$$\log F_0=-2\mu\int_0^{\epsilon}\frac{\epsilon}{\epsilon_0^2}d\epsilon.$$

Since $$f_1=-\epsilon_0\partial f_0/\partial\epsilon$$

the solution of Eq. (2) is

$$f_0=j\frac{3m^2}{8\pi eE}\frac{1}{F_0}\int_{\epsilon_1}^{\epsilon}\frac{\epsilon_0}{\epsilon}F_0d\epsilon.$$

When the cross section is reasonably constant the integral is readily evaluated in terms of exponential integrals $\bar{E}i$ tabulated in Jahnke Emde[8]

$$f_0=B[\exp -2\mu\epsilon^2/\epsilon_0^2][\bar{E}i(2\mu\epsilon_1^2/\epsilon_0^2)-\bar{E}i(2\mu\epsilon^2/\epsilon_0^2)].$$

This distribution function should hold up to the first resonance potential where it should be

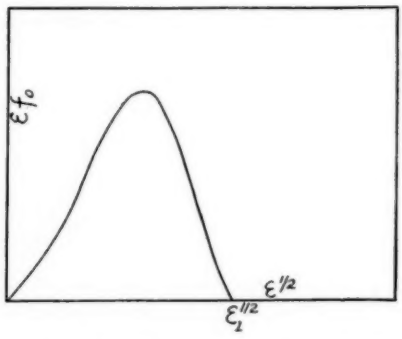

FIG. 3. Distribution with inelastic impacts. This distribution is probably correct over most of the range but should go rapidly to zero instead of cutting the axis at $(\epsilon_1)^{\frac{1}{2}}$.

[4] R. Seeliger and R. Hirchert, Ann. d. Physik (5) **11**, 817 (1931).
[5] O. Groos, Zeits. f. Physik **88**, 714 (1934).
[6] J. A. Smit, Physica **6**, 453 (1936).
[7] Morse, Allis and Lamar, Phys. Rev. **48**, 412 (1935).
[8] Jahnke and Emde, *Tables of Functions*, second edition (B. G. Teubner, Leipzig, 1923).

joined by some other function whose form will depend on the total inelastic cross section at all energies above the resonance potential. As this is an unknown quantity some simpler assumption must be made. The simplest is to keep the above distribution function up to the point where it crosses the axis for $\epsilon=\epsilon_1$ leaving ϵ_1 as an adjustable parameter which should, however, fall between the first resonance potential and the ionization potential. There is some justification for assuming that there are practically no electrons above a certain energy in the measurements of Kelly[9] who finds that in helium the distribution follows a smooth curve attaining the axis at about the second resonance potential (Fig. 3).

Another point should be mentioned. f_0 has a logarithmic infinity at the origin. This is because the electrons suffering inelastic collisions have been assumed to lose all their energy and therefore tend to accumulate somewhat at the origin. Better assumptions might be made but they would not change the drift velocities or "temperatures" as the slow electrons do not contribute appreciably to these quantities.

3. Results

Helium

The "temperature" curve starts with a slight positive curvature corresponding to a falling cross-section curve, but breaks away from this trend at $E/p=2$. The "temperatures" are always most sensitive to inelastic impacts and so were used to fix the parameter ϵ_1. In this case setting it at the first excitation potential, 19.7 volts, gives a calculated curve agreeing exactly with the data of Townsend and Bailey.[10]

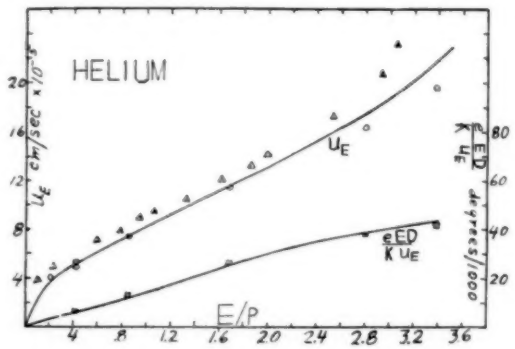

FIG. 4. Electron "temperatures" and drift velocities in helium. The experimental points □ are "temperatures" obtained by the Townsend method. The experimental points ⊙ and △ are drift velocities obtained by the Townsend method and by Neilsen, respectively. The same symbols are used in Figs. 5 and 6. The full line curves are computed using the distribution function corrected for ionization.

[9] H. C. Kelly, Doctor's Thesis, Massachusetts Institute of Technology, June 1936.

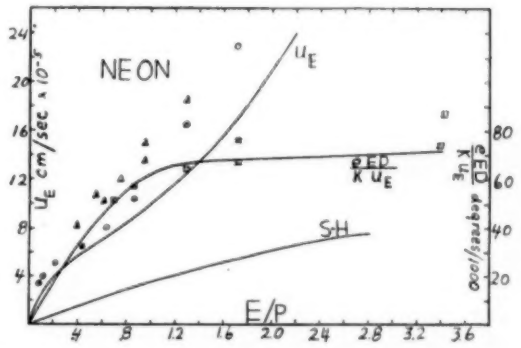

FIG. 5. Electron "temperatures" and drift velocities in neon. The curve marked *S–H* gives "temperatures" derived from the probe measurements of Seeliger and Hirchert. The theoretical curves were obtained using a constant cross section $Q=2.5$ sq. *A*.

The drift velocity curve starts as a parabola but soon curves upward since drift velocities vary as $\lambda^{\frac{1}{2}}$ and λ is increasing. The calculated curve is the same whether ϵ_1 is taken at 19.7 volts or at infinity. Inelastic collisions increase the drift velocity through decreasing the mean energy $\bar{\epsilon}$. In helium this also increases ϵ_0 thus tending to decrease the drift. The two effects seem to compensate exactly (Fig. 4).

Neon

The formulae for a constant cross section may here be used and give a straight line for the "temperature" and a parabola for the drift. The former agrees exactly with the results of the Townsend method as applied by Bailey[11] and the latter fairly well with Bailey[11] and with Neilsen[12] up to about $E/p=0.6$. Putting ϵ_1 at the ionization potential, 21.5 volts, brings exact agreement for the "temperatures" whereas the drift velocities would seem to require a lower value. The "temperatures" from the probe measurements of Seeliger and Hirchert[4] are also shown on the figure although they seem to have no relation to the other values (Fig. 5).

[10] J. S. Townsend and V. A. Bailey, Phil. Mag. **46**, 657 (1923).
[11] V. A. Bailey, Phil. Mag. **47**, 379 (1924).
[12] R. A. Neilsen, Phys. Rev. **50**, 950 (1936).

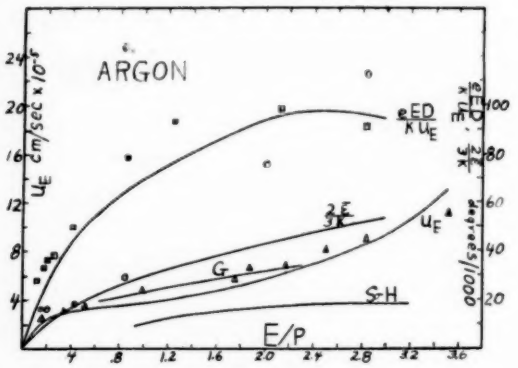

FIG. 6. Electron "temperatures" and drift velocities in argon. The curves marked *S–H* and *G* are "temperatures" derived from the probe measurements of Seeliger and Hirchert and of Groos, respectively.

Argon

Argon has the greatest Ramsauer effect of any gas. The result is that its "temperature" defined by formula (1) instead of being very nearly equal to $2\bar{\epsilon}/3k$ as it is when the cross section is constant, is very much greater. The two quantities are shown in Fig. 6 and it is seen that Townsend's[13] measurements agree fairly well with formula (1). On the other hand the probe measurements of Groos[5] and of Seeliger and Hirchert[4] are of the order of $2\bar{\epsilon}/3k$. Using $\epsilon_1=15.6$, the ionization potential, gives agreement at the top end of the curve.

Calculated drift velocities agree fairly well for low values of E/p though they are a bit low, as in the case of neon. At large E/p the use of 15.6 for ϵ_1 is quite inadequate to give the measured drifts, whereas $\epsilon_1=11.57$, the first critical potential gives excellent agreement with the measurements of Neilsen.[12] This value of ϵ_1, however, gives "temperatures" which are far too low. Townsend's measured velocities are far larger and are impossible of explanation on this theory.

In conclusion it may be said that "temperatures" and drift velocities may be calculated without any adjustable parameters and give excellent agreement with experiment for low values of E/p. The peculiarities of the "temperature" of argon are explained by its varying cross section. At large values of E/p where inelastic collisions are important their effect can in general be represented by choosing a single parameter, ϵ_1, which must lie in the range of the excitation potentials. The two measurements in argon cannot however be explained by the same parameters.

[13] J. S. Townsend and V. A. Bailey, Phil. Mag. **44**, 1033 (1922).

OCTOBER 1, 1937 PHYSICAL REVIEW VOLUME 52

Plasma Electron Drift in a Magnetic Field with a Velocity Distribution Function

LEWI TONKS, *General Electric Company, Schenectady, N. Y.*
AND
W. P. ALLIS, *Massachusetts Institute of Technology, Cambridge, Massachusetts*

(Received June 18, 1937)

Previous calculations of the drift motion of electrons moving through a gas under the combined action of electric and magnetic fields and concentration gradient have been based upon inexact averaging methods. For electrons which, like arc plasma electrons, have a Maxwell distribution to a first approximation, the first-order correction to the distribution function which arises from drift motion is now calculated. This permits exact averaging of component velocities to be carried out. The resulting equations are compared with Townsend's earlier results. Tonks' theorem that "the drift speed is the same as would occur if the components of concentration gradient and electric field perpendicular to it, as well as the magnetic field itself did not exist" is found to hold within 12 percent.

THE detailed analysis in terms of a distribution function of the motion of electrons in a magnetic field given by W. P. Allis and H. W. Allen[1] makes it possible to replace the previously approximate expressions for the drift motion of electrons[2] in a magnetic field with exact expressions.

[1] W. P. Allis and H. W. Allen, Phys. Rev. **52**, 703 (1937).

[2] J. S. Townsend, *Electricity in Gases*, §§89–92. L. G. H. Huxley, Phil. Mag. **23**, 210 (1937).

The case to be treated is that in which the magnetic field is in the z direction. The electric field and concentration gradient components in the z direction are assumed to be zero, since motion in this direction is independent of H and takes place according to well-known laws. With Allis and Allen we assume that the distribution function f giving the number of electrons per unit volume of ξ, η, ζ, x, y, z (velocity-displacement) phase space is

$$f=f_0(v, x, y)+(\xi/v)f_1(v, x, y)+(\eta/v)f_2(v, x, y), \quad (1)$$

where $v^2=\xi^2+\eta^2+\zeta^2$.

This is in accordance with the reasoning of Morse, Allis, and Lamar.[3] The analysis leads to three equations between f_0, f_1 and f_2 (Allis and Allen's Eqs. (28), (29), and (30)), of which the first gives the energy balance and the second and third the momentum balance in the x and y directions respectively.

The first equation is of importance in determining f_0 from the energy transfers which involve the electrons. The equation is based on two types of interchange. The first is the work done on the electrons by the electric field and the second is the energy elastically transferred to atoms on impact. In an arc plasma, however, other transfer mechanisms operate, namely loss of energy in inelastic impacts and probably direct interchange of energy between electrons. We must, therefore, abandon this equation and in its place use for f_0 the Maxwell distribution

$$f_0=\pi^{-\frac{3}{2}}w^{-3}n\epsilon^{-v^2/w^2}, \quad (2)$$

to which experiment shows that electrons conform in many cases. Here n is the electron density and w^2 is 2/3 of the mean square velocity C^2. In terms of electron temperature T and average electron speed $\bar{c}$

$$w^2=2kT/m=(\pi/4)\bar{c}^2. \quad (3)$$

The second and third equations have to be filled out by the inclusion of a y component of electric field E_y and also by concentration gradient terms which can obviously be added on the basis of the Morse-Allis-Lamar Eq. (7). We then have

$$\begin{aligned} eE_x\partial f_0/\partial v+mv\partial f_0/\partial x-Hef_2&=-mvf_1/\lambda,\\ eE_y\partial f_0/\partial v+mv\partial f_0/\partial y+Hef_1&=-mvf_2/\lambda, \end{aligned} \quad (4)$$

from which to determine f_1 and f_2. We shall assume that λ is independent of v, although it will appear that theoretically its variation with v can be included in the treatment.

Substitution in Eqs. (4) from (2) gives

$$\begin{aligned} -\pi^{-\frac{3}{2}}w^{-3}\epsilon^{-v^2/w^2}n\lambda b_x-(v_h/v)f_2+f_1&=0,\\ -\pi^{-\frac{3}{2}}w^{-3}\epsilon^{-v^2/w^2}n\lambda b_y+(v_h/v)f_1+f_2&=0, \end{aligned} \quad (5)$$

where

$$\begin{aligned} b_x&=eE_x/(kT)-\partial \ln n/\partial x,\\ b_y&=eE_y/(kT)-\partial \ln n/\partial y, \end{aligned} \quad (6)$$

$$v_h=\lambda eH/m. \quad (7)$$

It is worth noting that the electric field and density gradient components enter Eqs. (5) through the b's only and that the b's are themselves gradients of the function

$$B=-eV/(kT)-\ln n,$$

which is directly related to the Boltzmann equation. In the absence of magnetic field $(\lambda\bar{c}/3)B$ is the velocity potential for electron drift. Its space derivatives are still fundamental in the presence of a magnetic field. That the equations develop in this way is a consequence of the fact that a magnetic field does not destroy the validity of Boltzmann's equation.[4]

It is evident that v must enter f_1 and f_2 in Eqs. (5) in the exponential form. Accordingly, we set

$$f_1=\pi^{-\frac{3}{2}}w^{-3}nA_1\epsilon^{-v^2/w^2}, \quad f_2=\pi^{-\frac{3}{2}}w^{-3}nA_2\epsilon^{-v^2/w^2} \quad (8)$$

with A_1 and A_2 to be determined by substitution in Eqs. (5). The solution of the resulting simultaneous equations gives

$$\begin{aligned} A_1&=\lambda[b_x+(v_h/v)b_y]/[1+(v_h/v)^2],\\ A_2&=\lambda[b_y-(v_h/v)b_x]/[1+(v_h/v)^2], \end{aligned} \quad (9)$$

thus completing the specification of f_1 and f_2.

The flux of electrons in the x direction is

$$n\bar{\xi}=4\pi\int_0^\infty \xi v^2 f dv=4\pi\int_0^\infty v\xi^2 f_1 dv$$

[3] P. M. Morse, W. P. Allis, and E. S. Lamar, Phys. Rev. **48**, 412 (1935).

[4] L. Tonks, Phys. Rev. **51**, 744 (1937).

and since ξ^2 can be replaced[3] by $v^2/3$,

$$n\bar{\xi}=(4\pi/3)\int_0^\infty v^3 f_1 dv.$$

In the course of the indicated integration we require the value of

$$J=\int_0^\infty \frac{\epsilon^{-px^2}}{1+x^2}dx=\pi^{\frac{1}{2}}\epsilon^p\int_{p^{\frac{1}{2}}}^\infty \epsilon^{-z^2}dz,$$

which does not appear in the tables. The value given was found by the process

$$\epsilon^p\int_\infty^p \frac{d(J\epsilon^{-p})}{dp}dp,$$

the x integration being carried out after taking the derivative with respect to p.

The result of the integration is

$$\bar{\xi}=(\lambda\bar{c}/3)(\alpha b_x+\beta b_y), \tag{10}$$

where
$$\alpha=1-h^2+h^4\epsilon^{h^2}Ei(h^2), \tag{11}$$

$$\beta=(\pi^{\frac{1}{2}}/2)h[1-2h^2+2\pi^{\frac{1}{2}}h^3\epsilon^{h^2}\text{erf }(h)], \tag{12}$$

$$h=v_h/w, \quad Ei(x)=\int_x^\infty(\epsilon^{-x}/x)dx,^5$$

$$\text{erf }(x)=2\pi^{-\frac{1}{2}}\int_x^\infty \epsilon^{-x^2}dx. \tag{13}$$

In terms of the Larmor precession, $\omega=eH/m$

$$h=\omega\lambda/w. \tag{14}$$

For the y drift

$$\bar{\eta}=(\lambda\bar{c}/3)(\alpha b_y-\beta b_x). \tag{15}$$

For small values of h

$$\alpha=1-h^2+h^4(\ln h^2+0.5772+\cdots), \tag{16}$$

$$\beta=(\pi^{\frac{1}{2}}/2)h[1-2h^2+2\pi^{\frac{1}{2}}h^3+\cdots]. \tag{17}$$

For large values of h

$$\alpha=2h^{-2}[1-3h^{-2}+12h^{-4}+\cdots]. \tag{18}$$

$$\beta=(3/4)\pi^{\frac{1}{2}}h^{-1}[1-(5/2)h^{-2}+(35/4)h^{-4}+\cdots]. \tag{19}$$

[5] This is in accord with G. A. Campbell and R. M. Foster, "Fourier Integrals for Practical Application," Bell Telephone System Monograph B-584 (1931). Jahnke-Emde, *Tables of Functions* (1933) on p. 78 denote this integral as $-Ei(-x)$.

The table gives values for α and β for a range of values of h.

h	0	0.2	0.4	1.0	2.0	5.0	10.0
α	1.0	0.964	0.882	0.595	0.300	0.0716	0.0194
β	0.0	0.1671	0.295	0.457	0.44	0.243	0.130

In the present notation Townsend's result (amended[4]) is

$$\bar{\xi}=(\lambda\bar{c}/3)\frac{b_x+(\pi^{\frac{1}{2}}/2)hb_y}{1+(\pi/4)h^2}. \tag{20}$$

For small h this gives both α and β correctly to the lowest order in each. For large h, and again to the lowest order, his α is $2/\pi$ and his β is $8/(3\pi)$ of the proper value. Thus the agreement is surprisingly good. Considering ease of mathematical manipulation Eq. (20) is probably as good a simple approximation over the whole range of h as is possible where the basic distribution is Maxwellian.

Of particular interest is the modification which may be necessary to the theorem that the motion in the direction of drift is that which would be caused by the potential and concentration gradients in that direction alone with all other components and also the magnetic field eliminated.[4]

Since any deviations will be most marked for a drift perpendicular to the magnetic field, we shall assume that the drift lies in the xy plane and shall orient the x and y axes so that the flow is in the x direction. Then $\bar{\eta}$ is zero and

$$b_y=(\beta/\alpha)b_x,$$

whence
$$\bar{\xi}=(\lambda\bar{c}/3)(\alpha+\beta^2/\alpha)b_x. \tag{21}$$

Accordingly, for small h, using Eqs. (17) and (18)

$$\bar{\xi}=(\lambda\bar{c}/3)[1-(1-\pi/4)h^2]b_x$$
$$=(\lambda\bar{c}/3)[1-0.2146h^2]b_x \tag{22}$$

and for large h, using Eqs. (19) and (20),

$$\bar{\xi}=(\lambda\bar{c}/3)(9\pi/32)[1+(64/9\pi-2)h^{-2}]b_x, \tag{23}$$
$$=0.883(\lambda\bar{c}/3)[1+0.2635h^{-2}]b_x.$$

Thus the theorem is accurate to within 12 percent over the whole range of field strength.

Note added July 11, 1937. Expressions corresponding to our α and β are given without references in Knoll, Ollendorf and Rompe, Gasentladungstabellen, Sections *f*7 and *f*12. In the former, on page 47, the ratio of transverse

diffusion coefficient with magnetic field to that without magnetic field is given. This agrees, as it should, with our α. In the latter, on page 51, the ratio of drift parallel to the electric field with magnetic field to that without is given and also the ratio of transverse drift with magnetic field to parallel drift without. These should, but do not, agree with our α and β, respectively. In the absence of references it has not been possible to determine the source of the differences, but it probably lies either in the method used in averaging over the velocity distribution or in the assumptions, perhaps tacit, regarding that distribution.

OCTOBER 1, 1937 PHYSICAL REVIEW VOLUME 52

The Coupling of p Electron Configurations

HOWARD A. ROBINSON* AND GEORGE H. SHORTLEY
Mendenhall Laboratory of Physics, Ohio State University, Columbus, Ohio

(Received July 15, 1937)

The structure and type of coupling of the observed p^2, p^3, and p^4 configurations is considered in detail in terms of the intermediate-coupling theory, in particular for the long isoelectronic sequences which have recently been analyzed. The theoretical values of the ratios of various intervals in these configurations are plotted as functions of the single parameter which specifies the type of coupling. The experimental values have been fitted to these curves and the parameters evaluated. The points fit the theoretical curves fairly well; and the departures of the experimental points of an isoelectronic sequence from these curves are sufficiently regular to enable accurate prediction of unknown levels. This method has yielded new classifications in K IV and Ca VII. For the configurations p^3 and p^3s, interval ratios are found which are predicted to be entirely independent of coupling. The parameters are plotted for the isoelectronic sequences of sp, p, p^2, p^3, p^4, p^5, and p^5s configurations. The electrostatic interaction parameter F_2 is found to be a linear function of Z to a good approximation; the spin-orbit parameter ζ_p is accurately proportional to $(Z-S)^4$ for all but the first few members of each sequence. The screening constants (S) for ζ_p are much smaller than the corresponding screening constants for F_2. A complete bibliography of data for those atoms with p electrons in the normal configuration is appended.

Introduction

Recent progress[1] in the analysis of isoelectronic spectra has now made possible a thorough comparison of the intermediate-coupling theories with experiment for those elements containing equivalent p electron groups. The manner in which the energy of the various levels is predicted to vary with the coupling is shown by Fig. 1. These diagrams, but with only a few data superposed, were given by Condon and Shortley.[2] The size of the parameter χ measures essentially the departure from Russell-Saunders coupling ($\chi=0$). For pure jj coupling $\chi=\infty$ $(1/\chi=0)$. χ is defined as the ratio of the spin-orbit interaction integral ζ_p (C-S 4[5]4) to the electrostatic integral $5F_2$ (C-S page 177). Diagrams of this type are very compact and give a clear picture of the manner in which the relative values of the various energy intervals vary with the coupling. In actual practice, however, they are inconvenient to apply to experimental results because of the various scale factors involved and are inadequate for either extreme, $\chi\ll1$ or $\chi\gg1$, where certain of the intervals become very small compared to the rest. These difficulties are obviated in what follows by using ratios between directly observed energy intervals; these are calculated from theory and plotted directly against χ.

In the theory for the p^2, p^3, and p^4 configurations, the ratio of any two intervals (e.g. $^1S_0-{}^1D_2$ and $^3P_2-{}^3P_1$) is completely determined by χ alone. Thus in these configurations, if *any* three levels are known, χ may be predicted and the positions of the other levels as well. For example, a knowledge of the Landé ratio for a triplet term should predict absolutely the position of the two singlet terms arising from a p^2 or p^4

* Now at Central Technical Laboratory, Armstrong Cork Company, Lancaster, Pennsylvania.

[1] For a complete bibliography see the last section of this paper.

[2] Condon and Shortley, *Theory of Atomic Spectra* (Cambridge, 1935). For the general theory and notation used in this paper see chapters XI and XIII of this book. In what follows this reference will be denoted as C-S.

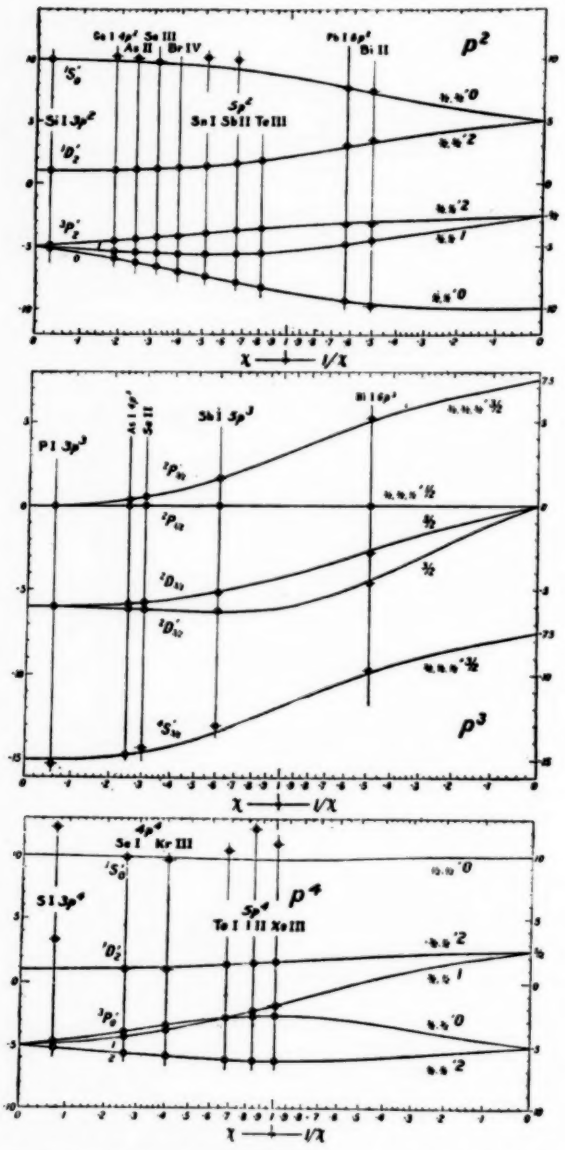

FIG. 1. *The configurations np^2, np^3, and np^4 in intermediate coupling.* Here are plotted quantities such as $(^1D-F_0)/F_2(1+\chi^2)^{\frac{1}{2}}$ [cf. Eq. (1)], that is, the energy intervals here are measured in units $F_2(1+\chi^2)^{\frac{1}{2}}$. Superposed are all data for $n=4$, 5, 6, and the first member of each sequence for $n=3$. In the original figures of C-S, the χ value and scale to use for the p^2 and p^4 data was determined by making $^3P_1$, the mean of $^1S_0$ and $^3P_0$, and the mean of $^1D_2$ and $^3P_2$ fit exactly. Near *LS* coupling this method of choosing χ has little significance when the configurations are somewhat perturbed; e.g., it gives a *negative* value for χ for S I $3p^4$. Since $\chi=\zeta_p/5F_2$ and since the triplet splitting essentially measures ζ_p and the distance between terms is a measure of F_2, it seems most significant to choose χ by making a pair of intervals—one a term splitting, the other a distance between terms—fit precisely. The intervals chosen are: for p^2, $^3P_2-{}^3P_0$ and $^1D-{}^3P_c$; for p^3, $^2P_{1\frac{1}{2}}-{}^2P_{\frac{1}{2}}$ and $^2P_c-{}^2D_c$; for $3p^4$ and $4p^4$, $^3P_1-{}^3P_2$ and $^1S-{}^1D$; for $5p^4$, $^3P_1-{}^3P_2$ and $^1D-{}^3P_c$. $6p^2$ and $6p^3$ are plotted as in C-S. This is the method used in obtaining the parameters of Tables VI, VII, and VIII.

configuration. It is our purpose to test these conclusions in detail.

The only other configurations for which all interval ratios are a function of but one parameter are those of the type *ls* and $l^{m-1}s$ (*ps*, p^5s, *ds*, d^9s, etc.). These are considered in C-S, pp. 272, 304. In certain of these cases the theory has proved of considerable use in locating the singlet by means of the observed Landé ratio of the triplet.[3]

We shall consider only the "Russell-Saunders half" of the diagrams ($\chi=0$ to $\chi=1$) as most of the experimental values lie in this range. We shall for convenience use the *LS* term designation throughout. In general other types of ratios than those which we consider would be of interest in the "*jj* half" ($\chi=1$ to $\chi=\infty$).

The p^2 configuration

The secular equations for this configuration are given in C-S, page 274. If we write the equation for ^1D in the form

$$(^1D-F_0)/F_2=-2+\tfrac{1}{45}\zeta_p/F_2 + [9-\tfrac{3}{25}\zeta_p/F_2+\tfrac{9}{16}(\zeta_p/F_2)^2]^{\frac{1}{2}} = -2+\tfrac{3}{4}\chi+[9-\tfrac{15}{2}\chi+\tfrac{225}{16}\chi^2]^{\frac{1}{2}}, \quad (1)$$

with similar equations for the remaining four terms, expressions for such ratios as $(^3P_2-{}^3P_0)/$

TABLE I. *Configuration p^2: Theoretical interval ratios as a function of χ.*

χ	$\frac{^3P_2-{}^3P_0}{^1S-{}^1D}$	$\frac{^3P_2-{}^3P_0}{^1S-{}^3P_c}$	$\frac{^3P_2-{}^3P_0}{^1D-{}^3P_c}$	$\frac{^1S-{}^1D}{^1D-{}^3P_c}$	$\frac{^3P_2-{}^3P_1}{^3P_1-{}^3P_0}$
0	0	0	0	1.5	2
0.02	0.0168	0.0101	0.0252	1.4999	1.932
.04	.0335	.0201	.0503	1.4989	1.867
.08	.0674	.0404	.1009	1.4952	1.751
.12	.1015	.0607	.1510	1.4880	1.643
.16	.1357	.0810	.2010	1.4801	1.546
.20	.1700	.1012	.2495	1.4683	1.460
.24	.2040	.1210	.2970	1.4538	1.378
.28	.2380	.1402	.3415	1.4365	1.307
.32	.2720	.1598	.3860	1.4168	1.238
.36	.3060	.1782	.4270	1.3946	1.175
.40	.3400	.1962	.4655	1.3704	1.117
.48	.4065	.2307	.535	1.3168	1.012
.56	.473	.2640	.596	1.2584	0.926
.64	.539	.2940	.645	1.1975	0.844
.72	.605	.3215	.687	1.1361	0.774
.80	.670	.3470	.720	1.0760	0.713
.88	.736	.3713	.749	1.0180	0.659
1.00	.835	.403	.782	0.9367	0.592

[3] E.g., H. A. Robinson, Phys. Rev. **49**, 301 (1935), Table V.

$(^1S-^1D)$ in terms of χ follow immediately. The ratios whose numerical values are listed in Table I and plotted in Fig. 2 are of three types. The first type consists of ratios between the triplet splitting and the distances between terms; in what follows they will be called *coupling ratios* inasmuch as they are all zero for pure LS coupling and start increasing linearly with χ. If ^3P_c denotes the centroid of the triplet term (the mean of the levels weighted according to $2J+1$), these ratios are given by $(^3P_2-^3P_0)/(^1D-^3P_c)$; $(^3P_2-^3P_0)/(^1S-^1D)$; and $(^3P_2-^3P_0)/(^1S-^3P_c)$.

The second type is the familiar *Landé ratio* $(^3P_2-^3P_1)/(^3P_1-^3P_0)$. In the LS limit this ratio is 2 but it departs rapidly from this value, decreasing linearly with χ. When the triplet has as yet only 0.085 of the total configuration spread ($\chi=0.18$), it has already fallen to 1.5. It begins to decrease according to the relation

$$(^3P_2-^3P_1)/(^3P_1-^3P_0)=2-\tfrac{7}{2}\chi+{}^{1\,2}\tfrac{5}{2\,4}\chi^2+\cdots.$$

This relation may be obtained either from the energy formulas or from third-order perturbation theory.

The third type of ratio $(^1S-^1D)/(^1D-^3P_c)$ we shall call the *Slater ratio* inasmuch as Slater first showed that in pure LS coupling its value should be $\frac{3}{2}$. It decreases quadratically from this value according to the relation

$$(^1S-^1D)/(^1D-^3P_c)=\tfrac{3}{2}-{}^{2}\tfrac{5}{3\,6}\chi^2+\cdots.$$

Of these five ratios only three are independent—the Landé ratio and any two of the other four ratios. If these three fit the observed data then the other two must also.

We have determined the χ values at which to plot the empirical ratios by making the observed value of $(^3P_2-^3P_0)/(^1D-^3P_c)$ fit the theoretical curve exactly. A coupling ratio was chosen inasmuch as near LS coupling it is related to ζ_p/F_2 more directly than the other types; the triplet splitting essentially measures ζ_p and the term separations F_2. We chose this particular coupling ratio because the ^1D is observed further along the sequence than is the ^1S. With this choice of χ the other ratios are seen to fit rather poorly for $2p^2$, very well for $3p^2$ and $4p^2$, somewhat less well for $5p^2$. For $3p^2$ the discrepancy in the Landé ratio is of the order of the experimental uncertainty. There is a curious drop in the $4p^2$ Landé ratio at Br IV.

The p^4 configuration

The secular equations for the p^4 configuration are immediately obtained from those for p^2 by reversing the sign of ζ_p. The ratios of Table II and Fig. 3 are similar to those considered for p^2. The principal difference occurs in the Landé ratio which here *increases* rapidly according to the equation

$$\text{Landé ratio}=2+\tfrac{7}{2}\chi+{}^{1\,2}\tfrac{5}{2\,4}\chi^2+\cdots,$$

and becomes infinite at $\chi=\frac{2}{3}$ (cf. Fig. 1). For this reason we have plotted the reciprocal of the usual Landé ratio. This is positive for $\chi<\frac{2}{3}$, negative for $\chi>\frac{2}{3}$.

TABLE II. *Configuration p^4: Theoretical interval ratios as a function of χ.*

χ	$\frac{^3P_1-^3P_2}{^1D-^3P_c}$	$\frac{^3P_1-^3P_2}{^1S-^1D}$	$\frac{^3P_1-^3P_2}{^1S-^3P_c}$	$\frac{^1S-^1D}{^1D-^3P_c}$	$\frac{^3P_0-^3P_1}{^3P_1-^3P_2}$
0	0	0	0	1.5	0.5
0.04	0.0339	0.0226	0.01354	1.4989	.4653
.08	.0686	.0458	.02747	1.4959	.4313
.12	.1038	.0696	.04167	1.4914	.3984
.16	.1396	.0940	.0562	1.4870	.3653
.20	.1754	.1187	.0708	1.4778	.3333
.24	.2112	.1437	.0855	1.470	.3017
.28	.2467	.1688	.1002	1.461	.2706
.32	.2819	.1941	.1149	1.452	.2401
.36	.3164	.2192	.1295	1.4434	.2102
.40	.3503	.2443	.1439	1.4344	.1808
.48	.4157	.2934	.1720	1.4173	.1237
.56	.4775	.3407	.1988	1.4018	.0690
.64	.5354	.3857	.2242	1.388	.0168
.72	.5893	.4277	.2479	1.3777	−.0327
.80	.6392	.4670	.2698	1.3688	−.0797
.88	.6853	.5031	.2901	1.3622	−.1237
1.00	.7478	.5516	.3174	1.3558	−.1848

TABLE III. *The invariant ratio $(^3P_1-C_{1\frac{1}{2}})/(^3P_1-^3D_{2\frac{1}{2}})$ for p^3. (Theoretical value = 1.167.)*

$2p^3$ NORMAL		$3p^3$ NORMAL		$4p^3$ NORMAL	
N I	1.333	P I	1.182	As I	1.161
O II	1.320	S II	1.181	Se II	1.155
F III	1.316	Cl III	1.182		
Ne IV	—	A IV	1.181	$5p^3$ normal	
Na V	1.295*	K V	1.186*	Sb I	1.132
Mg VI	1.325*	Ca VI	1.20*		
Al VII	1.295*	Sc VII	1.195*	$6p^3$ normal	
Si VIII	1.301*			Bi I	1.093
$2p^3$ DISPLACED†		$3p^3$ DISPLACED			
C II	0.82	P III	0.872		
N III	0.87				
O IV	0.90*				
F V	0.93*				
Na VII	0.95*				

* No intercombinations; doublet-quartet intervals may be in error.
† Several such displaced configurations are known for p^2 and p^4, but have not been plotted. The displaced p^4 seem to show approximately the same χ values as the normal p^3 in the same ion.

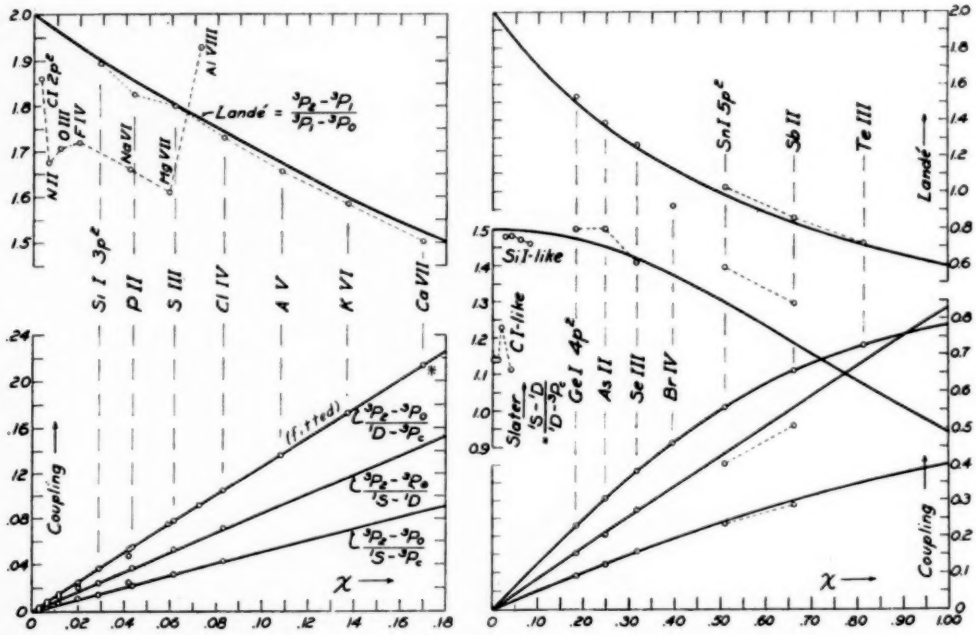

FIG. 2. Interval ratios for p^2 for $\chi=\zeta_p/5F_2\leq 1$. The plot on the left is an enlargement of part of that on the right. The curve coordinates are given in Table I.

In this case we have determined χ for $2p^4$, $3p^4$, and $4p^4$ from the coupling ratio[4] $(^3P_1-{}^3P_2)/(^1S-{}^1D)$ since many of the intercombinations are missing. For $2p^4$ the agreement with theory for the Slater ratio is poor but the Landé ratio agreement is much better than in $2p^2$; $3p^4$ is not so good as $3p^2$—it is poor at both ends of the sequence but good in the middle, although the Landé ratio is predicted remarkably well along the whole sequence; $4p^4$ is good. For $5p^4$ the Slater ratios have unreasonably large values.

[4] For Cl II, Si VII and Fe XI this ratio is not observed; the χ values are interpolated or extrapolated values.

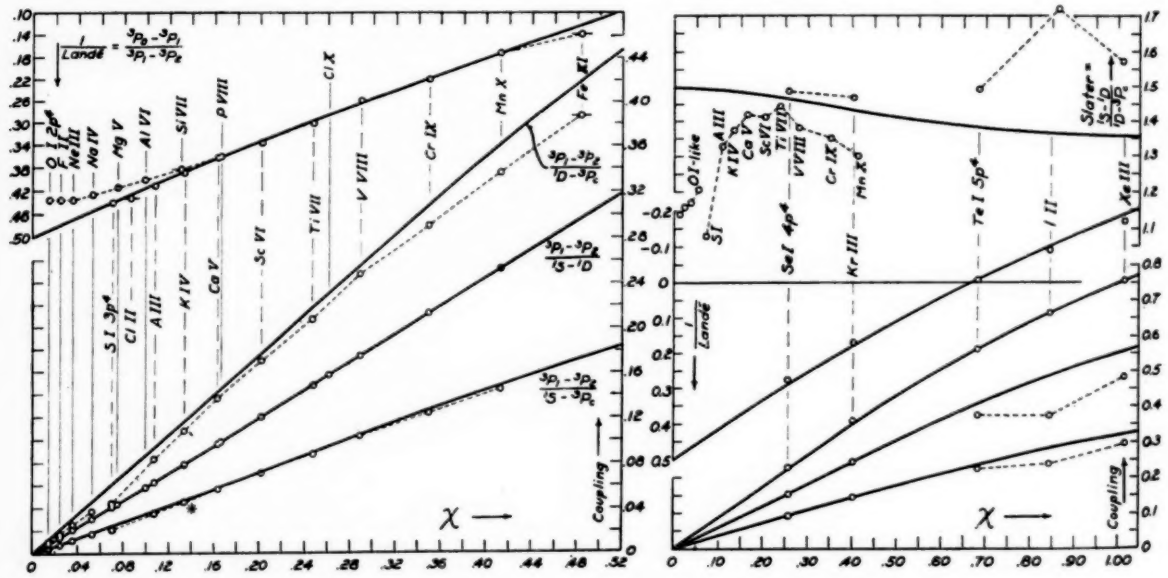

FIG. 3. Interval ratios for p^4 for $\chi=\zeta_p/5F_2\leq 1.05$. The plot on the left is an enlargement of part of that on the right. The curve coordinates are given in Table II.

Reasonable χ values in this latter case can only be obtained from the coupling ratio $(^3P_2-{}^3P_1)/(^1D-{}^3P_c)$; this is seen in Fig. 3 to predict the Landé ratios very well. One would infer that it is only the ^1S which is badly perturbed but this is not sensible since any perturbations push the ^1S *down*, and it is *high* relative to the balance of the configuration.

The p^3 configuration

This configuration occupies an exceptional position because the diagonal elements of its spin-orbit interaction matrix are all zero in LS coupling. As a result, the term splitting near LS coupling is very small, a quadratic function of χ rather than the usual linear one. Because of the vanishing of the diagonal elements, the traces of the energy matrices are functions of F_2 alone, and we can find a ratio which is completely *independent of coupling*. Such an invariant ratio exists only for the configurations p^3 and p^3s. If we denote by $C_{1\frac{1}{2}}$ the centroid of the levels for which $J=\frac{3}{2}$ $[C_{1\frac{1}{2}}=\frac{1}{3}(^2P_{1\frac{1}{2}}+{}^4S_{1\frac{1}{2}}+{}^2D_{1\frac{1}{2}})]$, then $^2P_{\frac{1}{2}}-C_{1\frac{1}{2}}=7F_2$; $^2P_{\frac{1}{2}}-{}^2D_{2\frac{1}{2}}=6F_2$; and in any coupling the ratio of these intervals is predicted to have the value $\frac{7}{6}$. The empirical values found for this ratio are listed in Table III. It will be noticed that even where they do not agree with the theoretical value, the ratios are approximately constant along an isoelectronic sequence.

TABLE IV. *Configuration p^3: Theoretical interval ratios as a function of χ.*

χ	$\frac{^2P_c-{}^2D_c}{^2D_c-{}^4S}$	$\frac{^2P_{1\frac{1}{2}}-{}^2P_{\frac{1}{2}}}{^2P_c-{}^2D_c}$	$\frac{^2P_{1\frac{1}{2}}-{}^2P_{\frac{1}{2}}}{^2D_{2\frac{1}{2}}-{}^2D_{1\frac{1}{2}}}$
0	0.667	0	1.32
0.06	.669	0.00392	1.32
.09	.674	.00911	1.32
.12	.678	.01603	1.32
.145	.683	.0230	1.32
.185	.693	.0367	1.34
.20	.697	.0424	1.34
.248	.718	.0627	1.347
.30	.730	.087	1.357
.35	.749	.113	1.37
.40	.770	.139	1.40
.45	.792	.167	1.41
.50	.815	.194	1.423
.55	.838	.222	1.450
.60	.862	.249	1.473
.65	.884	.275	1.495
.70	.905	.300	1.522
.75	.928	.325	1.545
.80	.947	.350	1.581
.85	.965	.372	1.613
.90	.983	.395	1.641
.95	.998	.416	1.672
1.00	1.010	.437	1.713

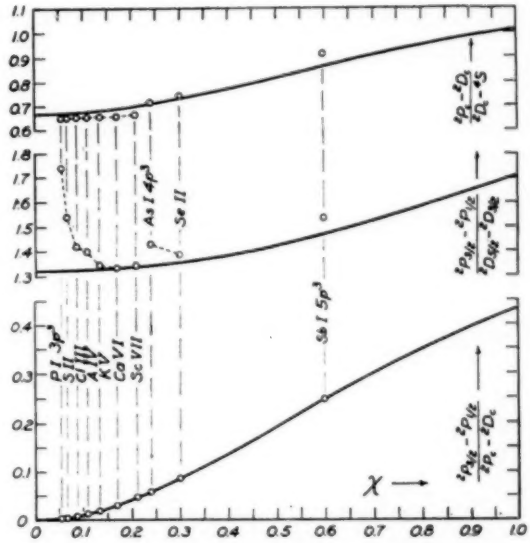

FIG. 4. Interval ratios for p^3 for $\chi=\zeta_p/5F_2\leq 1$. The curve coordinates are given in Table IV.

In Fig. 4 we have plotted three interval ratios as functions of χ. The lowest curve is the ratio of the ^2P splitting to the distance between the center of gravity of the ^2P and ^2D terms. This is analogous to a coupling ratio but starts quadratically in χ according to[5]

$$(^2P_{1\frac{1}{2}}-{}^2P_{\frac{1}{2}})/(^2P_c-{}^2D_c)$$
$$=5\tfrac{5}{48}\chi^2-16\tfrac{55}{6912}\chi^4+\cdots.$$

The middle curve gives the ratio of the ^2P splitting to the ^2D splitting. This is therefore a Landé type ratio. It has the value $3\frac{3}{25}=1.32$ for $\chi=0$ and departs from this slowly according to the relation

$$(^2P_{1\frac{1}{2}}-{}^2P_{\frac{1}{2}})/(^2D_{2\frac{1}{2}}-{}^2D_{1\frac{1}{2}})=3\tfrac{3}{25}+20\tfrac{9}{450}\chi^2+\cdots.$$

The top curve gives the Slater ratio between the $^2P_c-{}^2D_c$ separation and the $^2D_c-{}^4S$ separation. This is $\frac{2}{3}$ in LS coupling and departs from this value slowly according to the relation

$$(^2P_c-{}^2D_c)/(^2D_c-{}^4S)=\tfrac{2}{3}+125\tfrac{1}{162}\chi^2$$
$$-2312\tfrac{5}{23328}\chi^4+\cdots.$$

[5] Because of the occurrence of a cubic equation, the asymptotic forms for the p^3 levels are troublesome to compute. We give here explicitly the series for the energies (apart from the additive constant $3F_0$), as functions of $\chi=\zeta_p/5F_2$, measured in terms of F_2:

$$^2D_{2\frac{1}{2}}/F_2=-\ 6,$$
$$^2D_{1\frac{1}{2}}/F_2=-\ 6-\tfrac{125}{24}\chi^2+\tfrac{71875}{10368}\chi^4+\cdots,$$
$$^2P_{1\frac{1}{2}}/F_2=\quad\tfrac{55}{8}\chi^2-\quad\tfrac{2585}{384}\chi^4+\cdots,$$
$$^2P_{\frac{1}{2}}/F_2=\quad 0,$$
$$^4S_{1\frac{1}{2}}/F_2=-15-\quad\tfrac{5}{3}\chi^2-\quad\tfrac{65}{324}\chi^4+\cdots.$$

TABLE V. *Parameter values for normal p^2 configurations.*

$2p^2$	χ	$F_2(\text{cm}^{-1})$	$\zeta_p(\text{cm}^{-1})$
C I	0.0032	1694	27.1
N II	.0067	2537	85.0
O III	.0120	3354	201
F IV	.0204	3970	405
Na VI	.0422	5826	1230
Mg VII	.0593	6554	1940
Al VIII	.0728	7282	2650
$3p^2$			
Si I	0.029	1020	148
P II	.044	1430	314
S III	.062	1790	555
Cl IV	.083	2130	885
A V	.108	2470	1330
K VI	.137	2800	1920
Ca VII	.170	3120	2650
$4p^2$			
Ge I	0.184	1000	924
As II	.248	1340	1660
Se III	.318	1600	2550
Br IV	.395	2050	4050
$5p^2$			
Sn I	0.510	875	2230
Sb II	.661	1120	3700
Te III	.815	1320	5370
$6p^2$			
Pb I	1.583	921	7290
Bi II	1.975	1168	11540

It is difficult to obtain accurate χ values for this configuration near *LS* coupling since all of these curves are very slowly varying in this region, and there are certainly perturbations on the levels which will have a large effect on the ratios involving the very narrow doublet splittings. The doublets are predicted to be *normal* at all values of χ, but in the $2p^3$ sequence, the perturbations are larger than the very small expected separations so that one or both doublets are narrow but *inverted* for the first six members of the sequence. Only for Al VII, Si VIII, and P IX are they both normal but the Landé ^2P-^2D splitting ratios are 4.63, 1.08, and 0.53, respectively, in place of the predicted 1.32. The Slater ratios, predicted to be 0.667, are: N I, 0.500; O II, 0.509; F III, 0.512; Ne IV, —; Na V, 0.527;[6] Mg VI, 0.528;[6] Al VII, 0.528;[6] Si VIII, 0.530.[6] It was not possible to obtain χ or ζ_p values for this sequence;[7] the F_2 values of Fig. 6 are calculated from the $^2P_c - ^2D_c$ interval.

For the $3p^3$ sequence the χ values were determined from the coupling-ratio curve (drawn to a much larger scale than Fig. 4). The Slater ratio is very good; the Landé ratio improves along the sequence. For the known members of $4p^3$ and $5p^3$ the agreement is fair.

[6] No intercombinations; doublet-quartet intervals may be in error.

[7] But see note to Table VI.

Parameter values

The parameters ζ_p, F_2 (and χ) are given in the theory in the form of integrals over the wave functions which in most cases have not been evaluated. As a result their values have only been obtained empirically by some method of fitting observed experimental results to theoretical curves. Where the theory is not exactly obeyed, the values obtained depend somewhat on the method of fitting, but even approximate values and their general trends when considered as a function of atomic number should be of considerable interest. Our values for these parameters, which appear in Tables V, VI, VII, have been obtained on the assumption that the two intervals (numerator and denominator) of the ratio which we used to obtain the χ values

TABLE VI. *Parameter values for normal p^3 configurations.*

$2p^3$	χ	$F_2(\text{cm}^{-1})$	$\zeta_p(\text{cm}^{-1})$
N I		1600*	†
O II		2280*	
F III		2910*	
Ne IV		3520*	
Na V		4140*	
Mg VI		4740*	
Al VII		5360*	
Si VIII		6020*	
P IX		6690*	
$3p^3$			
P I	0.056	1220	343
S II	.067	1610	538
Cl III	.085	1940	825
A IV	.108	2270	1230
K V	.136	2580	1760
Ca VI	.169	2890	2440
Sc VII	.210	3190	3340
$4p^3$			
As I	0.240	1210	1450
Se II	.300	1540	2310
$5p^3$			
Sb I	0.598	1080	3230
$6p^3$			
Bi I	2.05	990	10,100

* For $2p^3$ the F_2 values were obtained from the observed value of $^2P_c - ^2D_c$. The coefficients of F_2 for this separation were obtained from estimated χ values. These coefficients range from 6.00 for N I to 6.16 for P IX and are so insensitive to changes in χ that no significant error can thus have been introduced.

† Good estimates of these ζ_p values should be obtainable by interpolation between p^2 and p^4 in Fig. 5.

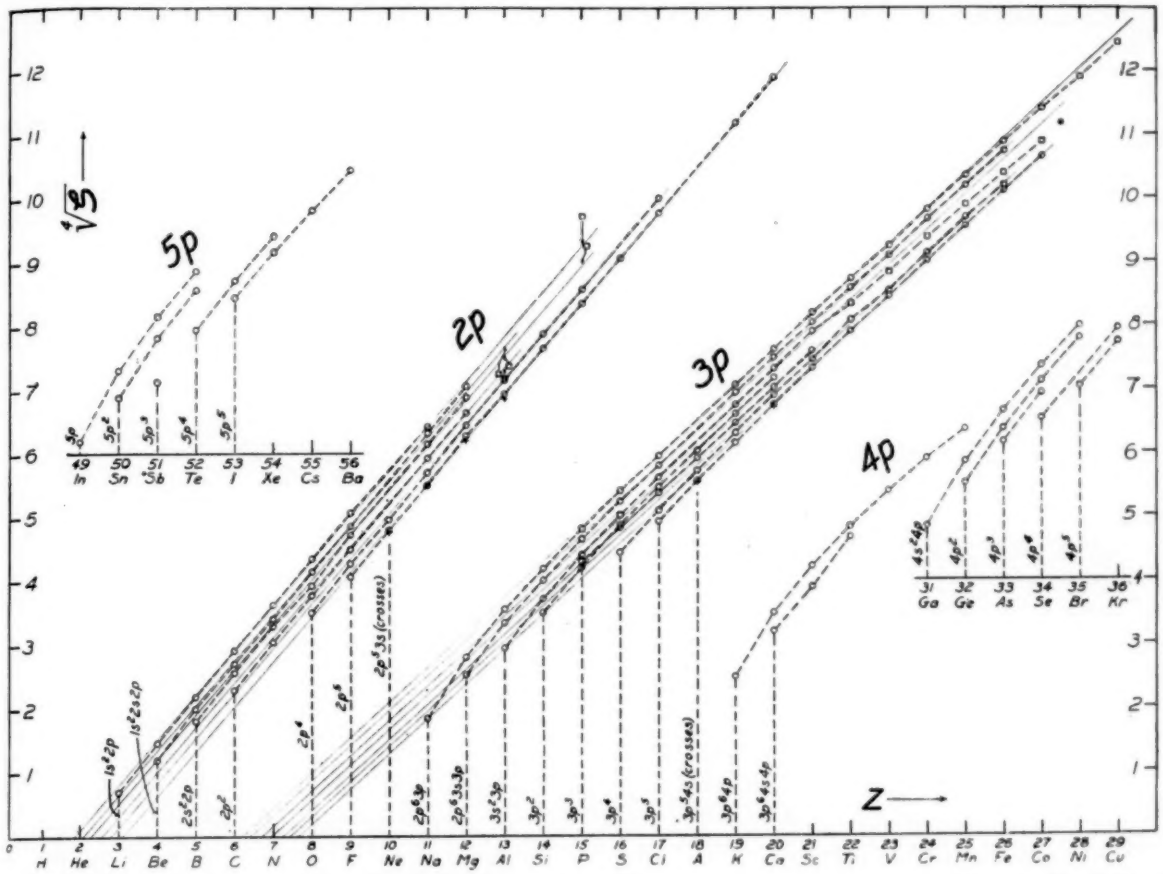

FIG. 5. The spin-orbit interaction parameter $\sqrt[4]{\zeta_p}$ in cm^{-1}. The broken lines connect the atoms of an isoelectronic sequence. The straight lines for $2p$ are plotted with hydrogenic slope. Squares show points which are uncertain because of poor experimental data. In the case of the last six members of the $3s^23p$ sequence (marked with an asterisk) the value of ζ_p was calculated from the difference between the ^2P and ^2D splitting in place of the ^2P alone. The ^2D splitting is not observed but is estimated to be approximately of the size necessary to bring these points up on to the straight line; it has the value 213 cm^{-1} in Ca VIII, about $\frac{1}{20}$ of the ^2P splitting.

(Figs. 2, 3, 4) fit the theory exactly.[8] These intervals are known functions of F_2 and χ. Since χ is known, the observed interval suffices to determine F_2 and hence ζ_p.

Corresponding values of ζ_p for p, sp, p^5, and sp^5 may also be found. In the p and p^5 configurations, $\zeta_p = \pm\frac{2}{3}$ the doublet splitting; in sp and sp^5, $\zeta_p = \pm\frac{2}{3}(^3P_2 - {}^3P_0)$ for any coupling. Values of $\sqrt[4]{\zeta_p}$ are plotted in Fig. 5 against Z. In the lower stages of ionization for the several sequences the curves bend down, but after this the relation $\zeta_p = K(Z-S)^4$ is remarkably well obeyed as is shown by the straight solid lines. Values of S may, of course, be found from the intercepts of the straight lines with the Z axis. The hydrogenic ζ are given by the

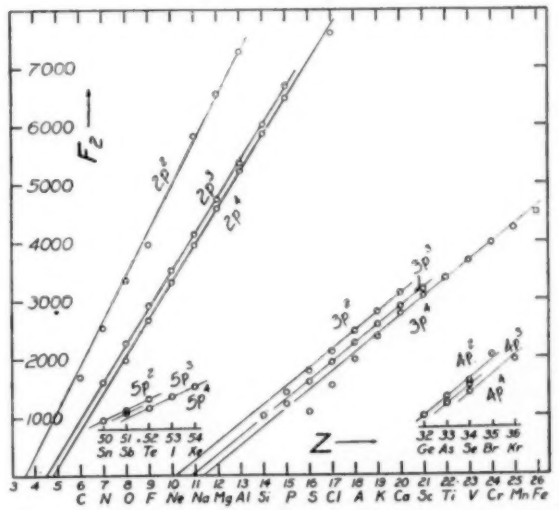

FIG. 6. The electrostatic interaction parameter F_2 in cm^{-1}. The straight lines for $2p^2$, $3p^2$, $3p^3$, $3p^4$ are drawn with hydrogenic slope.

[8] Compare with the legend of Fig. 1.

well-known formula

$$\zeta_{nl}=\frac{5.822\,Z^4}{n^3l(l+\frac{1}{2})(l+1)}\ \text{cm}^{-1}.$$

Thus

$$\sqrt[4]{\zeta_{2p}}=0.702\,Z\ \text{cm}^{-\frac{1}{4}};\quad \sqrt[4]{\zeta_{3p}}=0.518\,Z\ \text{cm}^{-\frac{1}{4}}.$$

The straight lines drawn through the $2p$ points have just the hydrogenic slope 0.702. The $3p$ points are not well represented by lines of slope 0.518. The slope chosen is 0.550. This corresponds to $n^*=2.86$ in place of $n=3$ in the hydrogenic formula. The data are as yet insufficient to decide whether the curves become linear at high ionization for $4p$ and $5p$.

The hydrogenic values of F_2, on the other hand, are linear in Z, so in Fig. 6 we plot F_2 directly against Z; the points lie fairly well on the indicated straight lines. It will be noticed that the screening constants corresponding to these lines are much larger than those found in Fig. 5. This may crudely be explained by the fact that ζ_p is essentially the average value of $1/r^3$ and so depends very strongly on the fields near the nucleus, where the screening is small. (Note that the ζ_p screening factors increase by only about $\frac{1}{5}$ for the addition of each $2s$ or $2p$ electron.) The contributions to F_2 are more uniformly distributed over the whole wave function. The hydrogenic values are $F_2(2p, 2p)=770\,Z\ \text{cm}^{-1}$; $F_2(3p, 3p)=320\,Z\ \text{cm}^{-1}$. The curves for $2p^2$, $3p^2$, $3p^3$, $3p^4$ are drawn with hydrogenic slopes!

TABLE VII. *Parameter values for normal p^4 configurations.*

$2p^4$	χ	$F_2(\text{cm}^{-1})$	$\zeta_p(\text{cm}^{-1})$
O I	0.015	1990	150
F II	.025	2670	330
Ne III	.036	3320	600
Na IV	.053	3960	1050
Mg V	.075	4590	1720
Al VI	.100	5230	2620
Si VII	.129*	5870*	3840*
P VIII	.166	6480	5370
Cl X	.262	7600	9950
$3p^4$			
S I	0.071	1090	386
Cl II	.087*	1540*	670*
A III	.108	1980	1070
K IV	.134	2370	1590
Ca V	.164	2770	2270
Sc VI	.202	3070	3100
Ti VII	.247	3370	4160
V VIII	.290	3670	5320
Cr IX	.350	3980	6950
Mn X	.413	4240	8760
Fe XI	.484*	4510*	10,910*
$4p^4$			
Se I	0.258	1410	1821
Kr III	.402	1980	3980
$5p^4$			
Te I	0.682	1160	3970
I II	.844	1360	5760
Xe III	1.014	1530	7780

* From interpolated or extrapolated χ values.

Inasmuch as χ is proportional to the ratio ζ_p/F_2 one would expect χ to vary as $(Z-S)^3$. This it does to a very good approximation. Because of the difference between the screening constant for ζ_p and the screening constant for F_2 there is some tendency for the curves of $\sqrt[3]{\chi}$ *vs.* Z to bend upward at low stages of ionization. Such an argument will perhaps account for the anomalous behavior of the ratio $\frac{3}{4}\zeta_p/G_1(s, p)$ in the sequence Ne I, Na II, Mg III ($2p3s$) and A I, K II, Ca III ($3p4s$) as shown in C-S, page 304. The ratio appears first to decrease and then to increase. The K II value shows also the effects of a perturbation from the configuration $3p3d$ with which it is completely mixed up.

Prediction of unknown levels

Figures 2, 3, and 4 show that the deviations of the experimental ratios from the theoretical curves are sufficiently regular that unknown interval ratios may be predicted by interpolation or extrapolation on the curves through the empirical points. Furthermore, the approximate linear variation of $\sqrt[3]{\chi}$, $\sqrt[4]{\zeta_p}$, and F_2 with Z may be used to predict unknown parameter values, where needed.

At the time that Fig. 3 was drawn the low states of Sc VI were unknown, but have since been published. As a typical example of the accuracy to be expected in interpolation, the following calculation was made (without recourse to the data) for this ion. The $\sqrt[3]{\chi}$ *vs.* Z was first plotted for the $3p^4$ sequence. The curve was smooth and gave the result $\chi=(0.588)^3=0.203$. The following ratios were read immediately from the dashed curves of Fig. 3:

$$(^3P_1-{}^3P_2)/(^1S_0-{}^3P_c)=0.071,$$
$$(^3P_1-{}^3P_2)/(^1S_0-{}^1D_2)=0.121,$$
$$(^3P_1-{}^3P_2)/(^1D_2-{}^3P_c)=0.170,$$
$$(^3P_0-{}^3P_1)/(^3P_1-{}^3P_2)=0.330.$$

Now near LS coupling any Landé interval such as $^3P_1-{}^3P_2$ will vary approximately as $(Z-S)^4$ along an isoelectronic sequence. We may therefore interpolate, numerically or graphically, in the table of $(^3P_1-{}^3P_2)^{\frac{1}{4}}$ to find for Sc VI, $^3P_1-{}^3P_2=(7.607)^4=3350$. Knowing this one value the other intervals follow at once. The results are listed in Table VIII. It will be noticed that the accuracy obtainable is about that which one would obtain by using the irregular-doublet law. In cases where predictions by means of the latter are precarious (as for example in interpolation between the first and third members of the sequence), the method here outlined may well give valuable information about the trend of the first difference.

Two other predictions made in this manner have allowed plausible classifications of hitherto unknown levels. These predictions are marked by means of an asterisk in Figs. 2 and 3. In these cases χ was known from the other levels. In the case of K IV $3p^4$ the ^1S was unknown. From Fig. 3 the ratio $(^3P_1-{}^3P_2)/(^1S-{}^3P_c)$ was predicted to be 0.0450. This predicts the unknown term at 37,160 cm^{-1}; two combinations have been found which locate the term at 37,778 cm^{-1}. In the case of Ca VII both the ^1S and ^1D were unknown. The ^1D was predicted at 21,910 cm^{-1} and found at 21,872 cm^{-1}. Lines giving the ^1S term could not be identified. The newly classified lines are listed in the following paper in this issue of the *Physical Review*.

Remarks on other configurations

The sp^3 configuration.—As mentioned previously, there exists for this configuration a ratio which is independent of the coupling. If 2_c denotes the centroid of the levels of $J=2$ $[2_c=\frac{1}{4}(^1D_2+{}^3D_2+{}^3P_2+{}^5S_2)]$ and 1_c denotes the centroid of the levels of $J=1$ $[1_c=\frac{1}{4}(^1D_1+{}^3P_1+{}^1P_1+{}^3S_1)]$, the ratio

$$\frac{16(^3P_0)+4(1_c)-20(2_c)}{^3P_0-{}^3D_3}=19.$$

That this relation holds fairly well may be seen from Table IX. Other relations may be expected to hold near LS coupling, e.g.

$^1P-{}^3P_c=^1D-{}^3D_c=\frac{1}{2}(^3S-{}^5S)$. (C-S page 199.)[9]

[9] In this reference, the ^3S, ^5S formula should read $+1$, $-3G_1$ in place of the coefficients given.

TABLE VIII. *Observed and estimated intervals for Sc VI $3p^4$.*

INTERVAL	ESTIMATED (this method)	OBSERVED	ESTIMATED (irregular-doublet law)
$^3P_1-{}^3P_2$	3350 cm^{-1}	3350 cm^{-1}	
$^3P_1-{}^3P_0$	1110	1126	
$^1D-{}^3P_2$	21,300	21,397	21,330 cm^{-1}
$^1S-{}^3P_2$	48,800	49,238	49,180
$^1S_0-{}^1D_2$	27,700	27,841	27,870

TABLE IX. *The invariant ratio $[16(^3P_0)+4(1_c)-20(2_c)]/(^3P_0-{}^3D_3)$ for sp^3. (Theoretical value = 19.)*

ELEMENT	CONFIGURATION	RATIO
N II	$2s2p^3$	18.21
O II	—	17.94
F IV	—	17.88
Na VI	—	18.32*
Mg VII	—	18.50*
Al VIII	—	18.56*
O I	$2p^33s$	21.35†
F II	—	20.27
P II	$3s3p^3$	19.4*
S I	$3p^34s$	19.20
Se I	$4p^35s$	19.09
Kr III	—	16.95†
Xe III	$5p^36s$	17.55†

* In these cases certain intercombinations are not accurately known.
† Partial overlapping with the p^3d configuration.

TABLE X. *Intervals in sp^3 configurations.* (Theory predicts that these should be equal in LS coupling.)

	$^1P-{}^3P_c$	$^1D-{}^3D_c$	$\frac{1}{2}(^3S-{}^5S)$
O I	2005	1526	1513
F II	−2324*	3189	3106
N II	57,547	51,943	54,231
O III	68,075	67,008	68,596
F IV	82,148	81,039	81,896
S I	1124	1407	1354
P II	26,011	12,462†	28,902

* Interaction between sp^3 ^1P and p^33s ^1P.
† The p^3 terms in P III are very irregular. There is also some interaction between sp^3 and s^2pd terms.

The empirical values are listed in Table X.

The pp configuration.—Early attempts to classify terms of this configuration in the first period led to erroneous term designations. As a result the relation[10] $R=(S_m-D_m)/(D_m-P_m)=3\frac{1}{2}$ which was predicted for the LS coupling case was thought to be entirely disobeyed (C-S, page 200). Recent revisions of these spectra show that the terms really lie in the right order to make this ratio positive; for C I, $R=1.13$; N II, $R=1.135$; O III, $R=9.3$. In the second period

[10] The subscript $_m$ denotes the mean of the singlet and the centroid of the triplet; e.g. $D_m=\frac{1}{4}(^1D+{}^3D_c)$.

Si I and P II give ratios which are negative because of the anomalous position of the ^1P term. In the third period the term order is correct: for As II, $R=1.20$. Ge I and Se III are not complete.

Sources of data

We present here a working bibliography which lists the sources of information on all ions having only s and p electrons in the normal configuration. In many cases the key paper only is given as usually previous data are therein listed. We have attempted to list also those papers which give supplementary data (usually by interpolation along an isoelectronic sequence) concerning a few terms in the spectra of other ions than those listed in the title. In several cases where more than one person has worked upon a single spectrum simultaneously we have only listed what appears to us on careful scrutiny to be the most reliable. Our choice has usually depended on further information which has appeared since the original publication and in no sense is to be construed as indicating that the efforts of a particular author are in general untrustworthy. In this list the roman numerals refer to the spectrum; the arabic to the reference.

This paper was completed while one of the writers (G. H. S.) was the guest of the physics department of Princeton University. He wishes to thank the members of this faculty for their generous hospitality.

Bibliography

He I, 1, 18.
Li I, 2; II, 1.
Be I, 2, 3, 4; II, 2; III, 1; IV, 5.
B I, II, III, 4; IV, 5.
C I, 4; II, 4, 7; III, IV, 4; V, 1.
N I, 2, 6; II, 4, 7, 15; III, IV, 4, 7; V, 4; VI, 1.
O I, 2, 2a; II, III, IV, 4, 8; V, 4, 76; VI, 4; VII, 1.
F I, 9, 10; II, III, 9, 11; IV, 11, 12; V, 11, 13; VI, 11, 14, 76; VII, 11, 14.
Ne I, 2; II, III, IV, 16.
Na I, 2; II–IX, 17.
Mg I, 2, 3; II, 2; III–IX, 17.
Al I, 2, 3, 18; II, 2, 3, 18; III, 2; IV–X, 17.
Si I, 2, 19, 22; II, III, 2, 20; IV, 21; V–IX, 17.
P I, 22; II, 22, 23; III, IV, V, 23; VI–XIII, 24.
S I, 25, 26; II, 26, 27, 22; III, 2, 27, 28; IV, 2, 20; V, 20; VI, 2, 28; VIII, 28.
Cl I, 2, 36; II, 2, 29; III, 30; IV, 30, 31; V, 30; VI, VII, 2; VIII, IX, 32.
A I, 2; II, 33, 36; III, 33, 34; IV, 33; V, 33, 35.
K I, 2, 10; II, 2; III, 2, 36, 41a; IV, 28, 37; V, 37; VI, 38, 28; VII, 38; VIII, 38, 39, 76; IX, 38, 40; X, 73; XI, 73, 76.
Ca I, II, III, 2; IV, 2, 36, 41a; V, VI, 37; VII, 38, 28; VIII, 38; IX, 39, 76; X, 40; XI, 73; XII, 73, 76.
Sc II, III, 2; IV–XI, 41, 41a, 41b, 41c; XII, 73.
Ti IV, 2; V, 41b; VI, 36; VII, 42; X, XI, 39; XII, 40; XIII, 73.
V V, 2; VII, 36; VIII, 42; XI, XII, 39; XIII, 40; XIV, 73.
Cr VI, 2, 41d; VIII, 36; IX, 42; XII, XIII, 39; XIV, 40; XV, 73.
Mn VII, 2, 41d; VIII, 41b; IX, 36; X, 42; XIII, XIV, 39; XV, 40.
Fe VIII, 41d; IX, 41b; X, 36; XI, 42; XIV, XV, 39; XVI, 40.
Co XI, 36; XV, XVI, 39; XVII, 40.
Ni XVIII, 40.
Cu XIX, 40.
Ga I, 2.
Ge I, 2, 43; II, 2.
As I, 45, 75; II, 44, 75; III, 2, 46, 75; IV, 50.
Se I, 47; II, 48; III, 49; IV, V, 50.
Br I, 2; II, 62; IV, 51; V, 52.
Kr I, 2; II–IV, 53, 54.
Rb I, 2.
Sr II, 2.
Y III, 2.
Zr IV, 2.
Cb V, 55.
Mo VI, 55.
In I, 2.
Sn I, II, 2.
Sb I, 2; II, 56; III, 2, 57.
Te I, 58; III, 59; IV, 60.
I I, 61; II, 62; IV, 74.
Xe I, 2; II, 63; III, 64.
Cs I, 2; III, 65.
Ba II, 2; IV, 65.
La III, 2, 66.
Ce IV, 66.
Tl I, 2.
Pb I, 2; II, 67.
Bi I, 2; II, III, 68.
Ra I, 69, 70; II, 71.
Th IV, 72.

References

1. H. A. Robinson, Phys. Rev. **51**, 14 (1937).
2. Bacher and Goudsmit, *Atomic Energy States* (1932).
2a. A. Fowler, *Series in Line Spectra* (1922).
3. F. Paschen, Ann. d. Physik **12**, 509 (1932).
4. B. Edlén, Nova Acta Reg. Soc. Scien. Upsal. IV, **9**, No. 6, Uppsala (1934). Certain of the data of this reference are reprinted in Zeits. f. Physik **84**, 746 (1933) and Zeits. f. Physik **85**, 85 (1933).
5. H. A. Robinson, Phys. Rev. **50**, 99 (1936).
6. E. Ekefors, Zeits. f. Physik **63**, 437 (1930) (this paper was overlooked by reference 2).
7. B. Edlén, Zeits. f. Physik **98**, 561 (1936).
8. B. Edlén, Zeits. f. Physik **93**, 726 (1935).
9. B. Edlén, Zeits. f. Physik **93**, 433 (1935).
10. B. Edlén, Zeits. f. Physik **98**, 445 (1936).
11. B. Edlén, Zeits. f. Physik **94**, 47 (1935).
12. B. Edlén, Zeits. f. Physik **92**, 19 (1934).
13. B. Edlén, Zeits. f. Physik **89**, 597 (1934).
14. B. Edlén, Zeits. f. Physik **89**, 179 (1934).
15 J. B. Green and H. N. Maxwell, Phys. Rev. **51**, 243 (1937).
16. J. C. Boyce, Phys. Rev. **46**, 378 (1934).
17. J. Söderqvist, Nova Acta Reg. Soc. Scien. Upsal. IV, **9**, No. 7, Uppsala (1934). Certain of the data of this reference are reprinted in Zeits. f. Physik **76**, 316, 756 (1932) and Zeits. f. Physik **79**, 634 (1932).
18. F. Paschen, Ann. d. Physik **18**, 867 (1933).
19. C. C. Kiess, Nat. Bur. Stand. J. Research **11**, 775 (1933).
20. I. S. Bowen, Phys. Rev. **39**, 8 (1932).

21. B.Edlén and J. Söderqvist, Zeits. f. Physik **87**, 217 (1933).
22. H. A. Robinson, Phys. Rev. **49**, 297 (1936).
23. H. A. Robinson, Phys. Rev. **51**, 726 (1937).
24. H. A. Robinson, unpublished data.
25. J. E. Ruedy, Phys. Rev. **44**, 758 (1933). The suggestion by I. S. Bowen, Rev. Mod. Phys. **8**, 78 (1936), that the ^1S term as given by Ruedy is incorrect, is in our view unsupported. Ruedy's data fit the trends rather better than Bowen's suggested correction.
26. K. M. Meissner, O. Bartelt, and L. Eckstein, Zeits. f. Physik **86**, 54 (1933).
27. A. Hunter, Trans. Royal Soc. **A233**, 303 (1934); O. Bartelt and L. Eckstein, Zeits. f. Physik **86**, 77 (1934).
28. H. A. Robinson, Phys. Rev. **52**, 724 (1937).
29. Murakawa, Zeits. f. Physik **96**, 117 (1935).
30. I. S. Bowen, Phys. Rev. **45**, 401 (1934).
31. I. S. Bowen, Phys. Rev. **46**, 377 (1934).
32. B. Edlén, Zeits. f. Physik **100**, 726 (1936).
33. J. C. Boyce, Phys. Rev. **48**, 396 (1936).
34. J. C. Boyce, Phys. Rev. **49**, 351 (1936).
35. H. A. Robinson, Nature **137**, 992 (1936).
36. B. Edlén, Zeits. f. Physik **104**, 407 (1937).
37. I. S. Bowen, Phys. Rev. **46**, 791 (1934).
38. A. E. Whitford, Phys. Rev. **46**, 793 (1934).
39. B. Edlén, Zeits. f. Physik **103**, 536 (1936).
40. B. Edlén, Zeits. f. Physik **100**, 621 (1936).
41. A. Beckman, Dissertation, Uppsala (1937); translation, with corrections, to appear shortly in Zeits. f. Physik; H. S. Pattin and P. G. Kruger, Phys. Rev. **51**, 1019 (1937) (abstract).
41a. P. G. Kruger and L. W. Phillips, Phys. Rev. **51**, 1087 (1937).
41b. P. G. Kruger, S. G. Weissberg, and L. W. Phillips, Phys. Rev. **51**, 1090 (1937).
41c. P. G. Kruger and L. W. Phillips, Phys. Rev. **52**, 97 (1937).
41d. P. G. Kruger and S. G. Weissberg, Phys. Rev. **52**, 314 (1937).
42. B. Edlén, Zeits. f. Physik **104**, 188 (1937).
43. J. S. Badami and K. R. Rao, Proc. Roy. Soc. **A140**, 397 (1933).
44. A. S. Rao, Proc. Phys. Soc. **44**, 343 (1932).
45. A. S. Rao, Proc. Phys. Soc. **44**, 594 (1932).
46. K. R. Rao, Proc. Phys. Soc. **43**, 68 (1930).
47. J. E. Ruedy and R. C. Gibbs, Phys. Rev. **46**, 880 (1934).
48. D. C. Martin, Phys. Rev. **48**, 938 (1935).
49. K. R. Rao and S. G. K. Murti, Proc. Roy. Soc. **A145**, 681 (1934).
50. K. R. Rao and J. S. Badami, Proc. Roy. Soc. **A131**, 154 (1931).
51. A. S. Rao and S. G. Krishnamurty, Proc. Phys. Soc. **46**, 530 (1934).
52. A. S. Rao and K. R. Rao, Proc. Phys. Soc. **46**, 163 (1934).
53. J. C. Boyce, Phys. Rev. **47**, 718 (1933).
54. C. J. Humphreys, Phys. Rev. **47**, 712 (1935).
55. M. W. Trawick, Phys. Rev. **46**, 63 (1934).
56. S. G. Krishnamurty, Ind. J. Phys. **10**, 83 (1936).
57. J. S. Badami, Proc. Phys. Soc. **43**, 538 (1931).
58. J. E. Ruedy, Phys. Rev. **41**, 588 (1932); S. G. Krishnamurty, Ind. J. Phys. **10**, 365 (1936).
59. S. G. Krishnamurty and K. R. Rao, Proc. Roy. Soc. **A158**, 562 (1937).
60. K. R. Rao, Proc. Roy. Soc. **A133**, 220 (1931).
61. S. F. Evans, Proc. Roy. Soc. **A133**, 417 (1931).
62. P. Lacroute, Ann. de physique **3**, 1 (1935).
63. C. J. Humphreys, T. L. de Bruin, and W. F. Meggers, Nat. Bur. Stand. J. Research **6**, 287 (1931).
64. C. J. Humphreys, Nat. Bur. Stand. J. Research **16**, 639 (1936).
65. M. A. Fitzgerald and R. A. Sawyer, Phys. Rev. **46**, 576 (1934).
66. R. J. Lang, Can. J. Res. **14A**, 127 (1936).
67. L. T. Earls and R. A. Sawyer, Phys. Rev. **47**, 115 (1935).
68. M. F. Crawford and A. B. McLay, Proc. Roy. Soc. **A143**, 540 (1934).
69. E. Rasmusson, Zeits. f. Physik **87**, 607 (1934).
70. H. N. Russell, Phys. Rev. **46**, 989 (1934).
71. E. Rasmusson, Zeits. f. Physik **86**, 24 (1933).
72. R. J. Lang, Can. J. Res. **14**, 43 (1936).
73. B. Edlén and F. Tyren, Zeits. f. Physik **101**, 206 (1936).
74. S. G. Krishnamurty, Proc. Phys. Soc. **48**, 277 (1936).
75. J. B. Green and W. M. Barrows, Phys. Rev. **47**, 131 (1935).
76. B. Edlén, unpublished data. We are indebted to Dr. Edlén for the unpublished Ca IX, K XI, and Ca XII data which appear on Fig. 5.

Additions to Certain Spectra of Sulphur, Potassium and Calcium

HOWARD A. ROBINSON*
Mendenhall Laboratory of Physics, Ohio State University, Columbus, Ohio

(Received July 15, 1937)

Twenty-seven lines have been classified in S III. These locate six of the important singlet levels accurately with respect to the known triplets. S VI has been completely revised. Fourteen new terms have been added which classify eighteen new lines. The revised ionization potential is 87.610±0.003 volts. Two new singlet terms with intercombinations have been found in K VI and Ca VII. One new singlet term has been added to K IV and three terms to S VIII. Several of these last few spectra have been investigated in order to test the conclusions drawn from the previous paper in this issue of the *Physical Review*.

IT has been possible to extend the classifications of certain sulphur spectra by means of spectrograms obtained in Professor Siegbahn's laboratory in Uppsala, Sweden. Previously published lists of sulphur lines[1–3] have also been used. Certain of the terms have already been published:[4] it was impossible at that time to list the newly classified lines. The new results are given in Tables I and II.

The new measurements show that 6 cm^{-1} must be subtracted from all terms higher than 140,000 cm^{-1}. Since these terms are very accurately known with respect to one another[3] the new values are not listed. The $3s3p^2 3d\ ^3D$ terms listed by L. and E. Bloch[1] are erroneous; the lines which they give as the $3s3p^3\ ^3D - 3s3p^2 3d\ ^3D$ transitions are in reality the $3s^2 3p^2\ ^3P - 3s3p^3\ ^3D$ transitions previously classified by Ingram.[5] Slightly more accurate values for the sp^3 triplet terms have also been added.

Extensions have also been possible in the case of S VI. (Tables III and IV.) The Rydberg denominators have been determined by means of the Princeton tables.[6] The absolute value of the ground state was obtained by setting n^* for $5g\ ^2G$ equal to 4.9990. This value was extrapolated from the corresponding terms in the other members of the isoelectronic sequence.

It has also been possible to identify the $s^2 2p^5\ ^2P - sp^6\ ^2S$ transition of S VIII. The lines

TABLE I. *S III Classified lines.*

INT.		λ(air)	ν(cm^{-1})	CLASSIFICATION
7		4677.67	21,372.20	$4s\ ^1P_1 - 4p\ ^3D_1$
5		4613.47	21,669.61	$4s\ ^1P_1 - 4p\ ^3D_2$
0		4125.4	24,233.3	$4s\ ^1P_1 - 4p\ ^3P_0$
3		4099.25	24,387.85	$4s\ ^1P_1 - 4p\ ^3P_1$
00		3899.27	25,638.59	$4s\ ^1P_1 - 4p\ ^3S_1$
00		3008.82	33,226.0	$sp^3\ ^1P_1 - 4p\ ^3D_2$?
1		2749.94	36,353.7	$sp^3\ ^1P_1 - 4p\ ^3P_2$
1		2593.87	38,540.9	$4p\ ^3P_1 - 5s\ ^1P_1$
2		2422.91	41,260.14	$4p\ ^3D_2 - 5s\ ^1P_1$
1		2405.63	41,556.5	$4p\ ^3D_1 - 5s\ ^1P_1$
1	2	λ(vac)	ν(cm^{-1})	CLASSIFICATION
8	2	1077.135	92,838.9	$3p^2\ ^1D_2 - sp^3\ ^1D_2$
00	–	911.77	109,677	$3p^2\ ^1S_0 - sp^3\ ^1P_1$
4	1*Bl*	836.315	119,572	$- 4s\ ^3P_1$
4	0	824.887	121,229	$- 4s\ ^1P_1$
4	5	796.692	125,519	$3p^2\ ^1D_2 - sp^3\ ^1P_1$
4	3	788.984	126,745	$- sp^3\ ^3S$
4	1	738.474	135,414	$- 4s\ ^3P_1$
2	–	736.25	135,834	$- 4s\ ^3P_2$
1	–	733.92	136,255	$- 3d\ ^3D_1$?
0	–	733.34	136,362	$- 3d\ ^3D_2$
0	–	732.98	136,492	$- 3d\ ^3D_3$
4	4	729.529	137,075	$- 4s\ ^1P_1$
4	3	735.251	136,008	$3p^2\ ^3P_2 - sp^3\ ^1P_1$
5	0	732.376	136,542	$^3P_1 - \quad ^1P_1$
3	0*n*	730.783	136,840	$^3P_0 - \quad ^1P_1$
2	0*n*	543.031	184,152	$3p^2\ ^1S_0 - 5s\ ^1P_1$
3	0	499.983	200,006	$3p^2\ ^1D_2 - 5s\ ^1P_1$

Intensities, col. 1 from L. and E. Bloch, reference 1.
Intensities, col. 2 from authors own measurements. All wave-lengths in vacuum from personal data except for those lines for which a dash is given in col. 2. Wave-lengths in air from references 2 or 3.

TABLE II. *S III term table.*

$s^2 3p^2\ ^3P_0$	0.0	$sp^3\ ^1D_2$	104,159?	$sp^3\ ^3D_1$	84,018.9
$^3P_1$	297.2			$^3D_2$	84,046.4
$^3P_2$	832.5	$^1P_1$	136,839	$^3D_3$	84,099.5
$^1D_2$	11,320	$4s\ ^1P_1$	148,397.8	$sp^3\ ^3P_2$	98,743.0
				$^3P_1$	98,765.6
$^1S_0$	27,163	$5s\ ^1P_1$	211,326.8	$^3P_0$	(98,771)
				$sp^3\ ^3S$	138,061.4

* Now at Central Technical Laboratory, Armstrong Cork Company, Lancaster, Pennsylvania.

[1] L. and E. Bloch, J. de phys. **6**, 441 (1935).
[2] L. and E. Bloch, Ann. de physique **12**, 5 (1929).
[3] A. Hunter, Phil. Trans. Roy. Soc. London **233A**, 303 (1934).
[4] H. A. Robinson, Nature **137**, 992 (1936).
[5] S. B. Ingram, Phys. Rev. **33**, 907 (1929).
[6] A. G. Shenstone, J. C. Boyce and H. N. Russell, *Rydberg Interpolation Table* (Princeton, N. J., 1934).

TABLE III. *Classified lines of S VI.*

INT.	λ(vac.)	ν(cm⁻¹)	CLASSIFICATION
5§	944.517	105,874	$3s\ ^2S - 3p\ ^2P_{1/2}$
4§	933.382	107,137	$^2S - ^2P_{3/2}$
3§	712.844	140,283	$3p\ ^2P_{3/2} - 3d\ ^2D_{3/2}$
4§	712.682	140,315	$^2P_{3/2} - ^2D_{5/2}$
6§	706.480	141,547	$^2P_{1/2} - ^2D_{3/2}$
1	650.430	153,744	$3d\ ^2D_{3/2} - 4p\ ^2P_{1/2}$
1	648.628	154,172	$^2D_{5/2} - ^2P_{3/2}$
10§	464.654	215,214	$3d\ ^2D - 4f\ ^2F$
8§	390.859	255,847	$3p\ ^2P_{3/2} - 4s\ ^2S$
6§	388.940	257,109	$^2P_{1/2} - ^2S$
6	328.605	304,409	$3d\ ^2D - 5f\ ^2F$
3	290.132	344,671	$3p\ ^2P_{3/2} - 4d\ ^2D_{5/2}$
2	289.092	345,911	$^2P_{1/2} - ^2D_{3/2}$
3	283.502	352,731	$3d\ ^2D - 6f\ ^2F$
0n	261.810	381,956	$3d\ ^2D - 7f\ ^2F$
2	251.905	396,975	$3p\ ^2P_{3/2} - 5s\ ^2S$
4	249.271	401,170	$3s\ ^2S - 4p\ ^2P_{1/2}$
4	248.985	401,631	$^2S - ^2P_{3/2}$
2	227.845	439,895	$3p\ ^2P_{3/2} - 5d\ ^2D_{5/2}$
2	227.197	440,147	$^2P_{1/2} - ^2D_{3/2}$
00	214.277	466,686	$3p\ ^2P_{3/2} - 6s\ ^2S$
0n	204.190	489,740	$3p\ ^2P_{3/2} - 6d\ ^2D$
00n	192.273	520,094	$3p\ ^2P_{3/2} - 7d\ ^2D$
0n	192.560	522,030	$3s\ ^2S - 5p\ ^2P_{1/2}$
00	192.480	522,248	$^2S - ^2P_{3/2}$
00n	171.327	583,679	$3s\ ^2S - 6p\ ^2P_{3/2}$

TABLE IV. *S VI term table with Rydberg denominators.*

$3s\ ^2S$	710,194§	2.3585	$3d\ ^2D_{3/2}$	462,774§	
$4s\ ^2S$	347,211§	3.3732	$^2D_{5/2}$	462,742§ (32)	2.9219
$5s\ ^2S$	206,082	4.3785	$4d\ ^2D_{3/2}$	258,409	
$6s\ ^2S$	136,371	5.3822	$^2D_{5/2}$	258,386 (23)	3.9101
$3p\ ^2P_{1/2}$	604,320§		$5a\ ^2D_{3/2}$	164,173	
$^2P_{3/2}$	603,057§ (1263)	2.5595	$^2D_{5/2}$	164,162 (11)	4.9056
$4p\ ^2P_{1/2}$	309,030§		$6d\ ^2D$	113,317	5.9043
$^2P_{3/2}$	308,573§ (457)	3.5780	$7d\ ^2D$	82,963	6.9007
$5p\ ^2P_{1/2}$	188,164		$4f\ ^2F$	247,541§	3.9949
$^2P_{3/2}$	187,946 (218)	4.5846	$5f\ ^2F$	158,346	4.9949
$6p\ ^2P_{3/2}$	126,515	5.5880	$6f\ ^2F$	110,024	5.9923
			$7f\ ^2F$	80,799	6.9924
$5g\ ^2G$	158,088§	(4.9990)			

§ Lines and terms previously classified: R. A. Millikan and I. S. Bowen, Phys. Rev. **25**, 295 (1925).

are of intensity 0, wave-length 202.605A (ν = 493,571 cm⁻¹) and 198.550A (ν = 503,652 cm⁻¹). This indicates a separation of −10,080 cm⁻¹ for the $p^5\ ^2P$ which is in good agreement with prediction.

Minor additions to the singlet spectra of

TABLE V.

INT.	λ(vac.)	ν(cm⁻¹)	CLASSIFICATION
2	501.649	199,343	$p^2\ ^1D_2 - sp^3\ ^3S$
10 d.	488.120	204,868	$p^2\ ^1D_2 - sp^3\ ^1P_1$
3	452.667	220,913	$p^2\ ^3P_2 - sp^3\ ^1P_1$
3	449.013	222,711	$p^2\ ^3P_1 - sp^3\ ^1P_1$

TABLE VI. *K VI term table.*

$s^2p^2\ ^3P_0$	0	$s^2p^2\ ^1D_2$	18,973
$^3P_1$	1131	$^1S_0$	—
$^3P_2$	2924	$sp^3\ ^1P_1$	223,840

TABLE VII.

6	433.609	230,623	$p^2\ ^1D_2 - sp^3\ ^1P_1$
2	402.551	248,416	$p^2\ ^3P_2 - {}^1P_1$
2	398.615	250,869	$^3P_1 - {}^1P_1$
2Bl	396.044	252,497	$^3P_0 - {}^1P_1$

TABLE VIII. *Ca VII term table.*

$s^2p^2\ ^3P_0$	0	$s^2p^2\ ^1D_2$	21,872
$^3P_1$	1629	$^1S_0$	—
$^3P_2$	4070	$sp^3\ ^1P_1$	252,495

K IV[7-9] show that the lines λ447.085 (ν = 223,671 cm⁻¹) and λ384.095 (ν = 260,352 cm⁻¹) are in all probability the transitions $3p^4\ ^1S_0 - p^3 3d\ ^1P_1$, and $3p^4\ ^1S_0 - p^3 4s\ ^1P_1$ respectively. This places tentatively the $p^4\ ^1S_0$ term at 37,778 cm⁻¹ ($p^4\ ^3P_0 = 0$).

Two of the singlet states of K VI[4] have also been located: the lines classified are given in Tables V and VI.

The corresponding transitions in Ca VII[7, 9] are given in Tables VII and VIII.

The additions to K IV and CaV II have been made jointly with Dr. George H. Shortley as part of the preceding paper in this issue of the *Physical Review*. They are listed here for convenience.

The writer is indebted to Professor Manne Siegbahn and Docent Bengt Edlén of the University of Uppsala, and wishes to thank the American Scandinavian Foundation for the award of the Irving Langmuir Fellowship which made the work possible.

[7] Wave-lengths from E. Ekefors, Dissertation, Uppsala (1931).
[8] I. S. Bowen, Phys. Rev. **46**, 791 (1934).
[9] A. E. Whitford, Phys. Rev. **46**, 793 (1934).

The $^1\Sigma^* - {}^1\Sigma$ Band System of Ionized Zinc Deuteride

JOSEPH W. GABEL AND R. V. ZUMSTEIN
Mendenhall Laboratory of Physics, Ohio State University, Columbus, Ohio

(Received August 13, 1937)

The $^1\Sigma^* - {}^1\Sigma$ bands have been photographed with a dispersion of about 1A/mm. Five bands of the system between λ2300 and λ2100 were analyzed. The isotopic coefficient ρ is in satisfactory agreement with the value obtained from atomic weights. The electronic isotope displacement of 6 cm^{-1}, relative to Zn^+H, is probably due to the small number of vibrational levels; three for each state of the molecule. A fine structure due to the zinc isotopes was indicated by a diffuseness of the lines.

THE band spectrum of the ionized zinc hydride molecule was discovered by Bengtsson and Grundström[1] who analyzed five bands of the system. Using an end on discharge tube of fused quartz and other equipment, which has been described,[2] we have photographed the analogous zinc deuteride spectrum.

[1] E. Bengtsson Knave, Nova. Acta. Reg. Soc. Upsaliensis **8**, 48 (1932).
[2] R. V. Zumstein, J. W. Gabel and R. E. McKay, Phys. Rev. **51**, 238 (1937).

EXPERIMENTAL

There was always a period of clean-up of the deuterium by the discharge followed by a release of absorbed gas. Considerable difficulty in operating the tube was experienced because of these wide variations of pressure. The spectra obtained were practically free from light hydrogen. One electrode was a small brass rod at the axis of the cylindrical discharge tube. The copper lines were thus emitted and served as

TABLE I. *Wave numbers of the ionized zinc deuteride bands.*

J	R	P	J	R	P	J	R	P	J	R	P
0−0 band			0−1 band			0−2 band			1−0 band		
2	46514.9*	46485.0	2	45190.5*	45160.5	7	899.1	814.3	15	351.3	176.3
3	514.9*	474.0	3	190.5*	150.5	8	894.8	798.2	16	330.9	143.7
4	514.9*	461.9	4	190.5*	138.5	9	889.2	780.6	17	307.6	110.0
5	512.4	448.0	5	190.5*	126.0	10	882.5	762.7	18	282.8	075.6
6	508.1	432.6	6	185.6	111.4	11	874.2	743.0	19	257.0	040.0
7	502.8	416.1	7	181.5	096.5	12	865.4	723.1	20	229.5	47000.8
8	495.9	397.4	8	176.1	078.2	13	854.6	700.5	21	200.8	46960.2
9	487.4	377.7	9	169.0	059.8	14	842.0	677.5	22	168.5	917.6
10	477.5	356.0	10	160.5	040.0	15	829.3	652.7	23	136.4	875.6
11	465.5	332.8	11	150.5	45018.3	16	814.2	627.7	24		830.5
12	452.6	308.3	12	138.5	44995.4	17	798.2	598.9	2−2 band		
13	437.1	282.0	13	126.0	971.9	18	780.6	573.3			
14	420.8	254.3	14	111.4	946.1	19	762.7	541.2	1		45786.7
15	402.2	225.0	15	096.4	919.6	20	743.0	512.4	2	45804.1	778.6
16	382.6	194.2	16	078.2	891.4	1−0 band			3	808.9*	769.0
17	361.5	162.0	17	059.8	861.6				4	808.9*	757.2
18	338.1	128.1	18	040.0	831.2	3	47473.8*	47433.2	5	808.9*	744.4
19	313.7	092.4	19	45018.3	798.3	4	473.8*	420.6	6	804.1	730.5
20	287.6	056.3	20	44995.5	764.5	5	471.1	407.2	7	799.0	714.9
21	259.8	46017.9	21	971.9	729.9	6	465.5	390.3	8	793.6	697.8
22	230.3	45977.9	22	946.1	695.1	7	459.4	374.7	9	786.7	680.1
23	199.6	937.0	23	919.6	659.0	8	452.2	354.9	10	778.6	660.4
24	167.9	894.5	24	891.1		9	442.0	334.0	11	769.0	640.3
25	132.8	850.9	0−2 band			10	431.4	311.8	12	757.2	616.9
26		805.8				11	418.4	287.5	13	744.0	592.9
27		757.2	4	43905.0*	43854.6	12	404.6	262.0	14		568.8
28		709.3	5	905.0*	842.0	13	388.9	235.0	15		542.5
			6	905.0*	829.6	14	370.5	207.6			

* Band head.

TABLE II. *Null lines.*

v' \ v''	0	1	2
0	46501.7	45176.5	43890.9
1	47460.9		
2			45794.1

TABLE III. *Constants from the rotational structure.*

v	B_v'	$-D_v'$	B_v''	$-D_v''$
0	2.905	0.00011	3.707	0.00011
1	2.869	0.000096	3.612	0.00012
2	2.821	0.000098	3.493	0.00008

TABLE IV. *Summary of constants.*

	$^1\Sigma$ lower state	$^1\Sigma^*$ upper state
ω_e	1364.8	974.4
$\chi_e\omega_e$	19.8	7.60
T_e	0	46693.9
B_e	3.818	2.944
α_e	0.13	0.046
D_e	−0.00010	−0.00010

ideal standards in this part of the spectrum. A thin coating of Eastman ultraviolet sensitizing solution was applied to ordinary photographic plates. This gives surprisingly sharp lines but they are inferior to the best Schumann plates.

ANALYSIS

The wave numbers that were measured are recorded in Table I. Since the copper comparison spectrum was obtained from the discharge tube there should be no appreciable shift between the two spectra. In the 0−0 band the resolved lines should be accurate to about 0.5 cm^{-1}. A characteristic feature of every band is that the P and R branch lines do not get in and out of step. In the 0−1, 0−2 and 2−2 bands the branches coincide. In the 0−0 and 1−0 bands the lines appear as doublets of about the same separation. The 1−3 and 2−4 bands could not be analyzed because the lines were very diffuse. This is probably due to the zinc isotopes. In no band was a resolution of the zinc isotopes observable. The constants D_v' and D_v'' in Table III do not show a regular variation and an average value has been used for D_e. This may originate in the overlapping of the P and R branch lines. If Bengtsson and Grundström's value of T_e, 46700, is assumed for ZnH we have an electronic isotope displacement of 6 cm^{-1}. It will be necessary to devise considerable improvement in experimental technique before this isotopic displacement can be evaluated with certainty.

TABLE V. *Isotope ratios Zn^+D: Zn^+H.*

	$^1\Sigma$	$^1\Sigma^*$
$(B_e^i/B_e)^{\frac{1}{2}}$	0.718	0.714
ω_e^i/ω_e	0.7123	0.7138
$(\mu/\mu_i)^{\frac{1}{2}}$	0.7127	

TABLE VI. *Other band heads observed but not analyzed.*

DESIGNATION	ν
1–3	43616.9
2–4	43358.1
0–3	42659.2
1–4	42412.8
2–5	42193.8
3–6	42005.4
4–7	41844.6
5–8	41707.9

Molecular Spectrum of Hydrogen in Mixtures of Hydrogen and Helium*

NOYES D. SMITH
Research Laboratory of Physics, Harvard University, Cambridge, Massachusetts

(Received August 10, 1937)

The anomalous rotation discovered by Richardson in the molecular spectrum of hydrogen mixed with helium was investigated. Helium was found to decrease vibration and increase rotation of the (0−0) bands in agreement with the results of O. W. Richardson and A. S. Roy. For high pressures of helium (400 mm) the rotation was also reduced. At liquid-air temperature the anomalous rotation was less marked than at room temperature. No anomalous rotation was observed in the (3−3) and (2−2) bands. These results agree with the process proposed by O. Oldenberg in which collisions between an excited hydrogen molecule and helium atoms change part of the vibration of the hydrogen molecule into rotation.

PROBLEM AND PREVIOUS WORK

MERTON and Barratt[1] in their tables of wave-lengths and physical properties of the hydrogen spectrum were the first systematically to record the effect of helium on the relative intensities of the different lines. Not until after the spectrum had been more carefully analyzed by Richardson and others did certain regularities appear. Richardson[2] found that in general the effect on the singlet systems was irregular. In the triplet systems some regularities were recorded. High vibrational bands were reduced in intensity and the high rotational lines of the (0−0) bands were enhanced. Roy[3] made further observations on the effect of helium, confirming Richardson's finding and showing that the triplet systems were enhanced with respect to the singlet systems.

Oldenberg[4] suggested that the anomalous rotation in this case appeared by a process similar to the one discussed by Rieke[5] in his investigation of the HgH bands. The anomalous rotation in the HgH spectrum when excited by sensitized fluorescence has been interpreted by Oldenberg and Rieke as follows. The HgH molecule is excited in a collision with a metastable mercury atom to an electronic state with high vibration. During the lifetime of the excited state collisions with nitrogen molecules transform vibrational energy into rotational energy.

The ratio of the atomic weights is important in the process converting vibrational into rotational energy. We can consider the vibration and rotation of the HgH molecule as essentially the motion of the light hydrogen atom with respect to the fixed heavy mercury atom. In collisions the energy of heavy bodies is not easily changed. However, vibration of the light hydrogen atom might change partly into rotation about the mercury atom during collisions with the heavy nitrogen molecule. In the case of the molecular spectrum of hydrogen the anomalous rotation is much less pronounced. This can be explained by the same process; for, since we are dealing only with light particles, the energy transfer will not be restricted to vibrational and rotational energy but will include translational energy. Hence the high vibrational energy will be more rapidly dissipated into heat. A detailed discussion of such processes has been given by O. Oldenberg and A. A. Frost.[6] The anomalous rotation should be less for the high vibration bands since the energy for the excess rotation comes from high vibrational states.

In the course of experiments[7] previously reported on the effects of helium and neon on the continuous spectrum of hydrogen a study of the discrete spectrum was made. It was found that 20 cm of helium were sufficient to reduce the vibration to practically zero. If the addition

* An extract from a thesis submitted in partial fulfillment of the requirements for the degree of Doctor of Philosophy at Harvard University.

[1] T. R. Merton and S. Barratt, Phil. Trans. **A222**, 369 (1922).

[2] O. W. Richardson, *Molecular Hydrogen and its Spectrum* (Yale University Press, 1934).

[3] A. S. Roy, Proc. Nat. Acad. Sci. **19**, 441 (1933).

[4] O. Oldenberg, Phys. Rev. **46**, 210 (1934).

[5] F. F. Rieke, Phys. Rev. **42**, 587 (1932) and **46**, 236 (1934).

[6] O. Oldenberg and A. A. Frost, Chem. Rev. **20**, 99 (1937).

[7] N. D. Smith, Phys Rev. **49**, 345 (1936).

of helium—after an initial increase—finally reduces the rotation to its thermal value, we should have the hydrogen spectrum in its simplest form. If some of the electronic energy is taken away in impacts of the second kind, the *total* intensity is reduced, but the intensity *ratios* in which we are interested are not changed. At low temperatures the simplification should be even greater. McLennan, Grayson-Smith, and Collins[8] studied the effects of cooling a hydrogen discharge with liquid air and found the rotational lines of low quantum number to be enhanced.

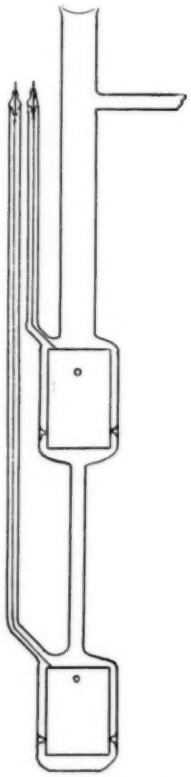

FIG. 1. Diagram of the discharge tube.

The object of this investigation was to test the predictions of the elementary processes suggested by Oldenberg and to produce the hydrogen molecular spectrum in its simplest form.

DISCHARGE TUBE

Figure 1 shows a diagram of the discharge tube. It was constructed of thin Pyrex, shaped so that the tube could be immersed in liquid air. The electrodes were made of thin sheet nickel. The capillary was 10 cm long and 3 mm in diameter and was platinized to aid the recombination of hydrogen atoms. The tube was mounted with the capillary vertical, and observations were made through the thin Pyrex window with a right-angle prism.

EXPERIMENTAL PROCEDURE

The tube was baked out with an electric furnace at 475°C and the electrodes heated to a bright red by an induction furnace while the tube was being evacuated. It was then filled with 0.6 mm of hydrogen purified by passage through a hot palladium tube. The helium was first purified by passage through an activated charcoal trap in liquid air and then by a misch metal arc.

For all exposures a constant current of 35 ma was used, furnished by a small transformer with 15,000 volts on the secondary. Exposures with various pressures of helium were made on Eastman type I-F plates with a concave grating of ten-foot radius giving a dispersion of 4.2 A/mm. At each pressure a plate was exposed with the tube in liquid air and then in a water bath. The times of exposure varied from a few minutes to an hour for the range of pressures up to 200 mm. A separate plate was used for each pressure of helium and the exposure times varied so that one exposure would have a good range of densities. One set of exposures was made with a small discharge tube with 400 mm of helium. This tube could not be water cooled and was operated with a current of 5 ma. Exposure times were of the order of twenty-four hours.

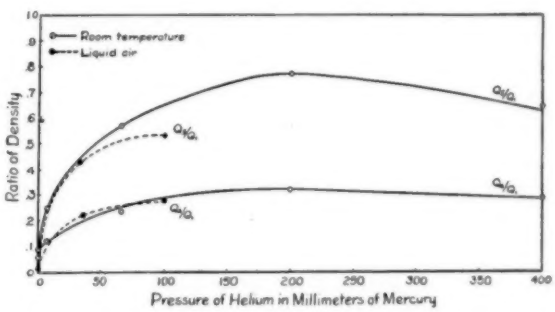

FIG. 2. Ratios of densities of $Q5$ to $Q1$ and $Q4$ to $Q1$ of the $\alpha(0-0)$ band of hydrogen as a function of the pressure of helium and the temperature.

[8] J. C. McLennan, H. Grayson-Smith, and W. T. Collins, Proc. Roy. Soc. **A116**, 277 (1927).

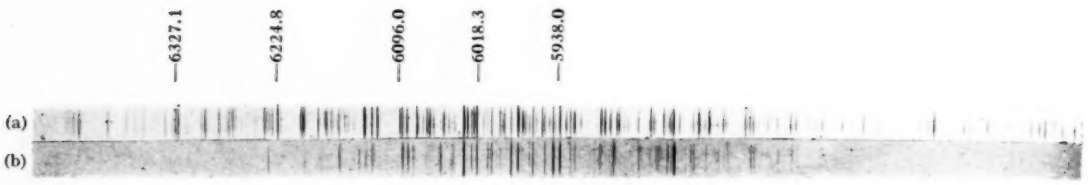

FIG. 3. Plate showing simplification of the hydrogen spectrum with the addition of helium. (a) 0.6 mm H_2; (b) 0.6 mm H_2+400 mm He.

RESULTS

The reduction in vibration due to the addition of helium was so prominent that it could be followed without recourse to photometric measurements. For a study of the rotational structure photometer tracings were made from exposures covering all the different conditions. In order to analyze the processes involved, it is sufficient to observe in what direction certain ratios of intensity vary. For this purpose ratios of *densities* were observed instead of *intensities*. This method does not give accurate quantitative results, but the order of the ratios cannot be mistaken. This procedure seems permissible considering the fact that the change of anomalous rotation with pressure is so clear that it was first noticed by Richardson without photometry.

The energy distribution in the rotational structure for pure hydrogen at room temperature was found to be expressed qualitatively by a Maxwell-Boltzmann distribution with a temperature under 100°C. When the tube was placed in liquid air the high rotational lines were reduced in intensity with respect to the low rotational lines, but the temperature was not that of liquid air.

Figure 2 shows the ratios of the densities of the fifth to the first and the fourth to the first member of the Q branch of the $\alpha(0-0)$ band plotted as a function of the pressure of helium in the tube. These lines were selected because of the freedom from overlapping by neighboring lines. The other triplet bands in this wave-length neighborhood show the same general effect. It will be noticed that the anomalous rotation reaches a maximum at about 200 mm and then slowly decreases for higher pressures of helium. The ratios at 400 mm should be regarded as an upper limit for the ratios of intensity, for the plate at this pressure was overexposed so that the line Q_1, which is more intense than Q_5, actually may have a higher intensity than indicated by its density. The anomalous rotation is less for liquid-air temperature. When the tube was placed in liquid air the pressure fell to half that at room temperature, a small volume near the window not being immersed. The actual pressure was used in plotting the results.

No anomalous rotation was found in the $(3-3)$ and $(2-2)$ bands. In the $(2-2)$ band, 7 mm of helium were sufficient to reduce the high rotational lines to nearly zero. At 33 mm only the lowest rotational line could still be observed. A detailed study of the high vibrational bands was not made because of their rapid decrease in intensity with increasing pressures of helium.

Figure 3 shows a comparison of a plate obtained from 0.6 mm of pure hydrogen with one from 0.6 mm of hydrogen and 400 mm of helium. The simplification introduced by the helium is striking and suggests that new hydrogen bands may be analyzed using this method of simplification.

It is with gratitude that the author acknowledges his indebtedness to Professor O. Oldenberg for many helpful discussions and suggestions.

Energy Bands in the Body-Centered Lattice*

MARVIN I. CHODOROW AND MILLARD F. MANNING**
Massachusetts Institute of Technology, Cambridge, Massachusetts

(Received July 23, 1937)

Slater's method of finding the structure of electronic energy bands in the body-centered lattices is extended so as to satisfy boundary conditions at fourteen points of the polyhedral cell surrounding an atom, instead of eight as in previous applications. Since this requires the use of all the "*d*" spherical harmonics, the method is now applicable to elements which have "*d*" electrons. Greater accuracy is also to be expected for other elements. The expansions of the determinants relating the energy E to k, the wave number vector, are given for all symmetry axes, and points, and in part for the symmetry planes. From group theory the places where various bands will stick together, i.e. degeneracies required by symmetry, are also determined.

I. INTRODUCTION

SLATER'S[1] extension of the method of Wigner and Seitz[2] has made possible an approximate determination of the detailed structure of electronic energy bands in crystals. In this method the crystal is divided into polyhedral cells of equal size, each cell surrounding one atom. In any one cell the wave function for an electron can be expanded as

$$\Psi=\sum_{m=-l}^{l}\sum_{l=0}^{\infty}A_{ml}u_l P_l^m(\cos\theta)e^{im\varphi},$$

where the u_l are radial functions (obtained by numerical integration) and $P_l^m(\cos\theta)e^{im\varphi}$ are surface harmonics. The constants A_{ml} are determined from the known periodicity conditions which the wave function and its slope must obey in a translation from one face of the cell to the perpendicularly opposite face. Since, to fulfill these conditions for the whole surface of the cell would be very difficult, in practice the boundary conditions are satisfied only at the midpoints of the faces, in which case we represent the wave function by a finite number of terms out of the above series. More exactly if we write

$$\Psi=G+iU,$$

where G is even with respect to inversion through the origin (taken at the nucleus in the center of the cell) and U is odd then the equations determining the A_{ml} are

$$U=\tan(K\cdot r_n/2)G,$$
$$G'=-\tan(K\cdot r_n/2)U'.$$

Here $r_n/2$ is the radius vector to the midpoint of one of the cell faces ($|r_n|$ is distance between midpoints of opposite faces), K is the reduced wave number vector,[3] the ($'$) denotes differentiation with respect to r, U, G, U', G' are evaluated at $r_n/2$. There is a pair of these equations for each pair of midpoints and therefore we will use as many terms in our polynomial for Ψ as the number of midpoints at which we wish to satisfy the boundary conditions.

These equations for A_{ml} are homogeneous and for a non-trivial solution the determinant of their coefficients must vanish. Setting this determinant equal to zero gives a relation between the energy E, which enters as a parameter in the numerical integration of the radial functions, and the wave vector K. A knowledge of E as a function of K throughout the whole Brillouin zone completely determines the structure of the band.

In previous applications to the body-centered lattice,[1,4] in which the cell is the familiar truncated octahedron with fourteen faces, eight between nearest neighbors, and six between second nearest neighbors, the boundary conditions were satisfied at the midpoints of the faces between nearest neighbors. The eight functions

* A preliminary report of this work with application to tungsten (unpublished) was given at a meeting of the American Physical Society in Rochester, N. Y. June, 1936, Phys. Rev. **50**, 399 (1936).

** Now at Toledo University.

[1] J. C. Slater, Phys. Rev. **45**, 794 (1934).

[2] Wigner and Seitz, Phys. Rev. **43**, 804 (1933) and **46**, 509 (1934).

[3] Cf. A. Sommerfeld and H. Bethe, *Handbuch der Physik*, Vol. 24; J. C. Slater, Rev. Mod. Phys. **6**, 209 (1934); Mott and Jones, *Theory of the Properties of Metals and Alloys*, Oxford, 1936.

[4] J. Millman, Phys. Rev. **47**, 286 (1935). F. Seitz, Phys. Rev. **47**, 400 (1935).

used in the expansion of Ψ were one s, three p, three d, and one f. Since the group[5] of a general K vector contains only the identity operation, there is no spatial degeneracy as in a free atom and an electronic level with a given l value in the free atom, which is always $2l+1$ fold spatially degenerate, splits up into $2l+1$ bands in the crystal. However, one cannot obtain, for instance, the five bands arising from an electronic d level, if an eight term polynomial is used for Ψ, containing only three d functions. Slater[1] pointed out that the method could be extended by fitting the boundary conditions at the midpoints of the six faces between second nearest neighbors, in which case fourteen functions would be used, including all of the d functions. When the d band in the metal is occupied, it is obviously necessary to use these extra functions and even for other cases, it should improve the accuracy of the results.[6] Moreover, Shockley,[7] in an attempt to check the accuracy of the method, has shown that although the use of eight functions gave quite good results in the first zone, it was in error by about 25 percent in the second. The more elaborate method would undoubtedly give more accurate results for the higher bands, and should therefore be used even for elements having only s and p valence electrons.

II. Method

For a general direction of propagation, the wave function for the value of K will contain all fourteen terms, and the resulting determinant will be of the fourteenth order, which is much too unwieldy for practical computation. For special directions of propagation (in symmetry planes, or along symmetry lines of the cell), i.e., where the group of K contains more than the identity operation, the wave functions will have symmetry properties which can be used to split the determinant into smaller ones. Under the operations of the group of K, the wave functions will transform by the irreducible representations of the group, and only those spherical harmonics which belong to the same representation will appear in the expansion of any one wave function. Due to these transformation properties of the wave functions, satisying the boundary conditions on one pair of faces, automatically satisfies them on all other pairs arising from the given pair by the symmetry operations of the group. Also for some representations the transformation properties are such that either the odd or even functions, or both, must vanish on certain pairs of faces, e.g., in the case of a symmetry plane, where the group contains two elements, those functions belonging to the antisymmetric representation must obviously vanish at all points lying in the plane. All this results in reducing the number of equations necessary to fit boundary conditions on all the faces, to exactly the number of spherical harmonics (out of the fourteen) belonging to the given representation. Therefore, instead of solving a fourteenth order determinant for all the K values (corresponding to the various zones) going with a given E, we solve several much smaller determinants, each for the K value or values,[8] corresponding to the zone (or zones) belonging to that representation.[9] Since, ultimately the constant energy surfaces in the Brillouin zones

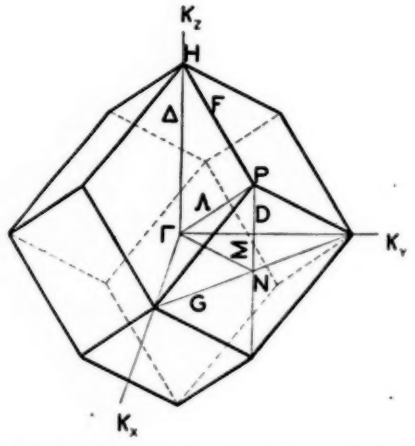

Fig. 1. Reduced Brillouin zone for the body-centered lattice.

[5] The group of a wave vector K contains those symmetry operations of the crystal class, i.e., rotations and reflections, which either leave the vector invariant or transform it into one belonging to an equivalent irreducible representation of the translation group, i.e., a vector differing from K by one of the translations of the reciprocal lattice. Cf. F. Seitz, Ann. Math. **37**, 17 (1936); Bouckaert, Smoluchowski and Wigner, Phys. Rev. **50**, 58 (1936).

[6] Unpublished calculations on potassium show that this improvement is appreciable.

[7] Doctoral thesis, M. I. T. (1936). Shockley applied the method to a case where the wave functions and energy were known exactly (constant potential) and compared the results obtained with those of the exact treatment.

[8] For some directions several zones may belong to the same irreducible representation.

[9] For classification of Brillouin zones according to their representations see paper by B. S. W. (reference 5).

are obtained by interlopation between known directions of K, as many possible directions as give manageable determinants must be examined. In the following section we give the results obtained.

III. Results

The reduced Brillouin zone for the body-centered lattice is shown in Fig. 1. For convenience we have used the notation of Bouckaert, Smoluchowski and Wigner[5] (to be referred to as B.S.W.) in labeling the axes of symmetry. We shall also use their notation for the various irreducible representations. For any direction of K, the functions are listed according to the representation to which they belong, the dimension of the representation,[10] and the expansion of the corresponding determinant given.

As has been pointed out by B.S.W., if we pass from a point of symmetry to an axis of symmetry, the group of the latter must be a sub-group of that of the former. The irreducible representations of the group of the point considered as representations of the sub-group (group of the axis), must either be irreducible representations of the group of the axis, or (if reducible) have the latter as their irreducible parts. The irreducible representation of any band along the axis must be contained in the irreducible representation of that band at the symmetry point. Since a point of symmetry always occurs at the intersection of two or more axes of symmetry, the above compatability relations between axes and points indicate which of the various band sections along the several axes may join. However, an irreducible representation along an axis may be compatible with several different irreducible representations at a point, and therefore this joining is not completely determined by symmetry, which only limits the possibilities, the actual numerical values being necessary for a complete determination. But inasmuch as these compatibility relations may not be violated, they serve as a valuable check on any numerical calculations. For this reason we include the representations at the various symmetry points, the functions belonging to them and the determinants. We have also given these data for the symmetry planes, $K_z=0$, $K_z=K_y$, but only for the anti-symmetrical representations. The determinants for the symmetrical representations are larger than can be conveniently handled.[11]

The fourteen functions used were

$$\text{even}\quad 1s\quad \frac{xy}{r^2}d\quad \frac{xz}{r^2}d\quad \frac{yz}{r^2}d\quad \frac{x^2-y^2}{r^2}d\quad \frac{3z^2-r^2}{r^2}d\quad \frac{5(x^4+y^4+z^4)-3r^4}{r^4}g;$$

$$\text{odd}\quad \frac{x}{r}p\quad \frac{y}{r}p\quad \frac{z}{r}p\quad \frac{x(5x^2-3r^2)}{r^3}f\quad \frac{y(5y^2-3r^2)}{r^3}f\quad \frac{z(5z^2-3r^2)}{r^3}f\quad \frac{xyz}{r^3}f;$$

s, p, d, f, g, refer to corresponding radial functions.

In using fourteen points we need the value of the radial functions and their slopes at two distances.

r_1 = half-distance between nearest neighbors $=(3)^{\frac{1}{2}}a/4$,

r_2 = half-distance between second nearest neighbors $=a/2$,

thus s_1, p_1, d_1, f_1, g_1, and s_1', p_1' d_1' f_1', g_1' will refer to value of the functions and slopes at the distance r_1, and s_2, f_2, etc. will refer to distance r_2. For convenience we shall use an abbreviated notation for the spherical harmonics omitting the denominator, thus x will mean x/r, $3z^2-1$ will mean $(3z^2-r^2)/r^2$ etc.

Also since certain symmetrical combinations of terms frequently appear in the expansions, we list these and the notation we use for them

$$\begin{aligned}
\sqrt{3}B_1&=3p_1'f_2'+2p_2'f_1', & S_1&=3s_1'g_2'+2s_2'g_1',\\
\sqrt{3}B_2&=3p_1'f_2+2p_2f_1', & S_2&=3s_1'g_2+2s_2g_1',\\
\sqrt{3}B_3&=3p_1f_2'+2p_2'f_1, & S_3&=3s_1g_2'+2s_2'g_1,\\
\sqrt{3}B_4&=3p_1f_2+2p_2f_1, & S_4&=3s_1g_2+2s_2g_1,\\
B_5&=p_1'f_1-p_1f_1', & S_5&=s_1'g_1-s_1g_1',\\
B_6&=p_2'f_2-p_2f_2', & S_6&=s_2'g_2-s_2g_2',
\end{aligned}$$

$$D_1=d_1'/d_1,\quad D_2=d_2'/d_2,\quad F=f_1'/f_1.$$

[10] As in the case of atomic levels an n-dimensional irreducible representation denotes an n-fold degeneracy.

[11] Shockley (Phys. Rev. **51**, 132–3 (1937)) has given a method for expanding such determinants by using the expansions along axes contained in the plane. In our case, however, the resulting transcendental equations would be much too complicated to solve without excessive calculations.

TABLE I. *Symbol of the representation, the degeneracy (in parentheses), the functions belonging to the representation and the expanded determinant.*

Point Γ	$K=(0,0,0)$	
Γ_1	$1s\ \{5(x^4+y^4+z^4)-3\}g$	$S_1=0$
$\Gamma_{15}(3)$	$xp\ yp\ zp\ x(5x^2-3)f\ y(5y^2-3)f\ z(5z^2-3)f$	$B_4=0$
$\Gamma_{25}'(3)$	$xyd\ xzd\ yzd$	$d_1'=0$
$\Gamma_{12}(2)$	$(3z^2-1)d\ (x^2-y^2)d$	$d_2'=0$
Γ_2'	$xyzf$	$f_1=0$
Point H	$K=(0,0,2\pi/a)$	
H_1	$1s\ \{5(x^4+y^4+z^4)-3\}g$	$S_3=0$
$H_{15}(3)$	$xp\ yp\ zp\ x(5x^2-3)f\ y(5y^2-3)f\ z(5z^2-3)f$	$B_2=0$
$H_{25}'(3)$	$xyd\ xzd\ yzd$	$d_1=0$
$H_{12}(2)$	$(3z^2-1)d\ (x^2-y^2)d$	$d_3=0$
H_2'	$xyzf$	$f_1'=0$
Point P	$K=(\pi/a,\pi/a,\pi/a)$	
P_1	$1s\ \{5(x^4+y^4+z^4)-3\}g\ xyzf$	$FS_4+S_2=0$
$P_3(2)$	$(3z^2-1)d\ (x^2-y^2)d$	$d_2=0$
$P_4(3)$	$xp\ yp\ zp\ xyd\ xzd\ yzd\ x(5x^2-3)f\ y(5y^2-3)f\ z(5z^2-3)$	$D_1B_3+B_1=0$
Point N	$K=(\pi/a,\pi/a,0)$	
N_1	$1s\ xyd\ (3z^2-1)d\ \{5(x^4+y^4+z^4)-3\}g$	$2D_1D_2S_4+2D_2S_2+D_1S_3+S_1=0$
N_2	$(xz-yz)d$	$d_1'=0$
N_3	$(xz+yz)d$	$d_1=0$
N_4	$(x^2-y^2)d$	$d_2=0$
N_1'	$(x+y)p\ \{x(5x^2-3)+y(5y^2-3)\}f$	$B_1=0$
N_3'	$zp\ z(5z^2-3)f\ xyzf$	$FB_4+B_2=0$
N_4'	$(x-y)p\ \{x(5x^2-3)-y(5y^2-3)\}f$	$B_3=0$
Line Δ	$K=(0,0,k)\qquad T_1=\tan(ka/4)\qquad T_2=\tan(ka/2)$	
Δ_1	$1s\ zp\ (3z^2-1)d\ z(5z^2-3)f\ \{5(x^4+y^4+z^4)-3\}g$	
	$T_2^2T_1^2B_1(2S_3+D_2S_4)-6T_2T_1D_2(S_5B_6+S_6B_5)+T_2^2B_3(2S_1+D_2S_2)+3T_1^2B_2D_2S_3+3D_2B_4S_1=0$	
Δ_2	$(x^2-y^2)d$	$d_2'=0$
Δ_2'	$xyd\ xyzf$	$FT_1^2+D_1=0$
$\Delta_5(2)$	$xp\ yp\ xzd\ yzd\ x(5x^2-3)f\ y(5y^2-3)f$	$B_2T_1^2+D_1B_4=0$
Line Σ	$K=(k,k,0)\qquad T=\tan(ka/2)$	
Σ_1	$1s\ (x+y)p\ xyd\ (3z^2-1)d\ \{x(5x^2-3)+y(5y^2-3)\}f\ \{5(x^4+y^4+z^4)-3\}g$	
	$T^4B_4(2D_1D_2S_4+D_1S_3+2D_2S_2+S_1)+T^2\{3D_2B_2(S_1+D_1S_3)+2D_1B_3(2D_2S_2+S_1)-12B_6S_5D_1D_2$	
	$-12B_5S_6D_1D_2\}+6D_1D_2S_1B_4=0$	
Σ_2	$(xy-yz)d$	$d_1'=0$
Σ_3	$zp\ (xz+yz)d\ z(5z^2-3)f\ xyzf$	$T^2(B_2+FB_4)+2D_1B_4=0$
Σ_4	$(x-y)p\ (x^2-y^2)d\ \{x(5x^2-3)-y(5y^2-3)\}$	$T^2B_3+D_2B_4=0$

In Table I we list first the symbol of the representation, in parentheses the degeneracy, if any, then the functions belonging to that representation and the expanded determinant.

In the section of Table I for line D, the symbols D_1, D_2 etc. used for the irreducible representations are not to be confused with the D_1 and D_2 defined previously in terms of the radial d functions and their derivatives. It is also to be noted that the vectors ending on line F of Fig. 1. do not actually have the form $K=(k,k,k)$ as indicated in Table I. However, the vectors along the line Λ do have this form and if we continue along this line past the point P we will be considering a line of an adjoining cell which, because of the symmetry of the reciprocal lattice, has the same energy values as the line F. Similarly the line G with $K=(-k+2\pi/a,k,0)$ has the same energy values as the line $K=(2\pi/a,k,k)$ and the plane $K_x=K_y$ has the same energy values as the plane $K_x+K_y=2\pi/a$.

Most of the compatibility relations between the various axes, points and planes have been given by B.S.W. and the reader is referred to their paper for these. We give below some, applicable to our results, which they have omitted.

N_1	N_2	N_3	N_4	N_1'	N_3'	N_4'	P_1	P_3	P_4
G_1	G_3	G_2	G_4	G_4	G_3	G_1	F_1	F_3	F_1F_3
D_1	D_4	D_3	D_2	D_3	D_1	D_4	D_1	D_1D_2	$D_1D_3D_4$
Σ_1	Σ_2	Σ_3	Σ_4	Σ_1	Σ_3	Σ_4			

As an example of how these compatibility relations are to be used, let us consider an energy at which $d_1'=0$. At this energy there will be three bands stuck together at the center of the

TABLE I.—*Continued.*

Lines Λ and F	$K=(k,k,k)$ $T_1=\tan(ka/4)$ $T_2=\tan(ka/2)$ $T_3=\tan(3ka/4)$	
F_1	$1s\ (x+y+z)p\ (xy+xz+yz)d\ xyzf\ \{x(5x^2-3)+y(5y^2-3)+z(5z^2-3)\}f\ \{5(x^4+y^4+z^4)+3\}g$	
	$16FB_1S_4T_1^2T_2^2T_3^2+T_1^2T_2^2(3D_1S_4+S_2)(3B_3F+B_1)+T_2^2T_3^2(FB_3+3B_1)(D_1S_4+3S_2)+$	
	$6T_2^2T_1T_3(D_1S_4-S_2)(B_1-FB_3)-24T_2T_1T_3(T_1+T_3)F(B_6S_5+S_6B_5)+16T_1^2T_3^2B_2FS_3$	
	$+T_1^2(B_2+3B_4F)(S_1+3D_1S_3)+T_3^2(3B_2+FB_4)(3S_1+D_1S_3)+16T_2^2D_1S_2B_3$	
	$+6T_1T_3(FB_4-B_2)(S_1-D_1S_3)-24T_2(T_1+T_3)D_1(B_6S_5+S_6B_5)+16D_1B_4S_1=0$	
$F_2(2)$	$(x-z)p\ (y-z)p\ (yx-yz)d\ (xy-xz)d\ (x^2-y^2)d\ (3z^2-1)d\ \{x(5x^2-3)-z(5z^2-3)\}f$	
	$\{y(5y^2-3)-z(5z^2-3)\}f$	
	$T_1^2T_2^2B_1+T_1^2D_2B_2+T_2^2D_1B_3+D_1D_2B_4=0$	
Line D	$K=(\pi/a,\pi/a,k)$ $T=\tan(ka/4)$ $C=\mathrm{ctn}\ (ka/4)$ $T_2=\tan(ka/2)$	
D_1	$1s\ zp\ (3z^2-1)d\ xyd\ z(5z^2-3)f\ xyzf\ \{5(x^4+y^4+z^4)-3\}g$	
	$12T_2(C-T)(F-D_1)(B_6S_5+B_5S_6)+6T_2^2\{(FB_3-B_1)(S_2-D_1S_4)+2(B_1S_4F+B_3S_2D_1)\}$	
	$+3T_2^2(T^2+C^2)(B_3F-B_1)(S_2+S_4D_1)-(T^2+C^2)\{2D_2(B_2+FB_4)(S_2+D_1S_4)-(B_2+FB_4)(S_1+D_1S_3)\}$	
	$-2\{2D_2[(B_2-B_4F)(S_2-S_4D_1)+2(B_2S_4F+B_4S_2D_1)]+(B_2-B_4F)(S_1-S_3D_1)$	
	$+2(B_2S_3F+B_4S_1D_1)\}=0$	
D_2	$(x^2-y^2)d$	$d_2=0$
D_3	$(x+y)p\ (xz+yz)d\ \{x(5x^2-3)+y(5y^2-3)\}f$	$T^2D_1B_2+B_1=0$
D_4	$(x-y)p\ (xz-yz)d\ \{x(5x^2-3)-y(5y^2-3)\}f$	$T^2B_1+D_1B_2=0$
Line G	$K=(-k+2\pi/a,k,0)$ $T=\tan(ka/2)$	
G_1	$1s\ (x-y)p\ xyd\ (3z^2-1)d\ \{x(5x^2-3)-y(5y^2-3)\}f\ \{5(x^4+y^4+z^4)-3\}g$	
	$T^4B_2\{2D_2(S_2+D_1S_4)+(S_1+D_1S_3)\}+T^4\{B_1(2D_2S_4+S_2)+12B_6D_2S_5+12B_5D_2S_6+3B_4D_2(S_1+D_1S_3)\}$	
	$+6D_2B_2S_3=0$	
G_2	$(xz+yz)d$	$d_1=0$
G_3	$zp\ (xz-yz)d\ z(5z^2-3)f\ xyzf$	$T^2D_1(B_1+FB_4)+2FB_2=0$
G_4	$(x+y)p\ (x^2-y^2)d\ \{x(5x^2-3)+y(5y^2-3)\}f$	$T^2B_1+D_2B_2=0$
Plane $K_x=K_y$	$K=(k,k,u)$ $T=\tan(ka/2)$ $R=\tan(ua/4)$	
–	$(x-y)p\ (xz-yz)d\ (x^2-y^2)d\ \{x(5x^2-3)-y(5y^2-3)\}f$	
	$T^2R^2B_1+T^2D_1B_3+R^2D_2B_2+D_1D_2B_4=0$	
Plane $K_z=0$	$K=(k,u,0)$ $T=\tan[(k+u)a/4]$ $R=\tan[(k-u)a/4]$	
–	$zp\ xzd\ yzd\ z(5z^2-3)f\ xyzf$	$2T^2R^2B_2F+D_1(FB_4+B_2)(T^2+R^2)+2D_1^2B_4=0$

zone and belonging to the representation Γ_{25}'. As we go out along the line Δ two of the bands will continue to stick together, having representation Δ_5 and the third with Δ_2'. Since Δ_5 is compatible with either H_{15} or H_{25}' the two degenerate bands may end at either the energy for which $d_1=0$ or $B_2=0$, and if we assume that the bands we are considering started at an energy lower than any other Δ_5 bands (two more start at energy for which $B_4=0$), they will end at the lower of these two energies, since bands of the same symmetry in general will not intersect, tending to repel each other. Let us consider the energy for $d_1=0$ as the lower. Since this belongs to H_{25}' which is triply degenerate there must be another band ending here, which had the representation Δ_2' (H_{25}' being compatible with $\Delta_2'\Delta_5$). This Δ_2' band may be either the one which started at the same point as the Δ_5 bands (i.e. $d_1'=0$, representation Γ_{25}') or one which started at $f_1=0$ (representation Γ_2'), in which case the former will end at $f_1'=0$ (H_2' also compatible with Δ_2'). The determining factors again are the numerical values and the fact that bands of like symmetry will not cross. Thus if $f_1=0$ occurs at a higher energy than $d_1'=0$, we have the two possibilities shown in Fig. 2. Here we have plotted the energy E (ordinate) as a function of $|K|$. (A) illustrates the case where the energy at which $d_1=0(H_{25}')$ is higher than that at which $f_1'=0(H_2')$. (B) illustrates the reverse case. It must be remembered that the curve Δ_5 represents two bands. In these diagrams the shape of the bands is not significant, the Δ_2' bands and Δ_5 bands may cross (accidental degeneracy) or in the case (B) the Δ_2' band starting at $d_1'=0$ may be above the Δ_5 bands. The correlations between beginnings and ends of bands here are significant, these being the

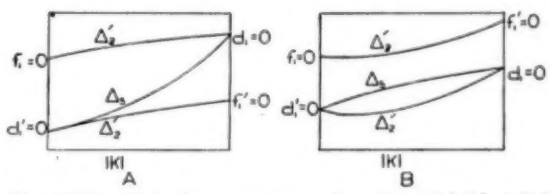

FIG. 2. The plot of energy E as a function of $|K|$. (A) illustrates the case where the energy at which $d_1=0$ is higher than that at which $f_1'=0$. (B) illustrates the reverse case.

only possibilities allowed, assuming $f_1=0$ at higher energy than $d_1'=0$. The possibilities for the opposite case follow in an analogous manner. It must be noted that results obtained here for degeneracies, the various bands which may stick together etc. are not dependent on our approximation. In an exact treatment (i.e., fitting boundary conditions over the whole surface of the cell) while the numerical values would be shifted, the spherical harmonics would still be classified according to representations, the compatibility relations would still hold and all the above results would follow. Thus, for example, the bands arising from a d atomic level would still have the same symmetry properties as above (determined essentially by the transformation properties of the various d functions). All the information we have obtained about these bands from their symmetry properties would still be valid in an exact treatment, or in any other method of approximation.

We wish to thank Professor Slater who suggested this problem and Dr. Shockley for many useful suggestions.

OCTOBER 1, 1937 PHYSICAL REVIEW VOLUME 52

The Zeeman Effect of the Rare Gases

J. B. GREEN
Mendenhall Laboratory of Physics, Ohio State University, Columbus, Ohio
(Received August 4, 1937)

The g values of the neutral rare gases have been calculated from the atomic coupling factors for the $np^5n'p$ configurations, and excellent agreement is shown to exist between theory and experiment in most cases. From curves of the g values, interesting conclusions regarding the the genealogy of the terms in these configurations are noted.

THE Zeeman effect of the neutral rare gases has been studied by a number of investigators, first among them Back[1] who showed, by means of his work on neon, the first discrepancies of the simple Landé theory and its failure to explain the anomalous g values that he had observed. At the same time, he gave the first evidence of the g sum rule.

A theoretical investigation by Houston[2] led the way to the interpretation of these g values and the possibility of their calculation from atomic coupling parameters. Pogany's[1(d), 1(e)] work on the rare gases has shown that excellent agreement exists between theory and experiment for the first excited state of these atoms, the configuration $np^5(n+1)s$, the type of configuration studied by Houston and Condon and Shortley,[3] and Jacquinot[4] has extended the work of Pogany to include the higher series members of this type of configuration in neon, namely the $2p^53s$, $2p^54s$, $2p^55s$, and $2p^56s$ configurations. Although a comparatively large amount of experimental evidence exists, there seem to have been no other calculations made for any other configurations of the rare gases except the $2p^53p$ configuration of neon, where the agreement between theory and experiment is extremely poor.

It is the purpose of the present paper to give a comparison between the observed g values and the g values calculated from the parameters determined by Bartberger[5] from a least-squares solution of the problem as set up by Shortley[6] for the $np^5n'p$ configurations of the rare gases. Bartberger's parameters were determined from the matrix of the energy set up in JJ coupling as the zero-order approximation, but such a zero-order scheme is not suitable for the calculation of g values, since the weak-field magnetic interaction terms are not diagonal in jj coupling. They are, however, in LS coupling, and Bart-

[1] (a) Back, (neon), Ann. d. Physik **76**, 329 (1925); (b) Terrien and Dykstra, (argon), J. de phys. **5**, 439 (1934); (c) Bakker, (argon, krypton, xenon), Diss. Amsterdam, 1931; (d) Pogany (krypton) Zeits. f. Physik **86**, 729 (1933); (e) Pogany (argon, krypton, xenon) Zeits. f. Physik **93**, 364 (1935).
[2] Houston, Phys. Rev. **33**, 297 (1929).
[3] Condon and Shortley, Phys. Rev. **35**, 1342 (1930); see also Laporte and Inglis, Phys. Rev. **35**, 1337 (1930).
[4] Jacquinot, Comptes rendus **202**, 1578 (1936).
[5] Bartberger, Phys. Rev. **48**, 682 (1935).
[6] Shortley, Phys. Rev. **44**, 666 (1933).

berger's parameters were used in the matrices set up in the LS scheme. The electrostatic coupling parameters are given on page 298 and the electromagnetic interaction terms on page 268 of Condon and Shortley's *Atomic Spectra*,[7] to which the reader is referred. The only change to be noted is that the sign of the parameter ζ' as given by Bartberger is to be changed before introduction into the matrix.

The calculation of the g factor of a particular term is then comparatively simple. It has been outlined by Marvin,[8] but perhaps a brief resumé would not be out of place here. The value of the term is subtracted from the diagonal terms of the matrix. The determinant thus formed would then be equal to zero. If M_1, M_2, M_3 $\cdots$ represent the minors of the diagonal terms of this determinant and g_1, g_2, g_3 $\cdots$ the LS g values of the terms designating the rows and columns of the original matrix; then the g value in intermediate coupling of the particular term under consideration is given by

$$g=\frac{g_1M_1+g_2M_2+g_3M_3+\cdots}{M_1+M_2+M_3+\cdots}.$$

This method is very much simpler of application and identical in result with the method which diagonalizes the matrix and which may be written

$$g(\alpha j)=\sum_{\gamma sl} g(slj)\,|\,(\gamma slj|\,\alpha j)\,|^2.$$

In fact, it may be shown that the square of the transformation coefficient

$$|\,(\gamma slj|\,\alpha j)\,|^2=M_\alpha/\sum M_\alpha.$$

The calculations are summarized in Table I, II and III. The calculations for Ne $2p^53p$ are Shortley's.[9]

In addition to the configurations in the tables the $4p^56p$ of Kr has been determined experimentally,[1(e)] but the coupling parameters have not yet been calculated accurately. In addition, a serious discrepancy exists in the g sum of the terms for $j=1$.

In general, except for the lowest levels of argon and neon, the agreement between theory and experiment is very satisfactory. In all cases where there is a disagreement in the g value, there is also a disagreement between the observed and calculated positions of the levels.

But a much more significant result is found when we plot the observed g values against the ratio of electromagnetic to electrostatic coupling parameters. This is shown in Figs. 1 and 2. In order to show the complete transition from LS

TABLE I. *g values of Ne* $2p^5np$.

J	LEVEL	$2p^53p$ (obs.)[1(a)]	$2p^53p$ (calc.)(9)	$2p^54p$ (obs.)*	$2p^54p$ (calc.)
1	p_2	1.340	1.339	1.397	1.411
	p_5	.999	1.105	.685	.695
	p_7	.669	.561	.981	.964
	p_{10}	1.984	1.993	1.934	1.930
	Σg	4.992	5.000	4.997	5.000
2	p_4	1.301	1.415	1.178	1.190
	p_6	1.229	1.106	1.376	1.363
	p_8	1.137	1.146	1.116	1.114
	Σg	3.667	3.667	3.670	3.667

* Unpublished results of Green and Peoples, reported at Washington meeting of the American Physical Society, 1937.

TABLE II. *g values of A* $3p^5np$.

J	LEVEL	$3p^54p$ (obs.)[1(e)]	$3p^54p$ (calc.)	$3p^55p$ (obs.)[1(b)]	$3p^55p$ (calc.)
1	p_2	1.379	1.363	1.45	1.466
	p_4	.819	.887	.61	.643
	p_7	.840	.774	1.01	1.001
	p_{10}	—	1.976	1.90	1.890
	Σg	—	5.000	4.97	5.000
2	p_3	1.248	1.280	1.18	1.179
	p_6	1.302	1.271	1.42	1.378
	p_8	1.121	1.116	1.09	1.110
	Σg	3.671	3.667	3.69	3.667

TABLE III. *g values of Kr and Xe.*

		Krypton		Xenon		
J	LEVEL	$4p^55p$ (obs.)[1(e)]	$4p^55p$ (calc.)	LEVEL	$5p^56p$ (obs.)[1(e)]	$5p^56p$ (calc.)
1	p_3	1.425	1.461	p_2	—	1.494
	p_4	.631	.653	p_4	—	.639
	p_7	1.028	1.002	p_7	1.02	1.029
	p_{10}	1.891	1.884	p_{10}	—	1.838
	Σg	4.975	5.000	Σg	—	5.000
2	p_2	1.163	1.179	p_3	1.183	1.178
	p_6	1.400	1.365	p_6	1.402	1.391
	p_8	1.116	1.123	p_9	1.113	1.098
	Σg	3.679	3.667	Σg	3.698	3.667

[7] Condon and Shortley, *Theory of Atomic Spectra* (Cambridge University Press, 1935).

[8] Marvin, Phys. Rev. **44**, 818 (1933).

[9] Shortley, Phys. Rev. **47**, 295 (1935).

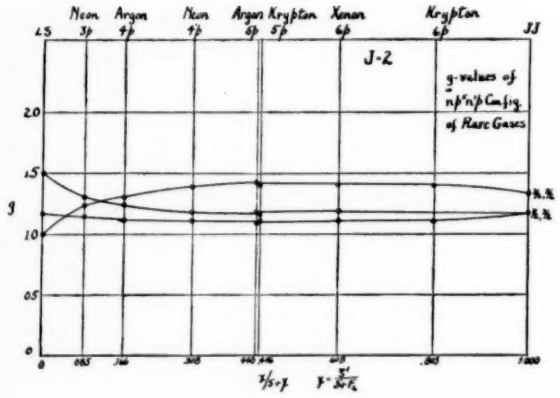

FIG. 1. g values of $np^5n'p$ of rare gases plotted against ratio of electromagnetic to electrostatic coupling parameter $J=1$. The g sum rule is indicated by the sum of the ordinates of the four curves being equal to 5.

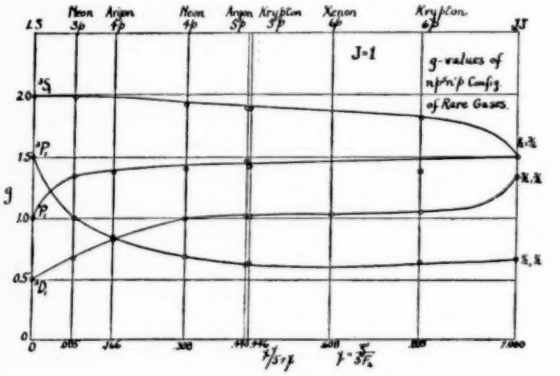

FIG. 2. g values of $np^5n'p$ of rare gases plotted against ratio of electromagnetic to electrostatic coupling parameter $J=2$. The g sum rule is indicated by the sum of the ordinates of the three curves being equal to 11/3.

coupling to JJ coupling on one graph, the g values of the levels have been plotted as ordinates, and $\chi/5+\chi$ as abscissae, where $\chi=\zeta'/5F_2$, ζ' being the electromagnetic and F_2 the electrostatic coupling parameter. Thus the abscissa is 0 for LS coupling and 1 for jj coupling.

All of the known g values have been plotted and members of the same series within each element joined together. Smooth curves were then drawn among the points so determined and all the elements joined together and extrapolated at both ends to the g values for LS coupling and jj coupling.

These curves bring out very clearly the genealogy of the levels of the rare gas configurations and show definitely the futility of the assignment of L and S values to the levels in these cases of intermediate coupling.

Thus, we see in the spectrum of neon that the levels p_5 and p_7, called $^1P_1$ and $^3D_1$ respectively in the $2p^53p$ configuration, have actually interchanged g values in the $2p^54p$ configuration and to be consistent, should now be called $^3D_1$ and $^1P_1$, respectively. It seems meaningless to designate members of the same series by different LS designations. A similar situation holds with respect to the levels p_4 and p_6 which also seem to interchange roles in going from the $2p^53p$ to the $2p^54p$ configurations.

It is also striking to note the sensitivity of the g values with respect to changes in the coupling. The $^3S_1$ changes very slowly until jj coupling is almost reached, and then changes very rapidly. $^3D_1$ changes rapidly at each end and very slowly at intermediate values and has a point of inflection. $^3P_1$ and $^3P_2$ drop very rapidly and then assume an almost steady value. $^1P_1$ rises rapidly at first, and then very gradually. $^3D_2$ drops very slowly and rises again near jj coupling. $^1D_2$ behaves almost oppositely.

In conclusion, the author wishes to express his thanks to Professor C. W. Ufford of Allegheny College, for supplying him with important data, and for some very valuable discussions.

Propagation of Potential in Discharge Tubes

L. B. SNODDY, J. R. DIETRICH AND J. W. BEAMS
University of Virginia, Charlottesville, Virginia
(Received July 27, 1937)

The speed of propagation of potential waves in long discharge tubes containing dry air has been measured as a function of pressure in three tubes with internal diameters of 1.7, 5 and 18 mm. Positive and negative impulsive potentials of approximately 125 kv were used. In general, in the low pressure range the speed increases with increasing pressure. From 0.02 to 0.2 mm the curves are steep; above this range there is a decided flattening. At relatively high pressures the speed decreases and the wave shape is greatly distorted. No appreciable difference between the speeds in dry air, CO_2 or H_2, could be detected in the 5 mm tube. The speed at constant pressure in dry air is approximately a linear function of the applied voltage (75–180 kv–5 mm tube). The initial wave which traverses the tube from high voltage end to the grounded end is followed immediately by a return discharge wave starting at the grounded end. The speed of this wave is about 10^{10} cm/sec. and is apparently independent of tube diameter. There is a slight increase in speed with pressure. Maximum currents in the initial wave were measured as a function of pressure. Voltage attenuation and some knowledge of the field in the wave fronts were obtained. The speed is found to obey the principle of similarity. Speeds in the 18 and 5 mm tubes are the same at pressures in the small tube 3.6 times those in the large tube. Speeds in the 1.7 mm tube are higher than they should be according to this principle. This is probably due to the high current density (4000 amp./cm²).

THE potential wave traversing a long discharge tube to which an impulse voltage is applied was shown in our earlier work[1] to have essentially the same characteristics as the accompanying wave of luminosity.[2] The time required for the potential wave to travel between two electrodes in the discharge tube was found to increase both with decreasing pressure and applied voltage and to be of the same order of magnitude as the time determined for the luminous wave to travel an equal distance. After this initial wave reached the grounded end of the tube a discharge wave starting at the grounded end and moving with about 1/3 the speed of light returned to the input end. Following this there were a few reflected waves rapidly decreasing in intensity superimposed upon the damped oscillation of the circuit as a whole.

The purpose of the present work was to investigate the times of travel as a function of pressure and voltage in tubes of different diameters. In addition to these measurements, the current-time curves and the values of maximum currents in the initial wave have been obtained together with some knowledge of wave fronts and voltage attenuation. Most of the measurements have been carried out with dry air although some were made with H_2 and CO_2.

[1] Snoddy, Beams and Dietrich, Phys. Rev. **50**, 469 (1936); **50**, 1094A (1936); **51**, 1008A (1937).
[2] Beams, Phys. Rev. **36**, 997 (1930).

APPARATUS AND METHOD

The apparatus is shown schematically in Fig. 1. It is essentially the same as that used in the preliminary investigation. Three Pyrex tubes (T) with internal diameters of 1.7, 5 and 18 mm were used. The lengths of tubing were joined by external glass sleeves waxed in place with Apiezon "W." Care was taken to keep all wax out of the discharge path. The terminal electrodes E_1, E_4 were brass rods with hemispherical ends and the electrodes E_2, E_3 short lengths of brass tubing. The oil pump and drying system were attached at P and the pressure read on a type of Pirani gauge at G. Pressures above the range of this gauge were read on a mercury manometer. A cold trap was placed in series with the manometer to prevent any appreciable amount of Hg vapor from diffusing into the system. The pump was shut off and the system allowed to come to equilibrium before observations were taken. As much H_2O vapor as possible was removed from the tube walls by long continued pumping and repeated discharging with a high current input. The applied potential was obtained from the Marx circuit C. A high speed, high voltage oscillograph of the Dufour type was used to determine the potential variations. The oscillograph circuit and the method used to synchronize the oscillograph and supply potential circuits are not shown as they followed standard

practice for such problems. The electrodes E_2, E_3 were connected to the oscillograph deflection plates through symmetrical capacity dividers in such a manner that simultaneous equal potentials at E_2 and E_3 would produce no displacement of the electron beam. With this arrangement a

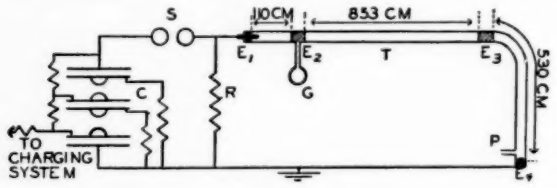

FIG. 1. Schematic diagram of apparatus showing input circuit and discharge tube.

potential wave passing down the tube produces a deflection of the beam when it arrives at E_2. This deflection is decreased when the wave arrives at E_3, the amount of decrease depending upon the voltage attenuation between E_2 and E_3. In like manner a return wave can be followed from E_3 to E_2. This oscillogram, together with a knowledge of the voltage variation at each electrode separately throughout the course of the discharge, furnishes a complete description of the traveling potential wave. Both negative and positive impulses were used.

As in the case of the luminous wave[2] the potential pulse starting at E_1 traveled relatively slowly at first. Times of travel consequently were not measured from the input electrode E_1 but from the second electrode E_2 placed about 110 cm down the tube. This distance depends upon the voltage, pressure, size of the tube and the initial degree of ionization. E_2 was placed at a point such that the wave fronts of successive discharges at constant pressure did not vary appreciably. This minimizes any effect due to a variation in the initial rate of propagation and eliminates the error involved in the time lag of the breakdown process at the entering electrode. In this work the average speed from E_1 to E_2 was about 1/3 of that from E_2 to E_3.

Current-time curves were obtained by connecting the deflection plates of the oscillograph across an electrolytic resistance of 240 ohms in series with the tube between S and E_1. Because of this resistance the voltage applied to the tube was not constant. It was found, however, that the speed of the potential wave and its form were not greatly altered provided the input voltage was adjusted to compensate approximately for the drop in the resistance. In most of the work only the maximum current in the initial wave was determined. For this the output end (E_4) of the tube was disconnected from the circuit and insulated. The current was computed from the voltage appearing across an electrolytic resistance of 40 to 80 ohms in series with the tube at the input end. This voltage was measured by a spark gap which was irradiated by ultraviolet light. While this method leads to an underestimation of the current due to the time lag of the measuring gap, the values obtained in this way are fair averages since the oscillograph showed that the current varied considerably from one discharge to the next.

RESULTS

A typical diagram of the voltage variations at the electrodes E_2 and E_3 is given in Fig. 2. In (1) the arrival of the wave at E_2 is shown at a and at b the wave has reached E_3. The time $b-c$ represents the time of transit of the initial wave from E_3 to E_4 plus the time necessary for the discharge wave to reach E_3 from the grounded end of the line. Since the gas is made highly conducting by the initial pulse, this discharge wave is similar to that obtained by grounding one end of a charged transmission line. As nearly as can be determined its speed is approximately 1/3 that of light. The part from c on represents voltage variations due to the discharge wave superimposed upon the slow damped oscillation of the circuit as a whole. At high pressures and high potentials the time $b-c$ is

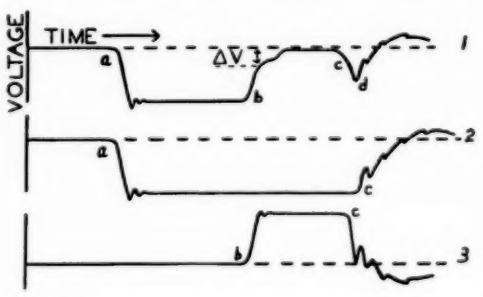

FIG. 2. General form of voltage variations observed with the oscillograph; (1) with electrodes E_2 and E_3 connected to deflection plates, (2) with E_2 alone—second deflection plate grounded, (3) E_3 alone.

variable, due at least in part to the practical difficulty of maintaining E_4 at constant potential when the gap S discharges. E_3 was placed at such a distance from E_4 that the time of transit from E_3 to E_4 and back to E_3 was always greater than the duration of the initial wave front. With this precaution the range of the measured times from a to b under conditions of constant pressure and voltage did not generally exceed 7 or 8 percent, although a few of the highest speed measurements show variations up to twice that amount. With E_4 disconnected from the circuit and insulated, the initial wave remains the same but the part from c on is lacking, showing that the last part is due to the discharge wave. ΔV represents the voltage attenuation of the wave front in traveling the distance E_2-E_3. In (2) and (3) typical voltage variations at E_2 and E_3 throughout the course of the discharge are given separately.

In Fig. 3 typical oscillograms of the voltage variations for positive and negative impulses are shown together with a current oscillogram for a positive impulse. The part $a-c$ in the current picture is characteristic of the initial wave, the part from c on shows the building up of the current after the discharge wave has returned to the input end of the tube.

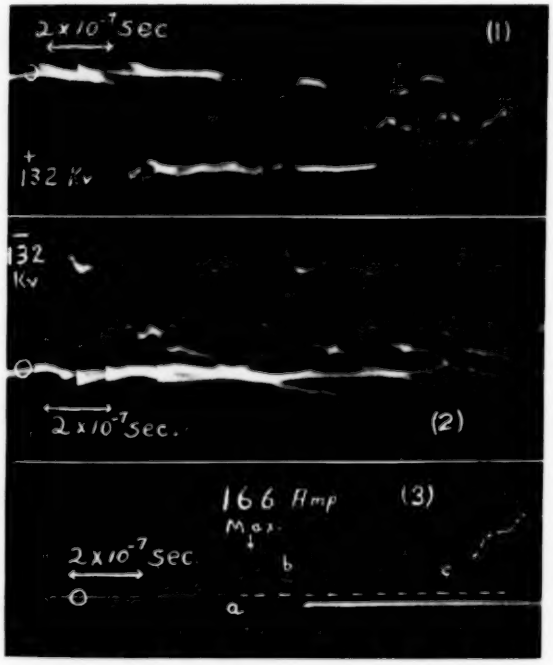

FIG. 3. Oscillograms of voltage and current. (1) Positive impulse pressure 0.18 mm 132 kv. (2) Negative impulse, pressure 0.11 mm 132 kv. (3) Voltage variation across 240 ohm resistance between S and E_1. Pressure 0.39 mm. Voltage of input condenser 160 kv.

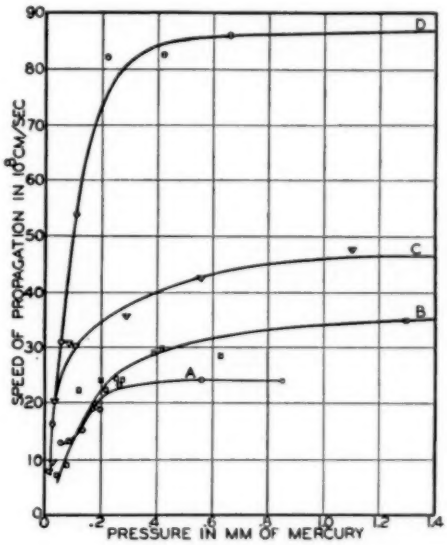

FIG. 4. Average speeds of propagation in dry air as a function of pressure. A, B, C, for positive impulse with tubes of internal diameter 1.7, 5 and 18 mm, respectively. D negative impulse 18 mm tube.

In Fig. 4 the average speeds of propagation in dry air are given as a function of pressure for tubes with inside diameter of approximately 1.7 (curve A), 5 (curve B) and 18 mm (curves C and D). The applied potential was kept constant at 125 kv for the 5 mm tube and at 132 kv for the other two tubes. Curves A, B and C are for the positive and D for the negative input voltage. The scattering of the points for a particular tube at the lower pressures is probably due to the difficulty of an exact determination of the pressure for each oscillograph trace arising from the liberation of gas from the walls of the tube by the discharges which are used to obtain proper synchronization between oscillograph and input circuits.

The negative wave is of particular interest as it probably closely resembles on a miniature scale the initial leader stroke of the lightning flash. This leader stroke travels from the cloud to ground either in a continuous or stepped manner with a maximum speed of approximately $3\text{–}5\times10^9$ cm/sec.[3]

[3] Schonland and Collins, Proc. Roy. Soc. **A143**, 654 (1934); Schonland, Malan and Collins, Proc. Roy. Soc. **A152**, 595 (1935); McEachron, Elect. J. **31**, 251 (1934); McEachron, Elect. World **104**, 15 (1934); Workman, Beams and Snoddy, Physics **7**, 375 (1936).

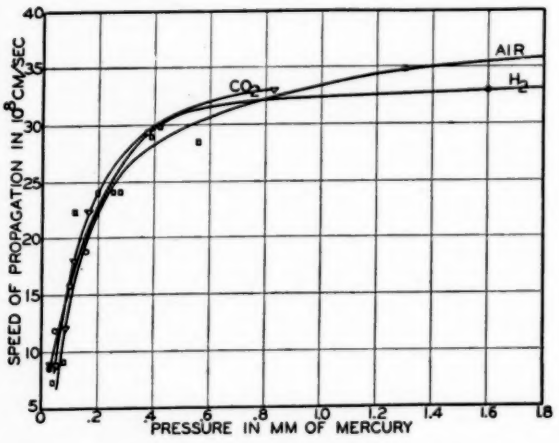

FIG. 5. Average speeds of propagation for dry air, CO_2 and H_2. Positive impulse (125 kv) in 5 mm tube.

Since the speed of the negative wave (curve *D*) seemed to be approaching with increase in pressure a value inconsistent with the observed values of leader velocity, one measurement was made at about 15 mm pressure. The speed had decreased to 47×10^8 cm/sec. indicating that the high value observed is probably a characteristic of the low pressure discharge, perhaps influenced in some way by the relatively small diameter tube used. In order to obtain a definite correlation with the lightning leader velocity it will be necessary to work over a much extended voltage and pressure range in a large tube. We are planning to do this in the near future.

Wave distortion and attenuation are very pronounced for the voltages used at pressures of a few mm changing entirely the character of the pulse from a wave type with a defined wave front to an approximately exponential rate of charging. As a consequence, only a few measurements were made above the range given in Fig. 4.

The speeds given here are the average speeds over the distance E_2-E_3. The time from a point halfway between E_2 and E_3 to E_3 was determined for a negative pulse (18 mm tube) at three pressures (0.021, 0.038 and 0.047 mm). The computed speeds were about 40 percent greater than the average, indicating an apparent increase in speed as the negative pulse travels down the tube. A similar determination for the positive wave (18 mm tube) over the first half of the tube gave a speed approximately 35 percent greater than the average, indicating a decrease in speed as the wave progresses. These measurements should be taken simply as an indication of the trend of the change of speed with distance down the tube for the two polarities since more work will have to be done with much longer tubes before the speed as a function of tube length can be determined with sufficient accuracy to compare absolute values.

The speed is greatly increased by the presence of appreciable ionization in the gas ahead of the wave. If two discharges are sent through the tube in rapid succession, the speed of the second pulse may be several times that of the first. Sufficient time was allowed between discharges to prevent any influence of this kind.

Figure 5 gives curves for the 5 mm tube for dry CO_2, H_2 and air with an applied voltage of 125 kv. Within the precision of measurement there is no apparent difference in speed over the pressure range used. Tank CO_2 and H_2 were used without purification other than rather careful drying over P_2O_5.

Figure 6 shows the speed as a function of positive voltage for the 5 mm tube at a constant pressure of 0.4 mm, which is above the range in which the speed varies rapidly with small changes in pressure. The relation between speed and voltage is quite accurately linear even though there was pronounced distortion and attenuation at the lower voltages.

The wave front appearing at *a*, Fig. 2, was not greatly influenced by changes in pressure over the range studied, although, at low pressures, it

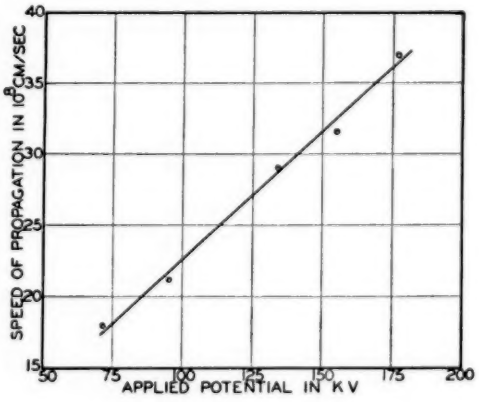

FIG. 6. Average speeds of propagation as a function of applied voltage at constant pressure of 0.4 mm. Dry air in 5 mm tube.

was measurably less steep than at high pressures. However, erratic variations due probably, in part, to distortion in the oscillograph, made a determination of the slope as a function of pressure of little value. Average values of the time from zero to 2/3 value are given in Table I.

To determine whether or not this slope was a characteristic of the input circuit rather than of the discharge, the discharge tube was replaced by a short electrolytic resistance of such a value that the maximum current through it was approximately the same as that through the tube. The rise in potential across it upon the breakdown of S was then measured. The slope of this wave was approximately the same as that at E_2 for the high pressure waves, but was definitely steeper than those at low pressure. This indicates that the wave front at E_2 is, at least in part, determined by the input circuit at high pressures but at low pressures is mainly a characteristic of the discharge tube itself.

The wave front at E_3, b of Fig. 2, and the attenuation ΔV were greatly changed as the pressure was increased. Usually, with an increase in pressure for any given voltage, the initial part of the wave front which is nearly linear became shorter and less steep, finally merging into a form represented approximately by $V(1-\epsilon^{-at})$. Values of attenuation, ΔV, are given in Table II.

TABLE I. *Average time of voltage rise at electrodes (0 to ⅔ value).*

Tube Diameter mm	Time to ⅔ Value	Sign of Applied Voltage
18	7.0×10^{-8} sec.	+
5	5.4	+
1.7	5.8	+
18	3.6	−

TABLE II. *Attenuation, ΔV, as a function of pressure for different tubes.*

Tube Diameter in mm	Pressure mm of Hg	ΔV Average in kv	Sign of Impulse
18	0.034	0	+
	0.56	22	
	1.1	45	
5	0.08	0	+
	0.20	25	
	0.56	40	
	1.3	60	
1.7	0.055	15	+
	0.22	25	
	0.56	31	
18	0.027	61	−
	0.055	27	
	0.22	23	
	0.42	33	
	0.66	33	

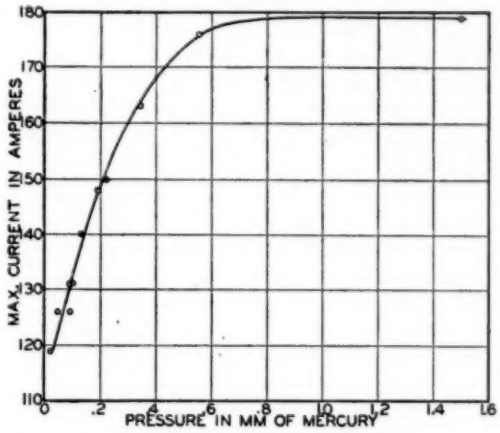

FIG. 7. Maximum current in initial wave as a function of pressure. Input condenser voltage 141 kv. Dry air in 5 mm tube.

The maximum current in the initial wave is given in Fig. 7 as a function of pressure for the 5 mm tube. The supply circuit voltage was 141 kv. For these measurements electrode E_4 was disconnected from the circuit and insulated. Curves of this type were not taken for the other tubes but the maximum current at a pressure beyond the range of rapid variation was measured. These are given in Table III.

The current-time oscillogram shown in Fig. 3 is apparently characteristic of the discharge at the higher pressures. At the lower pressures the decrease noted at b becomes more pronounced and for 0.07 mm the current at b is about 1/10 of the maximum. Beyond b it increases rapidly to a value which remains approximately constant throughout the initial wave.

The maximum voltage appearing at the output end of the tube (E_4) was determined both with the end insulated and with it connected to the return circuit through an electrolytic resistance. This voltage was measured by an irradiated spark gap. The shape of the voltage wave was also determined with the oscillograph. Curves of this type are shown in Fig. 8 for a positive impulse and 5 mm tube. Curves A, B, C give the voltage appearing across a resistance of 1.1×10^5

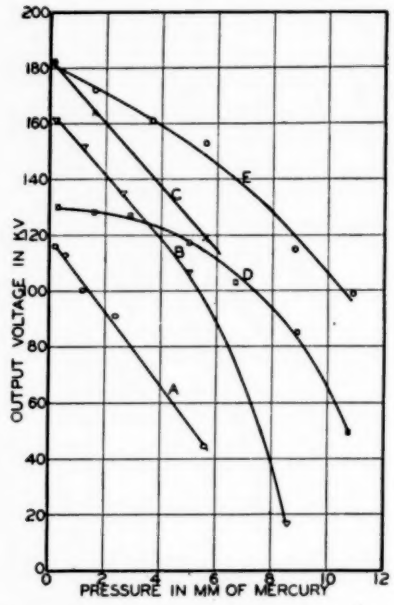

FIG. 8. Maximum voltage appearing at output end of tube (electrode E_4) as a function of pressure. A, B, C give voltages across 1.1×10^5 ohms for input voltages of 141, 180, and 194 kv respectively. For D and E, E_4 was insulated. Input voltage 141 and 194 kv, respectively. Dry air in 5 mm tube.

ohms as a function of pressure for applied voltages of 141, 180, and 194 kv respectively. For curves D and E the end of the tube was insulated ($R=\infty$). In Fig. 9 are shown several oscillograms of the voltage wave at the insulated end of the line. (Pressure 0.22 mm.)

The overvoltage at a in the oscillograms cannot be traced to any known oscillation or reflection in the circuit. It still appears when the output end of the line is shunted by a resistance as low as 30,000 ohms. At low pressures a similar although usually smaller increase can be observed in the wave appearing at the electrode E_3, even with E_4 grounded. With increasing pressure the amount of overvoltage rapidly decreases. It is apparently connected with the appearance of the minimum at b in the current-time curve (Fig. 3) and this is connected in some way with the initial building up of the propagation mechanism.

Because of this overshooting, the measured voltages in Fig. 8 at pressures below 0.4 mm are too high by amounts of approximately 3 kv for A to 8 kv for C.

The difference between the maximum voltage obtainable at E_4 at low pressure below the input voltage is about that to be expected on the basis of a sharing of charge between the capacity of the tube as a unit and the supply capacity.

If the corrected voltages for curves D and E are plotted against p^2, very good straight lines are obtained up to the pressures of about 9 mm.

The speed of the discharge wave returning from the grounded end of the tube to the input end is given in Table IV for two tubes at various pressures. As nearly as can be determined the speed is independent of the tube diameter and of the sign of the potential to which it is initially charged. It is thought, however, that the slight decrease in speed for the 18 mm tube at 0.034 mm pressure and the increase at 2.8 mm is real.

The speed of the luminous wave accompanying the potential wave was measured at a pressure of 0.1 mm and a positive voltage of 132 kv for the 18 mm tube. The method of Beams[2] which employs a high speed air turbine carrying a mirror was used. The light from two sections of the tube separated a distance of about 8 meters, after reflection from the rotating mirror was observed with a telescope fitted with a scale. The discharge in the tube supply circuit was tripped off by an auxiliary circuit which was started, when the mirror was in the proper position, by a discharge between two capillary gaps and two points extending a few mm from the rotating turbine. In this way very fair synchronization could be obtained between the mirror position and the time of discharge. For this work the output end of the tube was insulated.

These measurements were not made with any high degree of accuracy but were sufficient to show that, under the given conditions, the luminous wave and the potential wave traveled at speeds which did not differ by more than 20 percent. This of course gives no information

TABLE III. *Maximum current in initial wave for different tubes.*

Applied Voltage kv	Tube Diameter mm	Max. Current amp.	Pressure mm	amp./cm²
+132	18	230	0.6	90
+141	5	171	0.45	900
+180	5	143	0.08	750
+132	1.7	91	0.45	4000
−132	18	226	0.45	90

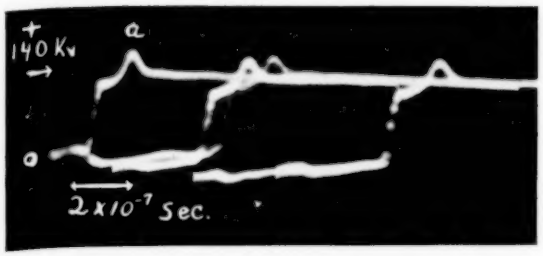

FIG. 9. Oscillograms of voltage wave at insulated end of line. Pressure (0.22 mm). 140 kv 18 mm tube.

concerning the relative positions of the potential and luminous wave fronts at any given time. A careful examination of the front of the luminous wave failed to show any characteristic shape. The wave front appeared quite straight with no apparent concentration either at the walls or toward the center of the tube. From this it would seem that the wave is not propagated as a surface discharge along the walls of the tube. It must be recognized, however, that faint luminosity $1\text{–}2\times10^{-8}$ sec. ahead of the main wave front probably would not be noticed.

DISCUSSION OF RESULTS

For an exact quantitative explanation of the propagation of a discharge of this type it is obvious that a number of other quantities should be known. A knowledge of electron densities, speed as a function of initial degree of ionization, ion current to the tube walls, etc., should be obtained. We are now starting work with a six inch tube about 42 feet long in which we hope that these quantities can be determined with some gas such as neon or argon.

However, there are a few relationships obtainable from this work which are of some interest. While the exact mechanism of the discharge is not known, it must depend upon a transfer of potential down the tube by ionization processes of the Townsend type. In the positive wave this necessitates a supply of electrons immediately ahead of the wave. These are probably formed by photoionization in the gas by light emitted in the wave front. It is possible of course that they may in part be derived from the tube walls. In the negative wave the electron supply is obtainable from the wave front where the electron density must be quite high. It is of interest to note, for the negative case, that the maximum speed of the initial wave approaches very closely to that of the discharge wave returning through the positive column left by the initial wave (0.89×10^{10} against 1×10^{10} cm/sec.).

One of the fundamental principles of the Townsend type of discharge is the principle of similarity. It states that a decrease in all linear dimensions of the discharge apparatus by a factor k must be compensated by an increase in pressure by the same factor to maintain some characteristic of the discharge such as the breakdown potential constant. For a constant applied potential the variation of the speed of propagation is the main characteristic and the tube diameter the only dimension to be considered. By a change in diameter from 18 mm to 5 mm, i.e., a factor of 3.6, it might be expected that the speed in the two tubes would be the same at pressures in the small tube, 3.6 times those in the large tube. Table V shows how accurately

TABLE IV. *Speed of discharge waves returning from grounded end to input end of tube.*

TUBE DIAMETER mm	PRESSURE mm	SPEED cm/sec.	VOLTAGE OF CHARGED TUBE
18	0.034	0.92×10^{10}	+132 kv
	0.29	1.03	
	0.56	1.00	
	1.1	1.11	
	3.9	1.07	
18	0.42	1.06×10^{10}	−132
	0.66	1.06	
	2.8	1.23	
1.7	0.055	1.07×10^{10}	+132
	0.086	1.07	
	0.18	.98	
	0.26	1.10	
	0.56	1.09	

TABLE V. *Illustration of principle of similarity.*

PRESSURE mm	TUBE DIAMETER IN mm	SPEEDS cm/sec.
0.016	18	8×10^{8}
0.0576	5	8
0.025	18	14
0.09	5	15
0.05	18	23
0.18	5	22.2
0.1	18	29.5
0.36	5	28
0.2	18	34.6
0.72	5	33.2
0.3	18	37.4
1.08	5	35

TABLE VI. *Field in wave front at electrodes E_2 and E_3.*

PRESSURE mm	POTENTIAL GRADIENT volts/cm E_2	E_3	
0.04	2300	2200	Applied voltage
0.08	1810	2800	+125 kv
0.12	870	910	
0.20	750	910	
0.42	920	740	
0.56	670	560	
1.3	420	340	

this relation holds over a considerable range of pressures for the positive impulse. This is in spite of the fact that the current density in the 5 mm tube is about 900 amp./cm². When this same principle is applied to the 1.7 mm tube the speed in it is about 9×10^8 cm/sec. too great at each pressure. Since the speed in this tube becomes practically independent of pressure at about 0.25 mm, the range available is not sufficiently great to determine whether or not this relation is accidental.

The discharge in the 1.7 mm tube is probably increased in speed by some additional process since the current density is about 4000 amp./cm². The presence of water vapor on the walls of the tube may have been a contributing factor since it is practically impossible to outgas thoroughly a tube of this diameter 50 feet in length. The independence of speed and pressure occurring at about 0.25 mm possibly means that the field in the positive column behind the wave front has become independent of pressure. This might be expected to happen in positive columns confined in very narrow tubes. In this way the energy supplied to the wave front is limited.

The speed in the 18 mm and 5 mm tubes for the positive impulse when plotted against log p can be fairly well represented by straight lines from pressures of 1.1 mm to 0.034 mm for the larger tube and from 5.4 mm to 0.11 mm for the smaller. Points below these pressures fall far off the curves. The ratio of pressures at which this relation fails is 3.2, which is nearly the ratio of tube diameters. This might be taken to mean that there is some change in the propagation mechanism when the mean free path becomes of the same order as the tube diameters.

The product of the attenuation ΔV times the maximum current I at any pressure when plotted against the speed at that pressure gives a linear relation (5 mm tube). This attenuation as measured represents the attenuation in the wave front and is not to be considered as uniformly distributed along the positive column back of the wave front. $\Delta V\times I$ is consequently proportional to the rate of energy loss in the wave front.

A rough idea of the magnitude of the field in the wave front can be obtained from the rate of potential rise at an electrode and the speed of propagation. Table VI gives these values at different pressures for the 5 mm tube and positive impulse of 125 kv. Although very erratic, the general decrease with pressure is evident. Presumably the speed would increase until the field in the wave front became independent of pressure.

By using the current-time oscillogram of Fig. 3 together with the known voltage, the total energy input was found to be 5.6 watt-seconds for the given pressure and voltage.

Magnetic Properties of Single Crystals of Silicon Iron

H. J. WILLIAMS
Bell Telephone Laboratories, New York, N. Y.

(Received July 29, 1937)

The magnetization curves for the [100], [110] and [111] directions of single crystals of iron containing 3.85 percent silicon were obtained from single crystal specimens cut in the form of hollow parallelograms so that the sides of each specimen were parallel to the tetragonal, digonal or trigonal axes, respectively. This method avoids the errors due to demagnetizing fields, inherent in previous measurements on single crystals. In addition to the well-known anisotropy at magnetizations above half of saturation, the data show for the first time considerable anisotropy at low magnetizations. A maximum permeability of 1,380,000 by far the highest ever reported for silicon iron, was observed in the [100] specimen after careful annealing. The magnetic anisotropy constants K_1 and K_2 were obtained from the magnetization curves and from torque measurements on a disk cut parallel to a (110) plane.

INTRODUCTION

THIS article describes three different ways of determining the ferromagnetic anisotropy constants K_1 and K_2 (see Eq. (1) below) of 3.85 percent silicon iron. This particular material was chosen because it is particularly easy to obtain in it very large single crystals of high permeability. The first way was to obtain the magnetization curves for the [100], [110] and [111] directions of a single crystal and then adjust the theoretical magnetization curves calculated according to the Akulov-Heisenberg theory to the experimental curves. A new method of measuring the magnetic properties of single crystals was employed. Single crystal specimens were used which formed closed magnetic circuits so that the specimens could be wound with primary and secondary windings and tested in the regular manner of testing toroidal specimens. The second method of evaluating the anisotropy constants was to measure the areas between the magnetization curves of these same specimens and then calculate the anisotropy coefficients from these areas as explained below. This method is, of course, essentially the same as the first. The third way of evaluating the coefficients was by means of torque measurements on a singe crystal disk. A disk was cut so that its plane was parallel to the (110) crystallographic plane. All three directions of interest lie along diameters of such a specimen. The disk was tested in a torsion magnetometer[1] and the theoretical torque curve which depends upon the anisotropy coefficients, was adjusted to fit the experimental curve.

[1] H. J. Williams, Rev. Sci. Inst. **8**, 56–60 (1937).

METHOD OF GROWING CRYSTALS

Large crystals of silicon iron were produced by melting silicon iron in an atmosphere of pure hydrogen and permitting the melt to solidify very slowly. Silicon iron containing 3.85 percent silicon was melted in an alundum boat 10 cm square and 2 cm deep. The furnace had an alundum muffle with a molybdenum winding and high grade alundum powder was used for external heat insulation. The melt was cooled at the rate of approximately 8°C per hour until it had completely solidified. The temperature gradient of the furnace was such that crystals grew across the melt resulting in a number of elongated crystals in the ingot. Some of these were approximately 1 cm wide, 2 cm deep, and extended in a somewhat irregular manner nearly 10 cm across the ingot. After etching it could be seen that these elongated crystals had tended to grow along a [100] crystallographic direction.

PREPARATION AND DESCRIPTION OF SPECIMENS

The approximate orientation of a (100) plane in a crystal was determined by naked eye observations, under a single source of light in a dark

TABLE I. *Dimensions of crystal specimens.*

DIRECTION OF SIDES	PLANE OF SPECIMEN	MEAN LENGTH OF SIDES (cm)	AREAS OF CROSS SECTION (cm²)
Tetragonal	(100)	1.72, 1.23	0.0697
Digonal	(100)	1.49, 1.17	0.0670
Trigonal	(110)	0.77, 0.77	0.0489

room, sticking a small mirror to the crystal so that it reflected a ray of light parallel to the rays reflected from etch planes. Since these are (100) planes of the crystal the plane of the mirror then lies parallel to a (100) plane. A flat surface was cut on the crystal parallel to the plane of the mirror. The orientations of this surface and of the axes lying in it were determined more accurately by means of x-rays and it was then possible to set the piece in a machine so as to grind any desired section to within half a degree or less of the desired orientation. It is possible to cut a parallelogram from a slice, properly located, so that each side of the parallelogram is parallel to any one of the three crystallographic directions, [100], [110] and [111] which are of most interest. The single crystal specimens were thus cut so that each may be described as a strip of metal forming a closed parallelogram having its sides parallel to a certain crystallographic direction.

Great care was taken in cutting the crystals to avoid straining them. After cutting, the specimens were etched to remove the strained material on the surface and then they were annealed in an atmosphere of hydrogen. They were etched again after annealing and since there were no signs of recrystallization, it was thought the specimens had not been unduly strained in earlier processes. Three magnetic test specimens of this sort were cut from the ingot. The first specimen had each side parallel to a tetragonal axis [010] or [001], the second specimen had each side parallel to a digonal axis, [011] or [01$\bar{1}$]. In each of these specmens the plane of the parallelogram was (100). The third specimen had each side parallel to a trigonal axis [1$\bar{1}$1] or [1$\bar{1}\bar{1}$], the plane of the parallelogram being (110). Table I gives the dimensions of the specimens, and the plane of the parallelogram.

The specimens are shown in Fig. 1.

Magnetic Tests

Magnetic data were obtained by winding each specimen with a primary and secondary winding and then testing with a Haworth fluxmeter.[2] Previous tests on single crystals have usually been made on ellipsoids or short rods and have the disadvantage that at low fields the effective magnetizing field is the difference between two relatively large quantities, the applied magnetizing field and the demagnetizing field of the specimen, so that small effective fields cannot be determined accurately. Therefore, the initial part of the magnetization curve up to approximately half the saturation value cannot be determined accurately nor can the residual induction be measured. The method described in this article eliminates this disadvantage. On the other hand the new method has the disadvantage that the flux at the corners may go in other crystallographic directions than those intended. In the specimens used these cross-corner distances are short in comparison to the total length of path and the cross-sectional area is slightly[3] greater at the corners.

Magnetization curves for the three specimens after annealing at 900°C for an hour and then reannealing at 1300°C for an hour are shown in Fig. 2. The curve for the [100] direction has a higher permeability than the other two curves. The maximum permeability is 624,000, the residual induction is 13,400 gauss and the coercive force is 0.028 oersted. The maximum permeability for the [110] direction is 64,000, the residual induction 10,400 gauss and the coercive force 0.043 oersted while the maximum permeability for the [111] direction is 19,300, the residual induction 2130 gauss and the

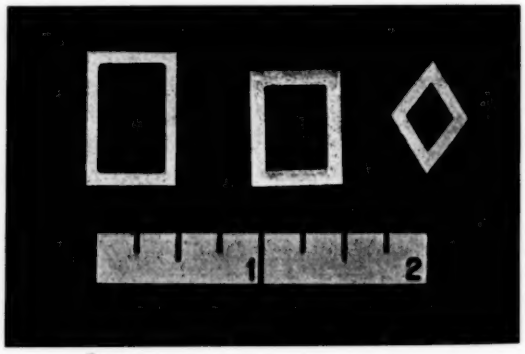

Fig. 1. Single crystal magnetic test specimens of 3.85 percent silicon iron. The first specimen has each side parallel to a tetragonal axis, the second specimen has each side parallel to a digonal axis and the third specimen has each side parallel to a trigonal axis. Scale in inches.

[2] F. E. Haworth, Bell System Tech. J. 10, 20–32 (1931).

[3] If the corners were rounded so as to give a uniform cross-sectional area the material cut away would amount to only about one percent of the total.

coercive force 0.11 oersted. Fig. 3 shows the permeabilities as functions of the induction. It should be noted that the [100] curve has not only a higher maximum permeability but also has much higher permeability at high flux densities. There are no points on the [100] curve for values of the induction between 2000 and 8000 gauss. This is because the magnetization curve is nearly vertical over this range. This gives a straight line when the permeability is plotted as a function of the induction.

The data of Figs. 2 and 3 show considerable anisotropy for values of magnetization less than half of the saturation value. This has not been previously observed nor has it been predicted by theory. However, a simple analysis shows that it should be expected. In this analysis the magnetization curves for the [110] and [111] are derived from the experimental curve for the

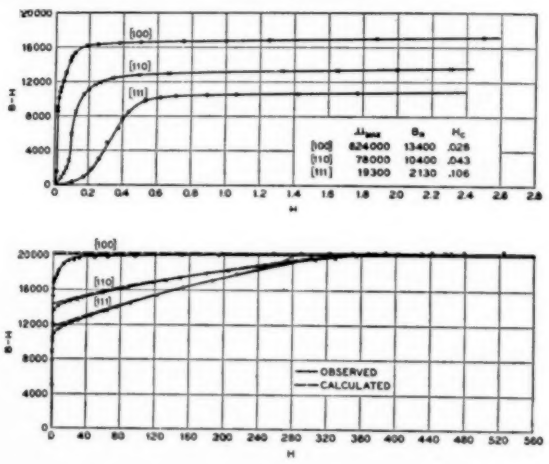

FIG. 2. The observed and calculated magnetization curves for the [100], [110] and [111] directions of single crystals of 3.85 percent silicon iron.

[100] by assuming that when H is applied along the [110] or [111] the component of H along a [100] will produce a magnetization in that direction given by a [100] magnetization curve; the projection of this value of I on the direction of the applied H gives the magnetization in that direction.

The [100] specimen was reannealed at 1300°C for two hours more and then tested. The maximum permeability was 1,180,000. Then it was heat treated at 600°C for three hours while a magnetic field of 10 oersteds was applied. The maximum permeability was then 1,030,000.

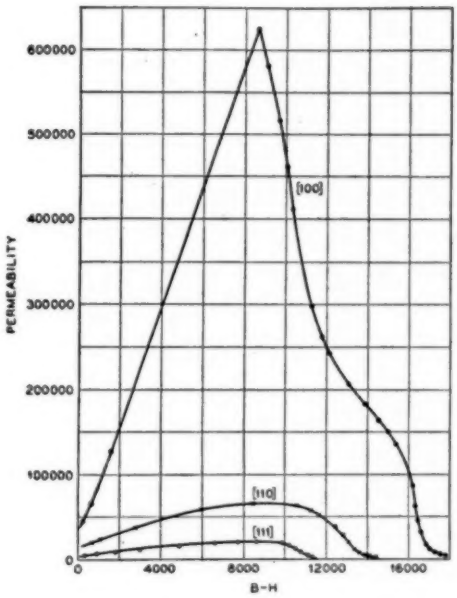

FIG. 3. Permeability *vs.* $B-H$ for the [100], [110] and [111] directions of single crystals of 3.85 percent silicon iron.

During this low temperature anneal the surface of the specimen became slightly oxidized so the specimen was etched to remove this coating. After etching the maximum permeability was 1,380,000. The permeability induction curves are shown in Fig. 4.

CONSTANTS BY FITTING CURVES

When a crystal is magnetized to saturation the expression for the energy of magnetization is to three orders of approximation,

$$E=K_0+K_1(S_1^2S_2^2+S_1^2S_3^2+S_2^2S_3^2)+K_2(S_1^2S_2^2S_3^2). \quad (1)$$

In this expression K_0, K_1 and K_2 are coefficients and S_1, S_2 and S_3 are the direction cosines of I_0, the saturation value of the local intensity of magnetization, with reference to the cubic axes. If the direction of magnetization is along a cubic axis the second and third terms in the expression are zero and so the energy of magnetization along a cubic axis is equal to K_0. To magnetize the crystal in any other direction, we may first magnetize the crystal along a cubic axis and then rotate the I_0 vector into the desired position. The second and third terms express the energy required to rotate the I_0 vector from a cubic

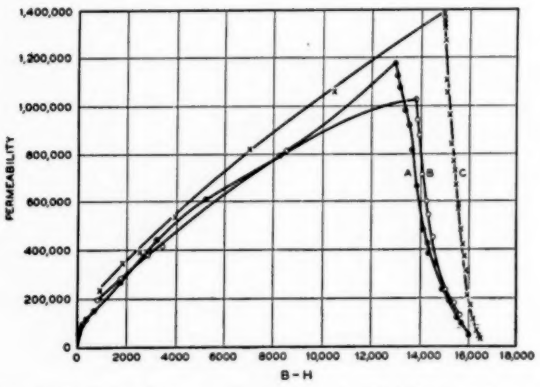

FIG. 4. Permeability *vs.* $B-H$ for the [100] direction. *A*, After heat treating the specimen at 900°C for one hour and 1300°C for three hours. *B*, After further heat treatment at 600°C for three hours in the presence of a magnetic field. *C*, After etching.

axis into any other position. The energy necessary to rotate I_0 is also equal to $-\int_0^{\alpha_0} L d\alpha$ where L is the torque and α_0 is the angle between the nearest cubic axis and the final position of I_0. It is assumed that the axis of L remains fixed. From this it is apparent that

$$L=-dE/d\alpha. \tag{2}$$

Let H make an angle α_0 with the nearest direction of easy magnetization. Then as H is increased I_0 will rotate from a position of easy magnetization and α, the angle between I_0 and the nearest direction of easy magnetization, will approach α_0. The equilibrium condition for a given value of H is that the torque due to the applied field is equal and opposite to the torque due to the forces of anisotropy which tend to keep the domains lined up in a direction of easy magnetization. The former is equal to the product of the normal component of I_0 and H, and the latter is equal to $dE/d\alpha$.

Equating these and solving for H gives

$$H=\frac{dE/d\alpha}{I_0 \sin(\alpha_0-\alpha)}. \tag{3}$$

The component of I_0 parallel to the applied field is given by the relation

$$I=I_0 \cos(\alpha_0-\alpha). \tag{4}$$

Eqs. (3) and (4) give the theoretical magnetization curves[4] for a single crystal. These curves intersect the I axis at $I_0 \cos \alpha_0$. The value of H required to saturate a material in the [110] direction is equal to $2K_1/I_0$, which gives a value of K_1. The values of K_1 and K_2 determined in this manner for the crystals of silicon-iron, are given in Table II.

CONSTANTS FROM AREAS

The energy required to magnetize a crystal to saturation in any direction $[hkl]$ is equal to

$$\int_0^{I_0} H_{hkl} dI_{hkl}.$$

Equating this to the expression for the energy given in Eq. (1) and then subtracting the energy of magnetization for the [100] direction from that for the [110] direction and the energy for [100] direction from that for [111] direction gives

$$E_{110}-E_{100}=\frac{K_1}{4}=\int_0^{I_0} H_{110} dI_{110}-\int_0^{I_0} H_{100} dI_{100}, \tag{5}$$

$$E_{111}-E_{100}=\frac{K_1}{3}+\frac{K_2}{27}$$

$$=\int_0^{I_0} H_{111} dI_{111}-\int_0^{I_0} H_{100} dI_{100}. \tag{6}$$

These equations give the anisotropy constants in

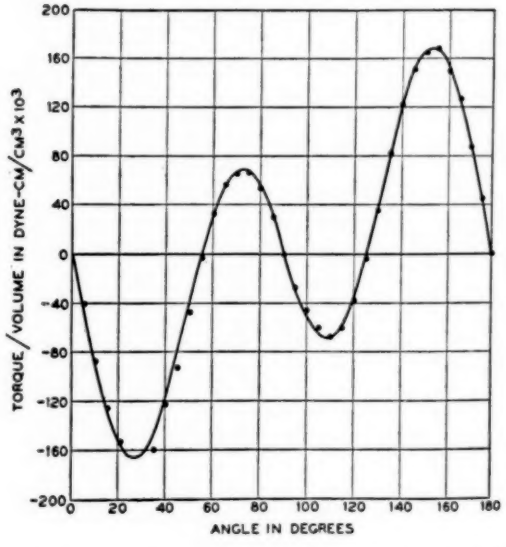

FIG. 5. Torque curve for a single crystal disk of silicon iron in the (110) plane, taken with an applied field of 5800 oersteds. The line is drawn according to Eq. (7) with $K_1=287{,}000$ and $K_2=100{,}000$.

[4] For a recent discussion of the theory of magnetization and torque curves involving K_1 and K_2, see R. M. Bozorth, Phys. Rev. **50**, 1076 (1936).

terms of the area between the magnetization curves. Values are given in Table II.

Constants from Torque Measurements

A third method of determining anisotropy constants is by means of torque measurements. A single crystal disk 1.77 cm in diameter and 0.222 cm thick was cut so the plane of the disk was parallel to (110). Torque measurements were made on this disk by means of a torsion magnetometer. Using the relation $L=-dE/d\alpha$ and substituting the direction cosines for a vector lying in the (110) plane gives the following expression for the torque.

$$L=-K_1(2\sin 2\alpha+3\sin 4\alpha)/8 -K_2(\sin 2\alpha+4\sin 4\alpha-3\cos 6\alpha)/64. \quad (7)$$

Fig. 5 shows the theoretical and experimental torque curves. K_1 and K_2 were determined by trial to make the theoretical curve fit the experimental curve as closely as possible.

Table II. *Values of anisotropy constants.*

Method	K_1 (erg cm^{-3})	K_2 (erg cm^{-3})
Measurement of areas between magnetization curves	272,000	150,000
Fitting theoretical magnetization curves to the experimental curves	280,000	100,000
Torque measurements	287,000	100,000

The values of K_1 and K_2 determined by the three methods are given in Table II.

I wish to thank F. E. Haworth for the careful x-ray determination of the crystal orientations, and R. M. Bozorth for valuable discussions.

OCTOBER 1, 1937 PHYSICAL REVIEW VOLUME 52

The Viscosity of Air

W. V. Houston
California Institute of Technology, Pasadena, California

(Received August 13, 1937)

The viscosity of air has been remeasured with the rotating cylinder apparatus used by Day and Bleakney. All of the constants have been redetermined, and especial attention has been given to the corrections to the simple theory. The value obtained at 22°C is $\eta=1.8243\pm0.0045$ c.g.s. units. This raises the oil drop value of e to 4.796 e.s.u. It is shown in the appendix that a correction must be applied for the opening between the suspended cylinder and the guard cylinders, and also a correction must be applied for the moment of inertia of the air carried around by the cylinder when determining its moment of inertia. Neglect of these corrections has introduced some additional uncertainty into other work.

THE viscosity of air has become of special interest within the last few years since the suggestion of Shiba[1] that an error in the adopted value of this quantity was responsible for the discrepancy between the values of e determined by the oil drop and the x-ray methods. The work of Harrington[2] was supposed to have established its value with the necessary precision, but Shiba concluded from an examination of other determinations that this precision might have been considerably overestimated. Because of this interest and the presence in this laboratory of a rotating cylinder apparatus suited to this purpose it seemed worth while to make a complete redetermination of the viscosity. Although since the work was started, about a year ago, the very careful work of Kellström[3] and a preliminary note from Bearden have appeared and have confirmed Shiba's supposition, it may be still of interest to have an independent determination.

It is not necessary to enter into a detailed description of the apparatus since it has been previously described.[4] No essential changes have been

[1] K. Shiba, Sci. Papers Inst. Phys. Chem. Res. Tokyo, **19**, 97 (1932).
[2] E. L. Harrington, Phys. Rev. **8**, 738 (1916).
[3] G. Kellström, Phil. Mag. **23**, 313 (1937); J. A. Bearden, Phys. Rev. **51**, 378 (1937).
[4] R. K. Day, Phys. Rev. **40**, 281 (1932); W. M. Bleakney, Physics **3**, 123 (1932).

made since the work of Bleakney but all of the dimensions have been redetermined.

The expression for the viscosity when determined by this method is

$$\eta=\pi(b^2-a^2)I\theta/la^2b^2P^2\Omega. \quad (1)$$

For convenience in discussion this may be divided into three parts. Let

$$K=QI=\{\pi(b^2-a^2)/la^2b^2\}I,$$
$$D=\theta/P^2\Omega,$$

where a is the radius of the inner suspended cylinder, b is the radius of the outer rotating cylinder, l is the effective length of the inner cylinder, I is the moment of inertia and P the period of oscillation of the inner cylinder, Ω is the angular velocity with which the outer cylinder is turned, and θ is the angular deflection of the inner cylinder. The quantity Q is determined by direct measurement, I by observation of periods of vibration, and the determinations of D constitute the measurement of the viscosity. K may be considered a constant of the instrument independent of the suspension used.

Determination of Q

The diameter of the inner cylinder was measured directly with two different micrometers. Each micrometer was checked on a standard block. Although no investigation of the standards was made it is certain that their error is entirely negligible compared with other errors which are present. Measurements were taken near the top, near the middle, and near the bottom. These are given in Table I. The uncertainties given are the root-mean-square deviations from the mean. The uncertainty indicated in the final value, in this as in all other tables, is either the root-mean-square deviation of the mean values given or $1/n^{\frac{1}{2}}$ times the square root of the mean square of the given uncertainties, whichever is the larger. There was evidence of slight ellipticity at the top and at the bottom.

Table I. *Diameter of inner cylinder.*

Readings	Position	Mean
20	Top	10.7173±0.0014
20	Middle	10.7176±0.0014
20	Bottom	10.7173±0.0006
	Mean	10.7174±0.0007

The inside diameter of the rotating cylinder was measured with two inside micrometers. The results are given in Table II.

Table II. *Diameter of outer cylinder.*

Readings	Position	Mean
14	Top	11.9070±0.0014
14	Middle	11.9078±0.0006
14	Bottom	11.9082±0.0009
	Mean	11.9077±0.0006

The length of the cylinder was measured with a steel scale and with a glass scale on a cathetometer. Both of these scales had previously been compared with a standard meter.[5] With the cathetometer, nine readings gave a mean of 25.482±0.018 cm when corrected for the error of the scale. Six readings with the steel scale gave 25.495±0.005. The mean is 25.489±0.013 cm.

The use of the length of the cylinder in Eq. (1) implies that all of the torque is applied to the outer surface of the cylinder. However, the air penetrates the opening between it and the guard cylinder and exerts a torque on the end and in fact on the inside surface of the suspended cylinder. This effect is small since the distance between the cylinders is small compared with the length, but it is not entirely negligible. The distance between the guard cylinders as measured with the steel scale was 25.587±0.015 cm so that the sum of the two openings was 0.098 cm. If the suspended cylinder and the guard cylinder had been identical in wall thickness, just half of this opening should be added to the length of the inner cylinder. However, the guard cylinder had walls some 3 mm thick while the thickness of the suspended cylinder wall was less than 0.5 mm. On this account more of the torque was applied to the guard cylinder than to the other and the correction added was 0.47 of the opening or 0.046 cm. A further discussion of this correction is given in the appendix.

With this correction the effective length of the cylinder was

$$l=25.535\pm0.015 \text{ cm}.$$

[5] J. S. Campbell and W. V. Houston, Phys. Rev. **39**, 601 (1932).

The relative uncertainty in the value of Q is

$$\Delta Q/Q=\{[\Delta a/(b-a)]^2+[\Delta b/(b-a)]^2+(\Delta l/l)^2\}^{\frac{1}{2}}.$$

Combining the above results gives

$$Q=8.1375\pm0.10 \text{ percent.}$$

Determination of I

The moment of inertia of the inner cylinder was determined by the customary procedure of measuring the period of the rotational oscillations with and without the addition of a ring whose moment of inertia was calculated from its dimensions. Since the torsion constant of a suspension depends upon the weight it supports, it was necessary to use a compensating weight when the ring was not in place. This weight had the form of a rod and was supported on the axis of the cylinder by three small wires extending to one of the ribs. The period was then measured under four different conditions.

Let T_0 be the period of oscillation of the cylinder alone, T_1 the period of the cylinder and the ring, T_2 the period of the cylinder and the weight, and T_3 the period of the cylinder with both the ring and the weight. Let these be the periods after the correction for the observed damping has been applied so that the square of the corrected period is proportional to the effective moment of inertia divided by the force constant. The correction was made in terms of the observed decrement. Let $\delta=\log_e(X_n/X_{n+1})$, where X_n and X_{n+1} are successive maximum displacements on one side. Then $T=T'/(1+\delta^2/8\pi^2)$, where T' is the observed period. In many cases this correction was entirely negligible.

The suspensions for the determination of I were steel and tungsten wires of various sizes. When first inserted they showed a tendency to change with the time, and the torsion constant always showed a slight change with the temperature. A determination of the moment of inertia thus involved an extended series of observations of each of the four periods until the permanent change was negligible and a curve of period against temperature could be established. The cylinder was mounted in a wooden case on a heavy block of concrete to be shielded from air currents and as much as possible from outside mechanical disturbances. In spite of these precautions it was found that the long period observations were erratic and not reproducible, so that no determinations were included in the final results for which T_0 was greater than 100 sec.

Table III. *Moment of inertia of rings and weights.*

No.	I_R	I_W	M_R	M_W
1	3264.5±1.0	43.5±0.5	116.10	118.16
2	6364.8±1.2	130.5±0.5	226.78	228.83

The oscillations were observed with a telescope and scale and the amplitude was recorded to compute the damping correction. The time between a passage through the central position and an integral minute on the clock was measured by means of a stopwatch. Part of the time the clock used was a chronometer loaned by the Mt. Wilson Observatory, but after the Institute power lines were connected to the Boulder Dam plant, the frequency was sufficiently constant to use an ordinary electric clock. Errors in the clock were treated as negligible. Observations were made of three passages through the center at the beginning of a run and again about 50 minutes later. The nine differences permitted averaging to minimize the end point errors so that the periods are believed to be correct to 0.005 percent.

Since these observations were made in air at atmospheric pressure it is necessary to make a correction for the moment of inertia of the air dragged around with the cylinder. This quantity is approximately proportional to $T^{\frac{1}{2}}$, and its exact form and development are given in the appendix. Let ΔI_0, ΔI_1, ΔI_2, ΔI_3 be the corrections to be added to the true moment of inertia of the cylinder under the four conditions of oscillation. Then

$$\begin{aligned}
T_0^2&=4\pi^2(I+\Delta I_0)/k,\\
T_1^2&=4\pi^2(I+\Delta I_1+I_R)/k(1+\epsilon),\\
T_2^2&=4\pi^2(I+\Delta I_2+I_W)/k(1+\epsilon),\\
T_3^2&=4\pi^2(I+\Delta I_3+I_W+I_R)/k(1+2\epsilon). \qquad (2)
\end{aligned}$$

I_R is the calculated moment of inertia of the ring, I_W that of the weight, and k is the torsion constant of the suspension when supporting the weight of the cylinder alone. In these equations it is assumed that the change in the

TABLE IV. *Determinations of I.*

SERIES SUSPENSION	1 8 mil steel	2 5 mil steel	3 8 mil W	4 5 mil W	5 5 mil W
Ring No.	2	1	2	1	1
Temp.	20.0	20.5	21.0	22.5	22.2
T_0	35.408	89.496	26.6174	56.637	
T_1	43.910	101.169	33.0030	63.990	63.969
T_2	35.618	89.775	26.7680	56.779	56.763
T_3	44.100	101.436	33.1340	64.103	
ΔI	37.5	58.0	31.5	47.5	
ΔI	41.6	61.3	36.0	50.2	50.2
ΔI_2	37.7	58.1	31.5	47.5	47.5
ΔI_3	41.7	61.3	36.0	50.2	
I'	11857	11839	11839	11824	
I''	11837	11850	11826	11862	
I'''	11835	11830	11834	11844	11847
Mean I	11843	11840	11833	11843	11847
Uncertainty	18	14	9	16	

Mean $I = 11841 \pm 10$

torsion constant is proportional to the weight added, and also that the small difference between the weights of the rings and the corresponding compensating weights is negligible.

From Eq. (2) it follows that

$$\begin{aligned}(1+\epsilon) &= \{1+(I_W+\Delta I_2-\Delta I_0)/ \\ &\qquad (I+\Delta I_0)\}T_0^2/T_2^2, \\ (1+\epsilon) &= \{1+(I_W+\Delta I_3-\Delta I_1)/ \\ &\qquad (I+I_R+\Delta I_1)\}T_1^2/T_3^2.\end{aligned} \tag{3}$$

An approximate value of I can be inserted in these equations to calculate $(I+\epsilon)$. The agreement of the two values obtained gives some indication of the consistency of the observations. The mean value was then used to determine I.

From Eqs. (2) it also follows that

$$\begin{aligned}I' &= T_0^2(I_R+\Delta I_1-\Delta I_0)/ \\ &\qquad [(1+\epsilon)T_1^2-T_0^2]-\Delta I_0, \\ I'' &= T_2^2(I+\Delta I_3-\Delta I_2)/ \\ &\qquad [(1+\epsilon)T_3^2-T_2^2]-I_W-\Delta I_2, \\ I''' &= T_2^2(I_R+\Delta I_1-\Delta I_2-I_W)/ \\ &\qquad (T_1^2-T_2^2)-I_W-\Delta I_2.\end{aligned} \tag{4}$$

The differences among these three values of I reflect the difference between the two values of $(1+\epsilon)$. The root-mean-square deviation of these three values from their mean gives an estimate of the consistency of the four observed periods and of the reliability of the mean value of I.

Table III gives the calculated moments of inertia of the rings and the weights and Table IV gives the observed periods and the values of I determined from them. In series 5 observations were made of T_1 and T_2 only so that no value of the dispersion can be given. The temperatures indicate those at which the periods were taken, but no correction to the standard temperature of 22.0° was made since the correction is well within the uncertainty.

The uncertainty in I given in Table IV is based on the consistency of the different results only. In addition the uncertainty in I_R and I_W must be included. The fact that two different rings are used with no apparent systematic difference in the results indicates that the difference between the errors in the two rings is within the dispersion of the measurements. However to make some allowance for these uncertainties the value was taken as

$$I = 11841 \pm 0.10 \text{ percent gram cm}^2.$$

DETERMINATION OF D

The rotating cylinder was driven at constant speed by a reed controlled motor. The reed was enclosed in a thermostated box and its temperature did not vary over 0.2°. The angular velocity of the cylinder, when connected to the motor by gears reducing the speed by a factor of 120, was determined from a run of several hours to be $\Omega_0 = 0.034967 \pm 0.002$ percent radians per second. In making observations several different gear ratios were used and the ratio of the angular velocity used to the one given above is tabulated in column 2 of Table V.

When the apparatus was assembled and the cylinder adjusted to be vertical and coincident with the guard cylinders a series of intermingled observations of P and θ were made. The observations of P were made with the apparatus

TABLE V. *Observations of D.*

$P(22.0°)$	Ω/Ω_0	TEMP.	θ	$D_T \times 10^5$	$D_{22} \times 10^5$	MEAN
275.42	9/14	21.7	0.032232	1.8912	1.8927	
	6/7	21.3	0.042935	1.8908	1.8943	1.8932
	1/1	21.6	0.050112	1.8905	1.8925	±0.0008
275.35	1/1	21.8	0.050168	1.8924	1.8934	
	4/3	21.8	0.066965	1.8942	1.8952	1.8941
	9/14	21.7	0.032260	1.8920	1.8935	±0.0008
	6/7	21.8	0.043045	1.8933	1.8943	
186.225	6/7	21.7	0.019642	1.8898	1.8913	
	9/14	21.9	0.014750	1.8922	1.8927	1.8909
	1/2	21.9	0.011448	1.8881	1.8886	±0.0017
186.049	1/1	22.0	0.022900	1.8916	1.8916	
	4/3	22.3	0.030563	1.8940	1.8925	1.8921
						±0.0005
186.070	4/3	22.3	0.030640	1.8974	1.8959	
	1/1	21.8	0.022935	1.8948	1.8958	1.8960
	6/7	22.2	0.019696	1.8978	1.8968	+0.0005
	4/3	23.3	0.030731	1.9020	1.8955	

Mean $D_{22} = 1.8933 \pm 0.0017$

evacuated since the moment of inertia was determined for the cylinder alone. The temperature was measured by means of four thermocouples at various points on the case of the apparatus. The whole was surrounded by an insulating housing to reduce the fluctuations in temperature, and although no great effort was made to control the temperature, it varied so slowly that the change during an observation of an hour was rarely as much as 0.1°C. The values of P were then plotted as a function of the temperature and the suitable value read from the curve for use with each value of the deflection. The value of P at 22.0° for each set of measurements is given in column 1 of Table V.

The air admitted to the apparatus was passed slowly through two tubes, a meter long, filled with calcium chloride and seemed to be adequately dried. To measure θ the motor was run first in one direction and then in the other. The equilibrium position for each direction was determined by observing a series of turning points as the cylinder oscillated through a small amplitude. Two observations of the deflection in each direction gave two values of the double deflection whose mean was then reduced to give the deflection of the cylinder. The scale readings were reduced to angular deflections by the suitable series expansion. The observed values of θ are given in column 4 of Table V and the corresponding temperatures are in the previous column.

The value of θ was then divided by the angular velocity of the outer cylinder and the square of the period at the given temperature to give the quantity D. Although D was observed at a number of temperatures, the temperature range was not sufficient to give a good value of the temperature coefficient. Hence the observed values were corrected to 22.0°C by the usual temperature coefficient of 0.00271 per degree.[6]

The results given in Table V are divided into five groups. The first two groups were made with a watch spring suspension of the type used by Day and Bleakney and the last three were made with a steel wire 0.003 in. in diameter. Each group represents a complete readjustment of the cylinders. The differences between the groups are somewhat larger than the dispersion within them and so are to be attributed to errors in the adjustment of the cylinders. According to Kellström an eccentric adjustment gives too low a value, so that the highest of the values should be considered the best. To make some allowance for this the adopted uncertainty in D was made fifty percent greater than that obtained from the dispersion of the values so that

$$D_{22}=1.8933\times10^{-5}\pm0.14 \text{ percent.}$$

Discussion of the Results

The combination of the adopted values of Q, I, and D given above gives

$$\eta_{22}=1.8243\pm0.25 \text{ percent}\times10^{-4} \text{ c.g.s. units.}$$

The combination of the uncertainties in the three quantities given above leads to 0.19 percent as the uncertainty of the result. To allow for other possibilities this is rounded off to 0.25 percent which is then to be regarded as an estimated limit of error.

With the usual temperature coefficient

$$\eta_{23}=1.8292\pm0.0045\times10^{-4} \text{ c.g.s. units}$$

which gives for the electronic charge as given by the oil drop experiments

$$e=4.796\times10^{-10} \text{ e.s.u.}$$

This value of η_{23} is a little lower than that given by Kellström although the difference is less than the sum of the two limits of error. It is not clear from Kellström's paper whether or not he applied the correction for the length of the cylinder. If this is applied to his result it becomes somewhat lower. Kellström also did not discuss the corrections to the moment of inertia due to the presence of air, but it appears from his description of the method used that this should be rather small and would tend to raise his value a little.

In conclusion I wish to acknowledge the assistance of Mr. F. C. Bennett who helped in making many of these observations.

[6] R. A. Millikan, Ann. d. Physik **41**, 759 (1913).

Appendix

Computation of end correction

The use of guard cylinders at each end of the suspended cylinder very much reduces the end effects and makes the end correction very small. Nevertheless a correction of the order of magnitude of the spacing between the inner cylinder and the guard cylinders must be added to the measured length. To determine the amount of this correction it is necessary to compute the excess of the torque on the inner cylinder over the torque computed in the simple theory.

Since the radius of the cylinders is large compared with the difference in radius it is sufficient to regard them as planes and to treat the problem in two dimensions. In the figure let AB represent a part of the inner surface of the outer cylinder, CD the end of the suspended cylinder and $EFGH$ the section of one guard cylinder. Since FG is about 3 mm and DF about 0.5 mm it is a sufficient approximation to prolong FG to FGJ. The thickness of the sheet CD is about 0.4 mm so it is treated as a thin sheet. The problem is now to find the motion of the fluid in the space surrounding these surfaces when CD and EFJ are fixed and AB is moving into the page with a constant velocity. When the motion of the fluid is known the force on the various surfaces can be found.

Under these circumstances all of the velocity is perpendicular to the page, and if v is the magnitude of the velocity at any point (x, y),

$$\partial^2 v/\partial x^2+\partial^2 v/\partial y^2=0. \qquad (1')$$

This equation and the accompanying boundary conditions are just those for the distribution of electrical potential between conducting sheets when AB is at one potential and the other surfaces are at another.

When the distribution of v is known the force per unit area on one of the surfaces is the normal component of $(-\eta \operatorname{grad} v)$ and the total force is the surface integral of this quantity. To determine the correct value of l for use in Eq. (1) it is only necessary to find the point P such that the lines of "flux" (grad v) from BP go to EFJ and those from AP go to CD. If P were joined to J by a surface normal to the figure and coincident with the grad v it follows from Gauss' theorem that the force on BP is equal and opposite to that on EFJ, and the force on AP is equal and opposite to that on CD. If the guard cylinder and the suspended cylinder were identical in section it would follow from symmetry that P would lie just midway between D and F. However, since this symmetry does not exist the problem was solved by means of a conformal transformation.[7] This shows that the fraction of the spacing to be added depends upon the ratio of the distance DF to the distance DP. As DF/DP approaches zero the correction approached $DF/2$, and for the dimensions used in this work 0.47 DF must be added to each end of the swinging cylinder. Since the thickness of CD is really almost as great as DF the correct result is between 0.47 and 0.50.

Since the wall of the cylinder is very thin the whole force is applied effectively at the surface, so the excess torque is simply given by this addition to the length. In other cases allowance would have to be made for the point on the end of the cylincer at which the force was applied.

Effect of the air on the period of the cylinder

When the cylinder is rotating about its axis in air a certain amount of the air, both inside and outside, rotates

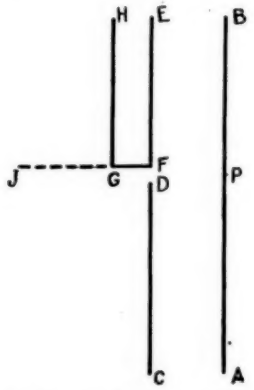

FIG. 1. Section at end of cylinder.

with it and contributes to the effective moment of inertia of the system. The correction necessary on account of this effect was computed by considering an infinite hollow cylinder. This is in error due both to the finite length of the cylinder and to the presence of the inside ribs but there seems to be no simple way to take these into account. Of course the moment of inertia could actually have been determined in vacuum but this presents considerable complication.

The treatment of problems such as this apparently goes back to Stokes[8] who gave a simple solution for an oscillating plane and worked out a number of more complicated cases. For a large enough cylinder and a short enough period of oscillation the approximation of a plane can be used. However, for the cylinder and the periods used in this measurement the error in such an approximation is considerable. I have been unable to find the cylindrical case treated in any of the standard works which I have consulted, and since it seems one which might have a number of applications I shall outline it here.

For the slow motion of a viscous fluid subject to no external volume forces, and in which the differences in pressure and density are negligible, the equation of motion is

$$\rho(\partial \mathbf{v}/\partial t)=\nabla^2 \mathbf{v}, \qquad (2')$$

where ρ is the density, η the viscosity, and $\mathbf{v}$ is the vector velocity of the fluid. For the problem in hand all the motion takes place in cylindrical laminae so that v is always perpendicular to the axis and to the radius. Expressed in cylindrical coordinates under these restrictions the equation is

$$\partial v/\partial t=(\eta/\rho)\{\partial^2 v/\partial r^2+(1/r)\partial v/\partial r-v/r^2\}, \qquad (3')$$

[7] I am indebted to Professor W. R. Smythe for assistance in working out this transformation. The method is described in his book, *Static and Dynamic Electricity* published by Edwards Brothers.

[8] G. G. Stokes, Math. and Phys. Papers, vol. III.

where v is now the scalar velocity. The velocity at any distance from the axis will vary harmonically with the time so let

$$v=A(r)\sin(2\pi t/T)+B(r)\cos(2\pi t/T). \quad (4')$$

Then
$$d^2A/dr^2+(1/r)dA/dr-A/r^2+\lambda B=0,$$
$$d^2B/dr^2+(1/r)dB/dr-B/r^2-\lambda A=0, \quad (5')$$

where $\lambda=2\pi\rho/\eta T$.

The general solution of these equations is

$$A=a\,ber_1(x)-b\,bei_1(x)+c\,ker_1(x)-d\,kei_1(x),$$
$$B=a\,ber_1(x)+b\,bei_1(x)+c\,ker_1(x)+d\,kei_1(x), \quad (6')$$

where $x=\lambda^{\frac{1}{2}}r$. For numerical computation it is a little more convenient to have these expressed in terms of the functions with the index zero, so by using the recursion formulas one obtained

$$A=\alpha\,ber'(x)-\beta\,bei'(x)+\gamma\,ker'(x)-\delta\,kei'(x),$$
$$B=\beta\,ber'(x)+\alpha\,bei'(x)+\delta\,ker'(x)+\gamma\,kei'(x). \quad (7')$$

The torque on length l of the cylinder due to the fluid is

$$L=\pm 2\pi lR^2\eta\{(dA/dr-A/r)\sin(2\pi t/T)+(dB/dr-B/r)\cos(2\pi t/T)\}. \quad (8')$$

The upper sign is to be used for the fluid outside the cylinder and the lower sign for that inside it. If θ is the angular displacement of the cylinder, let

$$\ddot{\theta}=(2\pi/RT)A_0\cos(2\pi t/T), \qquad \dot{\theta}=(A_0/R)\sin(2\pi t/T),$$

where R is the radius of the cylinder. The equation of motion of the cylinder is

$$\{I\mp(2\pi\rho lR^4/\lambda^{\frac{1}{2}}RA_0)(dB/dx-B/x)_{x=\lambda^{\frac{1}{2}}R}\}\ddot{\theta}+\{p\mp(2\pi lR^2\eta\lambda^{\frac{1}{2}}/A_0)(dA/dx-A/x)_{x=\lambda^{\frac{1}{2}}R}\}\dot{\theta}+k\theta=0, \quad (9')$$

in which p represents the damping constant due to sources other than the fluid in which the cylinder is immersed.

From Eq. (9') it is evident that the effect of the fluid is to add an additional moment of inertia to that of the cylinder and to increase the damping constant. Since only the correction to the moment of inertia is of immediate interest, the final expressions will be given for it only. The damping can be worked out in the various cases by similar methods.

In applying the boundary conditions it is convenient to consider three cases.

Case I. The fluid is inside the cylinder only.—In this case the velocity must vanish at the origin and so both A and B must vanish. Since $ker'(x)\to\infty$ as $x\to 0$, γ and δ must both be zero in this case.

Let $X=\lambda^{\frac{1}{2}}R$ where R is the radius of the inside of the cylinder. At $r=R$, $B(X)=0$, and $A(X)=A_0$. Hence

$$\alpha=\frac{A_0\,ber'(X)}{ber'^2(X)+bei'^2(X)}, \qquad \beta=-\frac{A_0\,bei'(X)}{ber'^2(X)+bei'^2(X)}. \quad (10')$$

From the equations which they satisfy it follows that

$$(d/dx)\,ber'(x)-ber'(x)/x=bei(x),$$
$$(d/dx)\,bei'(x)-bei'(x)/x=-ber(x).$$

Using these expressions in Eq. (9') it follows that

$$\Delta I=(\pi\rho lR^4/2)F(X)/X, \quad (11')$$

where
$$F(X)=4\frac{ber'(X)\,ber(X)+bei'(X)\,bei(X)}{ber'^2(X)+bei'^2(X)}.$$

The coefficient of $F(X)/X$ in Eq. (11') is just the moment of inertia of the fluid inside the cylinder if it were moving as a solid. This is its motion in the limit in which $X\to 0$. This limit can be approached by a low density, a high viscosity, a long period, or a small radius of the cylinder. The other limit in which $X\to\infty$ is that in which the approximation of the cylinder by a plane is justified. In this limit $F(X)\to 8^{\frac{1}{2}}$.

Case II. The fluid is outside the cylinder and extends to infinity.—In this case both A and B must vanish at infinity and B vanishes at $x=X$. Since $ber'(x)$ and $bei'(x)$ both go to infinity, α and β are both zero. These conditions give

$$\gamma=\frac{A_0 ker'(X)}{ker'^2(X)+kei'^2(X)}, \qquad \delta=\frac{-A_0 kei'(X)}{ker'^2(X)+kei'^2(X)}, \quad (12')$$

$$\Delta I=(\pi\rho lR^4/2)G(X)/X,$$

$$G(X)=-4\frac{ker'(X)\,ker(X)+kei'(X)\,kei(X)}{ker'(X)+kei'(X)}. \quad (13')$$

A few of the values of $F(X)$ and $G(X)$ which lie in the range needed for the moment of inertia determinations are given in Table VI.

TABLE VI. *Values of $F(X)$ and $G(X)$.*

X	$F(X)$	$G(X)$
0.0	X	
1.0	0.997	2.463
2.0	1.922	2.684
3.0	2.536	2.752
4.0	2.745	2.781
5.0	2.780	2.794
6.0	2.791	2.805
7.0	2.802	2.811
∞	2.828	2.828

Case III. Fluid enclosed between concentric cylinders.—In this case all four coefficients will be different from zero and must be determined by the solution of four simultaneous equations. Although laborious this solution presents no difficulties.

Since when the moment of inertia of the cylinder was determined the cylinder was enclosed in a house, this third case might have been of importance. However for the periods used it differed only negligibly from case II. With the dimensions of the cylinder used and approximate values for the density and viscosity of air $X=34.0/T^{\frac{1}{2}}$, and $\Delta I=152.5\{F(X)+G(X)\}/X$.

A Note on the Thomas-Fermi Statistical Method

E. FEENBERG
Institute for Advanced Study, Princeton, New Jersey
(Received July 16, 1937)

The accuracy with which binding energies can be computed using the statistical approximation is shown to depend strongly on the symmetry character of the wave function when the forces are of the short range saturation type met with in nuclear theory. Recent calculations on the relation between the neutron excess in heavy nuclei and the saturation properties of nuclear forces are reinterpreted in the light of this result.

THE Thomas-Fermi statistical method has been applied to fix upper bounds on the magnitude of nuclear forces[1] and to obtain necessary conditions for the occurrence of saturation in heavy nuclei.[2] These applications are legitimate because the method consists essentially in the calculation of an expectation value of the Hamiltonian operator with an especially simple wave function. Since an expectation value cannot lie below the true normal state eigenvalue, all forms of the interaction operator which yield too much binding energy in the statistical approximation must be rejected.

Recently the statistical approximation has been used to study the relation between the neutron excess, $A-2Z$, in heavy nuclei and the exchange properties of the nuclear forces.[3] In the statistical approximation a nucleus can be characterized qualitatively by the statement that it consists of a collection of "4" groups and "2" groups.[4] Two neutrons and two protons in one space orbit constitute a "4" group while two neutrons with opposed spins in a single space orbit form a "2" group. The wave function has a definite symmetry character[5] described by the partition quantum number $(4+4+\cdots+4+2+2+\cdots 2)$ with $\frac{1}{2}Z$ "fours" and $\frac{1}{2}(A-2Z)$ "twos." (Actually the symmetry character has little significance for heavy nuclei. The mixing effect of the spin exchange and Coulomb forces produces a state which is a linear combination of many different partitions.) For a fixed A, the value of $A-2Z$ which makes the energy as low as possible is determined by the conflict between the Coulomb interactions tending to increase the neutron excess and the saturation properties of the nuclear forces which tend to associate stability with a high degree of symmetry. Clearly the question of how the degree of accuracy of the statistical approximation depends on the symmetry character of the wave function must be answered before much significance can be attached to calculations of neutron excess in heavy nuclei.

To examine this question consider a generalized nuclear system with the Hamiltonian operator[6]

$$H=-\tfrac{1}{2}\sum\Delta_l-\sum_{i<j}J(r_{ij})(nP_{ij}+1)/(n+1) \quad (1)$$

subject to the condition that no more than n particles can occupy the same orbit. The physical possibilities include $n=2$ and $n=4$. Under these conditions the normal state binding energy plotted against the total mass will show an "n" group structure which gradually merges into a straight line for heavy nuclei. It is reasonable to suppose that the total binding energy of a collection of "n" groups will be somewhat greater than that of the separated n particle systems.

The binding energy of a single n particle system can be computed approximately by using the Gaussian wave function

$$\psi_n=C_n\exp\left[-(\nu/2)\sum_{i<j}r_{ij}^2\right]. \quad (2)$$

The expectation value of the energy is given by

[1] E. Majorana, Zeits. f. Physik **82**, 137 (1933); W. Heisenberg, *Rapport du Septieme Congres Solvay* (Paris, 1934); G. C. Wick, Nuovo Cimento **11**, 227 (1934); K. Nakabayasi, Zeits. f. Physik **97**, 211 (1935); C. F. v. Weizsacker, Zeits. f. Physik **96**, 431 (1935); H. A. Bethe and R. F. Bacher, Rev. Mod. Phys. **8**, 82 (1936).
[2] G. Breit and E. Feenberg, Phys. Rev. **50**, 850 (1936).
[3] H. Volz, Zeits. f. Physik **105**, 537 (1937).
[4] The discussion is limited to systems containing even numbers of neutrons and protons.
[5] E. Wigner, Phys. Rev. **51**, 106 (1937).
[6] P_{ij} is the Majorana exchange operator; the spin exchange operator Q_{ij} appears in Eq. (12).

$$\epsilon_n = 3n(n-1)\nu/4 - \tfrac{1}{2}n(n-1)(4/\pi^{\frac{1}{2}})\int_0^\infty J(r/(\tfrac{1}{2}n\nu)^{\frac{1}{2}})e^{-r^2}r^2dr. \quad (3)$$

Now we proceed to calculate the energy of a collection of "n" groups by means of the statistical method. Let N (an integral multiple of n) designate the number of particles in the system and $E(n, N)$ the energy value given by the statistical method. By comparing ϵ_n and $n/N\cdot E(n, N)$ something can be learned about the way in which the degree of accuracy of $E(n, N)$ depends on n. In the statistical model the radius R of the nucleus and the maximum momentum of the particles in the nucleus are connected by the relation $(RP)^3 = 9\pi N/2n$. The energy has the form

$$E(n, N) = 0.3NP^2 - n(n-1)/8 \cdot \int\cdots\int J(q-q')(q|\rho|q')^2 d\tau d\tau' \quad (4)$$

with[1]

$$(q-\xi/2|\rho|q+\xi/2) = (\sin \xi P/\xi - P\cos \xi P)/(\pi\xi)^2, \quad |q| \leqq R, \quad (5)$$
$$= 0, \quad |q| > R.$$

From Eqs. (4) and (5) we obtain the energy per "n" group

$$n/N\cdot E(n, N) = 0.3nP^2 - \tfrac{1}{2}n(n-1)(6/\pi)\cdot\int^\infty J(r/P)(\sin r - r\cos r)^2/r^4\cdot dr. \quad (6)$$

A great simplification is made possible by the fact that the function $1/9\cdot r^2\exp[-\lambda r^2]$ ($\lambda^{3/2} = 1/6\pi^{\frac{1}{2}}$) approximates very closely to $(\sin r - r\cos r)^2/r^4$ up to the first maximum of the latter function. The constant λ is determined by the condition

$$1/9\cdot\int_0^\infty r^2\exp[-\lambda r^2]dr = \int_0^\infty (\sin r - r\cos r)^2/r^4\cdot dr = \pi/6. \quad (7)$$

If $J(r)$ is an error function or a linear combination of error functions with positive coefficients, the potential energy in Eq. (6) is increased by the substitution of $1/9\cdot r^2\exp[-\lambda r^2]$ for $(\sin r - r\cos r)^2/r^4$. Thus, for a reasonably general form of potential function, we obtain a lower limit to $E(n, N)$ defined by the equation

$$n/N\cdot E'(n, N) = 0.3nP^2 - \tfrac{1}{2}n(n-1)(4/\pi^{\frac{1}{2}})\int_0^\infty J(r/P\lambda^{\frac{1}{2}})\exp[-r^2]r^2dr. \quad (8)$$

The substitution $3n(n-1)\nu/4 = 0.3nP^2$ transforms Eqs. (3) into

$$\epsilon_n = 0.3nP^2 - \tfrac{1}{2}n(n-1)(4/\pi^{\frac{1}{2}})\cdot\int_0^\infty J(r/P(n/5(n-1))^{\frac{1}{2}})\exp[-r^2]r^2dr. \quad (9)$$

The general assumption about the form of $J(r)$ made in the preceding paragraph and the inequality $n/5(n-1) > \lambda = 0.2068$ which is satisfied for $n < 31$ imply the relation

$$\epsilon_n < n/N\cdot E'(n, N) < n/N\cdot E(n, N). \quad (10)$$

Eq. (10) is still valid if E, E', and ϵ_n are replaced by the minimum values of the three functions defined by the Eqs. (6), (8) and (9), respectively. It is known that the Gaussian wave function for an n particle system is increasingly unsatisfactory as n is decreased.[7] In actual nuclear calculations the Gaussian wave function is very bad for $n=2$, but already surprisingly good for $n=4$. Thus ϵ_n is an increasingly bad upper limit on the true n particle eigenvalue as n is decreased.

The quantity

$$\theta(n) = (n/5\lambda(n-1))^{\frac{1}{2}} \quad (11)$$

is a monatonic decreasing function of n and greater than unity for $n < 31$. This quantity can be interpreted as the ratio of the effective ranges of the intranuclear forces in the n particle calculation and in the statistical calculation. More than half of the drop to the asymptotic value $(5\lambda)^{-\frac{1}{2}}$ occurs in passing from $n=2$ to $n=4$. The relation $\theta(n) > 1$ means that the statistical calculation yields no binding energy for a collection of "n" groups. This result must be ascribed to the inadequacy of the method.

From Volz's form of the Hamiltonian operator,

$$H = -\tfrac{1}{2}\sum\Delta_i - \sum_{i<j}V(r_{ij})(-5+14P_{ij} - 7P_{ij}Q_{ij} + 10Q_{ij})/12, \quad (12)$$

[7] E. Feenberg, Phys. Rev. **47**, 850 (1935).

we obtain the energy equation

$$E(4, N)=0.3NP^2$$

$$-(9/8)\int\cdots\int V(q-q')(q|\rho|q')^2 d\tau d\tau', \quad (13)$$

when the system contains equal numbers of neutrons and protons and

$$E(2, N)=0.3NP^2$$

$$-(1/8)\int\cdots\int V(q-q')(q|\rho|q')^2 d\tau d\tau', \quad (14)$$

when the system contains only neutrons. These equations are identical with Eq. (4) if for $n=4$ we take $J(r)=3/4\cdot V(r)$ and for $n=2$, $J(r)=\frac{1}{2}V(r)$. The same correspondences hold also for the four and two particle systems. Since the statistical approximation gives no binding energy between "2" groups and also none between "4" groups there is little likelihood that it is adequate for the calculation of the interactions within a mixed system containing both "2" and "4" groups.

Evidently the statistical method yields decidedly less accurate results for $n=2$ than for $n=4$. Although the problem considered here is not identical with that of determining the neutron excess in heavy nuclei, there is enough similarity to suggest that the values of $A-2Z$ given by the statistical approximation are too small by a large factor.[8] In view of this possibility the argument given by Volz for his special form of the symmetrical interaction operator must be considered inconclusive. Moreover the interaction operator proposed by Volz contains such large spin exchange terms[9] as to preclude the existence of a partition quantum number for even the lightest nuclei (with the single exception of the deuteron) and thus comes into conflict with the evidence presented by Wigner[10] for the usefulness of the partition quantum number in ordering the empirical material on the stability of isobars up to $A\sim 50$. Actually the simple theory without spin exchange forces discussed by Wigner begins to make $A-2Z$ too large in the neighborhood of $A\sim 50$. According to the calculations of Volz any discrepancy, with Wigner's choice of interaction operator, should be in the direction of making $A-2Z$ too small. However, for the comparison of isobars, Wigner's calculations are unquestionably much better than those based on the statistical approximation. One may conclude that the evidence available at present does not support the contention that very large spin exchange forces are required to account for the large neutron excess in heavy nuclei.

[8] In a letter to the writer Dr. Volz states that a calculation which will test this point is in progress.

[9] The sum of the Heisenberg and pure spin exchange operators is small, but each separately is large.

[10] E. Wigner, Phys. Rev. **51**, 947 (1937).

LETTERS TO THE EDITOR

Prompt publication of brief reports of important discoveries in physics may be secured by addressing them to this department. Closing dates for this department are, for the first issue of the month, the eighteenth of the preceding month, for the second issue, the third of the month. Because of the late closing dates for the section no proof can be shown to authors. The Board of Editors does not hold itself responsible for the opinions expressed by the correspondents.

Communications should not in general exceed 600 words in length.

A Theorem on the Effect of Vertical Divergence

Several corrections have been published[1-6] for the shift in the position of an x-ray line due to vertical divergence, but only those of Spencer[3] and Williams[4] check.

All writers agree that a monochromatic x-ray incident at an angle ψ with the horizontal plane containing the normal to the crystal, will be reflected at a horizontal angle $\theta+\delta\theta$ where θ is the Bragg angle and

$$\delta\theta=\tfrac{1}{2}D\lambda\psi^2=K\psi^2. \tag{1}$$

D is Allison's notation for the dispersion $d\theta/d\lambda$. For single crystal reflection $D\lambda=\frac{1}{2}\tan\theta$, while for the double crystal spectrometer $D\lambda=\frac{1}{2}(\tan\theta_A\pm\tan\theta_B)$.

The distribution of intensity in the vertical plane, which we shall call $f(\psi)$ is transformed into a horizontal distribution $F(x)$ where x stands for $\delta\theta$. We wish to study the nth moment of $F(x)$ defined by

$$\mu_n'=\int_{-\infty}^{\infty}x^nF(x)dx. \tag{2}$$

By substituting (1) and the transformation equation

$$F(x)dx=f(\psi)d\psi, \tag{3}$$

$$\mu_n'=K^n\int_{-\infty}\psi^2f(\psi)d\psi=K^n\mu'_{\psi 2n}. \tag{4}$$

Eq. (4) may be stated as a theorem: *The nth moment of the horizontal distribution is K^n times the 2nth moment of the vertical distribution.* This theorem obviates the necessity for changing variable.

Let us apply the theorem to the case in which radiation from a uniformly bright target is limited by two slits of total heights a and b with centers at the same height but distant L apart. The intensity distribution in the vertical plane is then a trapezoid, which is equivalent to the difference of two triangles

$$f(\psi)=L(\psi_2-|\psi|)-L(\psi_1-|\psi|), \tag{5}$$

where $$\psi_2=\tfrac{1}{2}(b+a)/L \quad\text{and}\quad \psi_1=\tfrac{1}{2}(b-a)/L. \tag{6}$$

Eq. (4) then becomes

$$\mu_n'=\frac{LK^n(\psi_2^{2+2n}-\psi_1^{2n+2})}{(n+1)(2n+1)}. \tag{7}$$

The center of gravity of $F(x)$, and hence, the shift in the center of gravity of the x-ray line, is

$$\mu_1'/\mu_0'=K(\psi_2^2+\psi_1^2)/6=(\delta_2+\delta_1)/6. \tag{8}$$

This agrees with the author's expressions[3] $\delta_m/6$ and $\delta_m/3$ for the special cases of $a=0$ and $a=b$. The maximum deviation is $\delta_m=\delta_2$. Eq. (8) also reduces to Williams' formula for the effective shift

$$\delta\theta_{eff}=[(a^2+b^2)/24L^2]\tan\theta, \tag{9}$$

which is to be applied to each crystal.

If (1) is divided by $D\lambda$, the fractional shift in the measured wave-length corresponding to $\delta\theta$ is

$$\delta\lambda/\lambda=\tfrac{1}{2}\psi^2. \tag{10}$$

If now we let $x=\delta\lambda/\lambda$ and $K=\frac{1}{2}$, (8) and (9) become

$$\delta\lambda/\lambda=(\psi_2^2+\psi_1^2)/6=(a^2+b^2)/24L^2, \tag{11}$$

which is the fractional shift in wave-length of the center of gravity of the x-ray line. When an error of a factor of 2 is rectified in Eqs. (16) and (17) developed by the author,[3] they are found to agree with (11).

The shift in the center of gravity approximates the shift in the peak, which is of greater importance. The peak may be located by means of the graphical solution developed by the author,[7] which makes use of the higher moments of $F(x)$.

ROY C. SPENCER

Brace Laboratory,
University of Nebraska,
September 6, 1937.

[1] S. K. Allison and J. H. Williams, Phys. Rev. **35**, 1476 (1930), p. 1480.
[2] A. H. Compton, R. S. I. **2**, 365 (1931), Eq. (3).
[3] R. C. Spencer, Phys. Rev. **38**, 618 (1931), Eqs. (11)–(17).
[4] J. H. Williams, Phys. Rev. **40**, 636(L) (1932).
[5] L. G. Parratt, Phys. Rev. **47**, 882(L) (1935).
[6] Compton and Allison, *X-Rays in Theory and Practice* (Van Nostrand), p. 737.
[7] See reference 3, pp. 625–628.

Unidentified Interstellar Lines

The following absorption lines appear in stellar spectra but are believed to be of interstellar origin:

λ	Intensity
5780.55±0.03	3
5797.13±0.04	1
6202.99±0.06	1−
6269.99±0.04	1
6283.91±0.03	6
6613.9 ±0.1	2

These lines differ from other interstellar lines in being slightly diffuse. Their characteristics will be described in detail in an article to be submitted to the *Astrophysical Journal*. In addition to the lines in the above list there is a vague feature near λ4430, which has been extensively

studied by Beals at the Dominion Astrophysical Observatory.

It has not been possible to identify these lines with any laboratory lines, and the evidence appears unfavorable to an atomic origin. It is conceivable that the lines are actually bands or portions of bands of molecular origin. The low density of interstellar space favors both ionization and dissociation but since neutral atoms (of sodium) are known to be fairly abundant, one can scarcely decide *a priori* against the existence of molecules. With very feeble excitation only a few quantum levels would be occupied and the structure of absorption bands might be quite different from that ordinarily observed in the laboratory. No conclusive identifications, however, have yet been suggested.

A third hypothesis is that the lines are produced by small solid particles. This possibility is emphasized by the fact that the correlation between stellar color excess and the intensity of λ6284 seems to point toward a physical relationship between space reddening (presumably caused by interstellar dust) and the formation of the spectral line. At room temperature only a few solids are known to produce narrow absorption lines, but at very low temperatures many substances probably have narrow lines.[1] It is therefore conceivable that at temperatures a few degrees above absolute zero the interstellar dust which causes the reddening of starlight might also produce certain absorption lines. A theoretical investigation of the formation of absorption lines by solids in the form of finely divided dust would be valuable, while positions of lines produced in the laboratory by solids at low temperatures should be examined for any possible correspondence with the interstellar lines.

PAUL W. MERRILL

Carnegie Institution of Washington,
Mount Wilson Observatory,
September 4, 1937.

[1] See for example F. H. Spedding and G. C. Nutting, J. Chem. Phys. **2**, 421 (1934).

Maximum Energy of the Protons from the Bombardment of Boron by Alpha-Particles

The maximum energy of the protons from the bombardment of boron by alpha-particles has been measured by a number of workers[1] and corresponds to a nuclear energy change of +3.3 (±0.2) Mev. According to the recently accepted values of nuclear masses a greater energy release would be expected corresponding to an energy change of +4.0 Mev. During the past eight months we have carried out a careful search for any long range group of protons of very small yield which would give better agreement with the known mass values.

A thick layer of boron was bombarded by polonium alpha-particles and the range of the protons measured with an automatic screen-changing device which made possible very long times of counting. Under our experimental conditions the protons in the 3.3 Mev group have a range of 79 cm; a group of 4.0 Mev would have a range of over 100 cm. Our first results[2] showed that at 89 cm and 100 cm counts were obtained which were above the background while at 110 cm the yield obtained was roughly equal to the background. We have, however, made a much more extended series of runs using a larger source with a counter having a lower background, which should have made the long range group six times as prominent. These later results show that if there is any longer range group of protons the yield is extraordinarily small. We give here a sample set of runs which enables a comparison to be made between the yield in the group of energy change +3.3 Mev and the possible yield of a long range group.

Absorption (cm)	43.2	89	97.2	∞
Counts	2905	278	305	196
Time (hours)	20	30	30	20
Number per hour	146.1	9.3	10.2	9.8

It can be seen that the yield beyond 80 cm is less than one two hundredth of the yield at 43 cm, which corresponds to the single group of energy change +3.3 Mev. Our full results in which over a thousand particles were counted at several absorptions confirm the above figures.

The reaction which occurs is $B^{10}+He^4 \rightarrow C^{13}+H^1$ so that the absence of a group of protons of sufficient energy to balance the mass-energy equation indicates that an excited state of C^{13} can exist having a relatively long lifetime.

We wish to express our thanks to Dr. Bearden and Dr. Kanne of Johns Hopkins University for the gift of a polonium source and to Professor A. F. Kovarik for advice and interest during the work.

ERNEST POLLARD
GORDON BRUBAKER

Sloane Physics Laboratory,
Yale University,
September 15, 1937.

[1] H. Bothe, Zeits. f. Physik **63**, 381 (1930); J. Chadwick, J. E. R. Constable and E. Pollard, Proc. Roy. Soc. **130**, 463 (1931); R. Paton, Zeits. f. Physik **90**, 586 (1934); H. Miller, W. E. Duncanson and A. N. May, Proc. Camb. Phil. Soc. **30**, 549 (1934).
[2] American Physical Society Washington Meeting, Phys. Rev. **51**, 1013 (1937).

Errata: On the Ultraviolet Light Theory of Magnetic Storms

(Phys. Rev. **52**, 155 (1937))

The following correction is noted. On page 155 in the heading of the article (Received March 25, 1936) should read (Received March 25, 1937).

A. G. MCNISH

Department of Terrestrial Magnetism,
Carnegie Institution of Washington,
Washington, D. C.,
September 3, 1937.